0017435

WHC-EP-0500

Geology and Hydrology of the 300 Area and Vicinity, Hanford Site, South-Central Washington

Prepared for the U.S. Department of Energy
Office of Environmental Restoration and
Waste Management

Westinghouse
Hanford Company Richland, Washington

Hanford Operations and Engineering Contractor for the
U.S. Department of Energy under Contract DE-AC06-87RL10930

DEC 1991
RECEIVED
EDMC

Approved for Public Release

LEGAL DISCLAIMER

This report was prepared as an account of work sponsored by an agency of the United States Government. Neither the United States Government nor any agency thereof, nor any of their employees, nor any of their contractors, subcontractors or their employees, makes any warranty, express or implied, or assumes any legal liability or responsibility for the accuracy, completeness, or any third party's use or the results of such use of any information, apparatus, product, or process disclosed, or represents that its use would not infringe privately owned rights. Reference herein to any specific commercial product, process, or service by trade name, trademark, manufacturer, or otherwise, does not necessarily constitute or imply its endorsement, recommendation, or favoring by the United States Government or any agency thereof or its contractors or subcontractors. The views and opinions of authors expressed herein do not necessarily state or reflect those of the United States Government or any agency thereof.

This report has been reproduced from the best available copy.
Available in paper copy and microfiche.

Available to the U.S. Department of Energy
and its contractors from
Office of Scientific and Technical Information
P.O. Box 62
Oak Ridge, TN 37831
(615) 576-8401

Available to the public from the U.S. Department of Commerce
National Technical Information Service
5285 Port Royal Road
Springfield, VA 22161
(703) 487-4650

Printed in the United States of America.

DISCLM-1.CHP (1-91)

WHC-EP-0500

UC-630

Geology and Hydrology of the 300 Area and Vicinity, Hanford Site, South-Central Washington

D. R. Gaylord
Washington State University
Pullman, Washington

E. P. Poeter
Colorado School of Mines
Golden, Colorado

Date Published
October 1991

Prepared for the U.S. Department of Energy
Office of Environmental Restoration and
Waste Management

Westinghouse Hanford Company P.O. Box 1970 Richland, Washington 99352

Hanford Operations and Engineering Contractor for the
U.S. Department of Energy under Contract DE-AC06-87RL10930

Approved for Public Release

ABSTRACT

The following report summarizes the findings of a joint Washington State University (WSU) and Colorado School of Mines (CSM) research team that investigated the geology and hydrogeology of the 300 Area during FY87-89. The primary goal of this research was to evaluate existing data and identify new and innovative techniques and/or methods necessary to characterize the 300 Area geology and hydrogeology.

Site characterization of the 300 Area demands the close integration of geologic and hydrogeologic research to achieve the most meaningful results. Geologic aspects of the research focused on the identification and analysis of both small- (i.e., sedimentary-textural characteristics) and large-scale (i.e., lithofacies and architectural elements) aquifer heterogeneities and on the derivation of fundamental compositional (i.e., mineralogy and geochemistry) data to assist in identification of marker beds. Hydrogeologic aspects of the research focused on identification and refinement of hydraulically significant, three-dimensional aquifer units termed hydrofacies and on preliminary inverse modeling of ground water flow in the 300 Area. Hydrofacies are fundamental units that will aid in site characterization, development of monitoring programs, and design of remedial action. Inverse modeling is used to improve estimates of the values of hydraulic parameters associated with each hydrofacies.

The WSU/CSM research team identified two major shortcomings of the geologic and hydrogeologic data base for the 300 Area. First the quality of geologic data from 300 Area drilling is far below that necessary to characterize either the geology or hydrogeology of the suprabasalt strata. Almost exclusive use of cable-tool drilling and the absence or near absence of continuous core or intact samples lend little insight into the in situ packing, size, sorting, and arrangement of sedimentary grains composing the aquifer. Second, the limited number of field-scale aquifer tests and the veritable lack of hydraulic testing of discrete aquifer intervals greatly limit attempts to accurately identify basic hydraulic parameters such as hydraulic conductivity and/or specific yield. Without this basic hydraulic data, numerical modeling has limited value.

CONTENTS

1.0 INTRODUCTON AND REGIONAL GEOLOGIC SETTING OF THE HANFORD SITE AND 300 AREA 1
1.1 COLUMBIA RIVER BASALT GROUP 1
1.2 ELLENSBURG FORMATION 2
1.3 SUPRABASALT STRATA 2
1.3.1 Ringold Formation 2
1.3.2 Plio-Pleistocene Unit 3
1.3.3 Early Palouse Soil 4
1.3.4 Pre-Missoula Gravels 4
1.3.5 Hanford Formation 4
1.3.6 Late Quaternary-Recent Surficial Deposits 4
1.4 REGIONAL STRUCTURAL GEOLOGY AND TECTONIC SETTING 5

2.0 HANFORD SITE AND 300 AREA LITHOFACIES AND AQUIFER HETEROGENEITIES 11
2.1 300 AREA STRATIGRAPHY 11
2.2 RINGOLD AND HANFORD FORMATION LITHOFACIES DESCRIPTIONS AND INTERPRETATIONS 12
2.2.1 Ringold Formation Lithofacies 12
2.2.2 Hanford Formation Lithofacies 15

3.0 STRATIGRAPHIC CORRELATION AND COMPOSITIONAL ANALYSES 24
3.1 METHODS 24
3.2 XRF ANALYSES 24
3.3 DISCUSSION OF XRF ANALYSES 25
3.4 ICP/MS--REE ANALYSIS 25

4.0 PRELIMINARY HYDROFACIES DEFINITION IN THE 300 AREA 39
4.1 DEFINITION OF HYDROLOGIC UNITS (HYDROFACIES) 40
4.2 CONSTRUCTION OF HYDROFACIES AND HYDROFACIES MAPS 41
4.3 INTRPRETATION OF HYDROFACIES MAPS 41
4.4 APPLICATION OF HYDROFACIES AND HYDROFACIES MAPS TO NUMERICAL MODELING 42
4.5 ESTIMATION OF HYDRAULIC CONDUCTIVITY OF THE HYDROFACIES 43
4.5.1 Hydraulic Conductivity Values Obtained from Aquifer Testing for Hydrofacies 43
4.5.2 Specific Yield and Hydraulic Conductivity Values Obtained from Hydrofacies Grain Size Analysis 44
4.5.3 Specific Yield 45
4.5.4 Hydraulic Conductivity 45

5.0 PRELIMINARY MODELING OF GROUND WATER FLOW IN THE HANFORD 300 AREA 59
5.1 HYDROGEOLOGIC UNITS USED IN THE MODEL 59
5.2 BOUNDARY CONDITIONS USED IN THE MODEL 60
5.3 MATERIAL PROPERTIES USED IN THE MODEL 60
5.4 MODEL RESULTS 61
5.5 SUMMARY 62

6.0 REFERENCES 75

CONTENTS (Cont)

APPENDIX A PREPARATION OF SAMPLES FOR XRF ANALYSIS A-1

APPENDIX B PROCEDURES FOR ICP/MS ANALYSIS B-1

APPENDIX C PROCEURES FOR ETIMATING HYDRAULIC CONDUCTIVITY AND SPECIFIC YIELD FROM GRAIN SIZE DISTRIBUTION C-1

ATTACHMENT PERMEABILITY THEORY (C. R. McKEE) . . . . . 1 of 8

FIGURES

1-1 Location Map of the Hanford Site, Washington, and the 300 Area . . . 6
1-2 Hanford Site, Washington, and Major Structural and Topographic Features 7
1-3 Basalt and Suprabasalt Strtigraphy at the Hanford Site, Washington 8
1-4 Stratigraphy of Suprabasalt Strata Within and Near the 300 Area 9
1-5 Structural Subprovinces of the Hanford Site and Surrounding Area 10
2-1 Thickly Laminated to Thinly Bedded Mud Exposed Along the White Bluffs and Analogous to Ringold Lithofacies M Elsewhere 19
2-2 Mixed Mud and Sand Exposed Along the White Bluffs and Analogous to Ringold Lithofacies MS Elsewhere 20
2-3 Cross Stratified Sand Exposed Along the White Bluffs and Analogous to Ringold Lithofacies SS Elsewhere 20
2-4 Crudely Stratified Pebble to Cobble Conglomerate Exposed Along the White Bluffs and Analogous to Ringold Lithofacies G Elsewhere 21
2-5 Hanford MS Lithofacies Interstratified with Climbing Ripple Laminated SS and G Lithofacies Exposed in Gravel Pit in Sec. 25, T12N, R28E 21
2-6 Hanford SS Lithofacies Illustrting Plane Bedding and Climbing Ripple Limination 22
2-7 Hanford G. Lithofacies of Cross-Stratified Coarse Pebble to Cobble-Sized Gravel Overlain by and Interstratified Lithofacies SS 22
2-8 Hanford CB and G Lithofacies Displaying High-Angle Foreset Beds Dipping West-Southwest from a Gravel Pit in Sec. 25, T12N, R28E 23
3-1 Location Map of the 300 Area and Borehole Locations 27
3-2 Scatter Diagrams of XRF Data from Glaciofluvial, Upper, and Lower Ringold Formation Strata 28
4-1 Contoured Isopach Map for Gravel Hydrofacies Bodies in the 300 Area (Main) 47
4-2 Contoured Isopach Map for Gravel Hydrofacies Bodies in the 300 Area (Accessory #1) 48
4-3 Contoured Isopach Map for Gravel Hydrofacies Bodies in the 300 Area (Accessory #2) 49

CONTENTS (Cont)

FIGURES (Cont)

4-4 Contoured Isopach Map for Sand Hydrofacies in the 300 Area (Main) 50
4-5 Contoured Isopach Map for Sand Hydrofacies in the 300 Area (Accessory #1) 51
4-6 Contoured Isopach Map for Mud/Silt Hydrofacies in the 300 Area (Main) 52
4-7 Contoured Isopach Map for Mud/Silt Hydrofacies in the 300 Area (Accessory #1) 53
4-8 Contoured Isopach Map for Mud/Silt Hydrofacies in the 300 Area (Accessory #2) 54
4-9 Hydrofacies Representative for Numerical Modeling 55
5-1 Hanford 300 Area Model Hydrofacies Maps/Grids [(a) through (j)] . . . 63
5-2 Example Geologic Cross Section of 300 Area 68
5-3a Example Water Table Map Used to Model 300 Area - February 16, 1977 69
5-3b Example Water Table Map Used to Model 300 Area - May 20, 1977 70
5-3c Example Water Table Map Used to Model 300 Area - May 27, 1977 71
5-4 Flow Field Based on Aquifer Head Map Prepared by Lindberg and Bond (1979) 72
5-5 Flow Field Based on Initial Estimates of Hydraulic Conductivity and Heads at Boundaries 73
5-6 Flow Field Based on Inverse Estimates of Hydraulic Conductivity . . . 74

TABLES

3-1 XRF Data from Glaciofluvial, Upper Ringold Formation, and Lower Ringold Formation Samples 37
3-2 Quantitative Results of ICP/MS Analyses 38
4-1 Hydraulic Conductivities for the Interpreted Hydrofacies as Estimated from Aquifer Tests 56
4-2 Hydrofacies Specific Yield Values Estimated from Grain Size Data . . 57
4-3 Hydrofacies Hydraulic Conductivity Values Estimated from Grain Size Data 58

1.0 INTRODUCTION AND REGIONAL GEOLOGIC SETTING OF THE HANFORD SITE AND 300 AREA

An accurate understanding of the hydrogeologic setting of the 300 Area of the Hanford Site is necessary for the development and implementation of waste remediation strategies. As part of an effort to better understand the hydrogeology of the 300 Area, a joint Washington State University (WSU) and Colorado School of Mines (CSM) research team, under the direction of the Pacific Northwest Laboratory (PNL), developed a hydrostratigraphic model for the 300 Area. This work, conducted from FY 87 to FY 89, used lithologic and hydrologic information available at the time. The following report summarizes the results of the WSU-CSM research effort. Data and insights gained into the hydrogeology of the 300 Area since the end of the WSU/CSM effort are not incorporated into this report.

Since FY 89, extensive characterization efforts have been initiated by Westinghouse Hanford Company (Westinghouse Hanford) as part of the 300-FF-5 Operable Unit remedial investigation. With the addition of 19 new groundwater wells the hydrogeology of the 300 Area is being reevaluated. Results of this effort will be described as part of the Phase I remedial investigation report.

Ground water and contaminant movement across the 300 Area (Figure 1-1) reflect both regional and local geologic and hydrogeologic variations at the Hanford Site. The Hanford Site is located in the Pasco Basin, a topographic and structural basin situated in the northern portion of the Columbia Plateau (Figure 1-2). The Pasco Basin is bounded on the south by the Rattlesnake Hills and Horse Heaven Plateau, on the west by the Umtanum and Yakima ridges, on the north by the Saddle Mountains, and on the east by the Jackass Monocline. Gable Mountain and Gable Butte effectively divide the Pasco Basin into northern and southern halves while the prominent White Bluffs (exposed along the eastern and northern banks of the Columbia River) bisect the basin and cut across the northern third of the Hanford Site.

The 300 Area is located along the southeastern margin of the Hanford Site, adjacent to the Columbia River (Figure 1-2). This area is similar to much of the rest of the site which (for purposes of ground water studies) consists of a two-tiered stratigraphy of basalt/basalt-related volcanic and sedimentary rocks and suprabasalt sedimentary deposits. The principal units at the Hanford Site are (from oldest to youngest) the: Miocene Columbia River Basalt Group, Miocene Ellensburg Formation, Miocene-Pliocene Ringold Formation, informally defined Plio-Pleistocene clastic sedimentary unit, Pleistocene early "Palouse" soil, Pleistocene pre-Missoula gravel, the Pleistocene Hanford formation, and Holocene eolian deposits (Figure 1-3). The CRBG and Ellensburg Formation are included within the basalt/basalt-related deposits while all others are included within suprabasalt deposits.

1.1 COLUMBIA RIVER BASALT GROUP

The Columbia River Basalt Group (CRBG) is characterized by a thick sequence of tholeiitic, continental flood basalts of Miocene age. These flows cover an area of more than 63,000 mi^2 (163,700 km^2) in Washington, Oregon, and Idaho, and have an estimated volume of about 40,800 mi^3 (174,356 km^3) (Tolan et al. 1989). Isotopic age determinations indicate basalt flows were erupted

from approximately 17 to 6 Ma, with >98% of this volume extruded between 17 and 14.5 Ma (Reidel et al. 1989a).

The Columbia River basalt flows were erupted from north to northwest-trending fissures or linear vent systems in north-central and northeastern Oregon, eastern Washington, and Western Idaho (Swanson et al. 1979). The CRBG is formally subdivided into five formations (from oldest to youngest): Imnaha Basalt, Picture Gorge Basalt, Grande Ronde Basalt, Wanapum Basalt, and Saddle Mountains Basalt. Of these, only the Picture Gorge Basalt is not known to be present in the Pasco Basin. The Saddle Mountains Basalt is divisible into the Ice Harbor, Elephant Mountain, Pomona, Esquatzel, Asotin, Wilbur Creek, and Umatilla members and forms the uppermost basalt across most of the Pasco Basin. The Elephant Mountain Member is the uppermost flow beneath most of the Hanford Site except north of the 200 Areas where erosion has removed all younger flows down to the Umatilla Member and near the 300 Area where the top-most unit is the Ice Harbor Basalt. Erosion also has exposed the Wanapum and Grande Ronde basalts on the anticlinal ridge crests bounding the Pasco Basin.

1.2 ELLENSBURG FORMATION

The Ellensburg Formation consists of all sedimentary units intercalated with the basalt flows of the CRBG. Strata of the Ellensburg Formation can be characterized as either volcaniclastic or siliciclastic rocks. The volcaniclastic rocks consist mainly of pyroclastic airfall and reworked pyroclastic deposits derived from volcanic terrains west of the Columbia Plateau. Siliciclastic strata in the Ellensburg Formation consist of reworked siliciclastic, plutonic, and metamorphic detritus derived from the Rocky Mountain and Okanogan Highland sources. These two lithologies occur as both distinct and mixed strata in the Pasco Basin. A detailed discussion of the Ellensburg Formation near the Hanford Site is provided by Reidel and Fecht (1981). Smith et al. (1989) provide a discussion of Ellensburg age-equivalent units on and adjacent to the Columbia Plateau.

1.3 SUPRABASALT STRATA

Numerous researchers have investigated both local and regional characteristics of the Hanford Site suprabasalt strata (e.g., Grollier and Bingham 1971; 1978; Tallman et al. 1979; Lindberg and Bond 1979; Myers and Price 1979; PSPL 1982; Bjornstad 1985; Fecht et al. 1985; DOE 1988; Lindsey et al. 1989; Lindsey and Gaylord 1990; Lindsey 1991). As a result, much is known in general about the history of these deposits. However, the general lack of readily laterally extensive marker beds often has complicated correlation of suprabasalt strata onsite and offsite.

The suprabasalt sedimentary sequence at the Hanford Site reaches a maximum of nearly 750 ft (230 m) thick in the west-central Cold Creek syncline and pinches out against the Saddle Mountains anticline, Gable Mountain/Umtanum Ridge anticline, Yakima Ridge anticline, and Rattlesnake Hills anticline. The suprabasalt sediments are dominated by the laterally extensive, late Miocene to Pliocene Ringold Formation and the Pleistocene Hanford formation. The informally defined Plio-Pleistocene unit, the early Palouse soil, and pre-Missoula gravels generally are laterally restricted and comprise the rest of the suprabasalt sequence.

Suprabasalt strata in the 300 Area are subdivided into (in ascending order) the Ringold Formation, Hanford formation (informal), and unnamed (younger) alluvial and eolian sediments (Figure 1-4).

1.3.1 Ringold Formation

Recent studies of the Ringold Formation in the Pasco Basin and Hanford Site indicate that significant, previously undocumented stratigraphic variations exist (Lindsey and Gaylord 1990; Lindsey 1991). The Ringold Formation at the Hanford Site is up to 600 ft (185 m) thick in the deepest part of the Cold Creek syncline south of the 200 West Area and 560 ft (170 m) thick in the western Wahluke syncline near the 100 B Area. Ringold strata pinch out against the Gable Mountain, Yakima Ridge, Saddle Mountains, and Rattlesnake Mountain anticlines and largely are absent in the northern and northeastern parts of the 200 East Area and adjacent areas to the north in the vicinity of West Pond.

The Ringold Formation consists of semi-indurated clay, silt, pedogenic mud, fine- to coarse-grained sand, and granule to cobble gravel that usually are divided into: (1) gravel, sand, and paleosols of the basal unit; (2) clay and silt of the lower unit; (3) gravel of the middle unit; (4) mud and lesser sand of the upper unit; and (5) basalt detritus of the fanglomerate unit (Newcomb 1958; Newcomb et al. 1972; Myers and Price 1979; Bjornstad 1984; DOE 1988). Ringold strata also have been divided on the basis of facies types (Tallman et al. 1981) and fining-upwards sequences (PSPL 1982). All of these strati-graphic divisions are of limited use either because they are too generalized to account for marked local stratigraphic variations or are defined in detail only for small areas (Lindsey and Gaylord 1990).

Ringold Formation strata originally were considered to be Pleistocene-aged (Merriam and Buwalda 1917; Newcomb 1958; Grollier and Bingham 1971; Newcomb et al. 1972). However, subsequent paleontologic, paleomagnetic, and palynologic studies have demonstrated an older age for the Ringold. Gustafson (1973; 1985) established a Pliocene age for upper Ringold strata from paleontologic evidence collected along the White Bluffs. Packer and Johnson (1979) suggested a Miocene to Pliocene age based on paleomagnetic data from Ringold exposures and drill core, while Leopold and Nickman (1981) determined a Miocene age for the oldest Ringold strata on the basis of pollen samples collected near the base of the Ringold Formation. Fecht et al. (1985) established a maximum age of 8.5 Ma for the Ringold Formation from potassium-argon whole-rock dating of the underlying Miocene basalt (McKee et al. 1977) and a minimum age of 3.9 Ma on the basis of paleomagnetic data and vertebrate fossil evidence.

Exposures of the Ringold Formation are limited because of an extensive Pleistocene-Holocene sedimentary cover and erosion by catastrophic, proglacial Pleistocene floods. However, informative outcrops exist: (1) on the White Bluffs across the Columbia River east and north of the Hanford Site; (2) in ravines and coulees between Wallula Gap and Moses Lake, Washington; and (3) near prominent basaltic uplifts including Rattlesnake Mountain, the Saddle Mountains, Gable Mountain, and the Frenchman Hills (Figure 1-1).

1.3.2 Plio-Pleistocene Unit

The laterally discontinuous Plio-Pleistocene unit unconformably overlies the Ringold Formation in the western Cold Creek syncline in the vicinity of 200 West Area (DOE 1988). This unit is up to 82 ft (25 m) thick and is divided into two facies: (1) basaltic detritus and (2) pedogenic calcrete. One or both facies may be present locally. The calcrete facies generally consists of interfingering carbonate-rich silt and sand and carbonate-poor silt and sand. The basaltic detritus facies consists of weathered and unweathered basaltic gravels deposited as locally derived slope wash, colluvium, and alluvium. The Plio-Pleistocene unit appears to be correlative to other alluvial and pedogenic deposits found near the base of the ridges bounding the Pasco Basin on the north, west, and south.

1.3.3 Early Palouse Soil

The early Palouse soil consists of up to 65 ft (20 m) of silt and fine-grained sand that overlies the Plio-Pleistocene unit in the western Cold Creek syncline near 200 West Area (Tallman et al. 1981; Bjornstad 1984; DOE 1988). Strata comprising the early Palouse soil are very loess-like in character and interpreted to be of eolian origin. The unit is differentiated from younger slackwater flood deposits (of the Hanford formation) by greater calcium carbonate content, massive structure in core, and high natural gamma response in geophysical logs (Bjornstad 1984). The upper contact of the unit is poorly defined and may grade upsection into the lower part of the Hanford formation.

1.3.4 Pre-Missoula Gravels

Pre-Missoula gravels are deposits of quartzose to gneissic clast-support pebble to cobble gravel with a matrix of quartzo-feldspathic sand that underlies the Hanford formation in the east-central Cold Creek syncline and at the east end of the Gable Mountain anticline east and south of 200 East Area (Lindsey 1991). These gravels, called the pre-Missoula gravels (PSPL 1982), are up to 82 ft (25 m) thick, contain less basalt than underlying Ringold gravels and overlying Hanford formation deposits, have a distinctive white or bleached color, and sharply truncate underlying strata. The nature of the contact between the pre-Missoula gravels and overlying Hanford formation is not clear. It also is not clear whether the pre-Missoula gravels overlie or interfinger with the early Palouse soil and Plio-Pleistocene unit.

1.3.5 Hanford Formation

The informally defined Hanford formation is composed dominantly of uncemented pebble to boulder conglomerate and less commonly of fine- to coarse-grained sand, silt, and silty clay. The bulk of these sediments were derived during Pleistocene Missoula floods though some also are attributed to pre-Missoula flood episodes (PSPL 1982). Coarse-grained deposits of the Pasco Gravels dominate the sedimentary sequence near and adjacent to the 300 Area. Unfortunately, the criteria that can be used to identify the Pasco flood gravels from the underlying pre-Missoula gravels in the geologic drill logs are poorly defined making differentiation of these units ambiguous. Bjornstad and Fecht (1989) report that the earliest of the Pleistocene floods that

affected the Hanford area occurred more than 800,000 years ago. The most recent proglacial, Missoula flood was approximately 13,000 years ago (Mullineaux et al. 1978).

Extensive scouring associated with the Missoula flood deposits was responsible for the erosion of an approximately north-south oriented paleo-channel that cuts across the western side of the 300 Area (Lindberg and Bond 1979). This channel, which was filled with coarse-grained, dominantly gravel detritus during Hanford time, merges with the modern Columbia River north of and at the extreme southern margin of the 300 Area.

1.3.6 Late Quaternary-Recent Surficial Deposits

Late Quaternary (dominantly Holocene) surficial deposits consist of silt, sand, and gravel that forms a thin (<16 ft [5 m]), discontinuous veneer across much of the Hanford Site. These sediments resulted from a complex mixture of eolian and alluvial activity.

1.4 REGIONAL STRUCTURAL GEOLOGY AND TECTONIC SETTING

The Columbia Plateau is a part of the North American continental plate and is situated in the back-arc east of the Cascade Range. The plateau is bound on the north by the Okanogan Highlands, on the east by the Northern Rocky Mountains and Idaho Batholith, and on the south by the High Lava Plains and Snake River Plain.

The plateau can be divided into three informal structural subprovinces (Figure 1-5): Blue Mountains, Palouse, and Yakima Fold Belt (Tolan and Reidel 1989). These structural subprovinces are delineated on the basis of their structural fabric, unlike the physiographic provinces that are defined on the basis of landforms. The Hanford Site is located near the junction of the Yakima Fold Belt and the Palouse subprovinces.

The Yakima Fold Belt is characterized by a series of segmented, narrow, asymmetric anticlines that have wavelengths between 3 and 19 mi (5 and 30 km) and amplitudes commonly <0.6 mi (<1 km) (Reidel et al. 1989b). Prior to deposition of the suprabasalt sediments, the Pasco Basin was a focal point for the accumulation of nearly 2 mi (3.2 km) of Miocene basalt (Hooper 1982). Deformation of these basalts began near the end of the Miocene and continued into at least the early Pliocene. This deformation led to the development of the anticlinal Rattlesnake Hills, Yakima Ridge, Umtanum Ridge, and Saddle Mountains that border the Pasco Basin on the south, west, and north (Myers and Price 1979) (Figure 1-2). In addition, the Cold Creek and Pasco synclines and the Gable Mountain anticline formed within the basin during this deformation. All three structures cross the Hanford Site. Deformation of the Yakima Fold Belt occurred under north-south compression and was probably contemporaneous with the eruption of the basalt flows (Reidel 1984; Reidel et al. 1989b). The fold belt was enlarging during the eruption of the CRBG and continued to enlarge through the Pliocene, into the Pleistocene, and perhaps to the present. Structural deformation seems to have been largely coeval with supra-basalt sedimentation, so most of these strata are similarly deformed or structurally tilted. The 300 Area lies along the axial trend of the Cold Creek syncline and strata in the area are essentially flat lying.

Figure 1-1. Location Map of the Hanford Site, Washington.

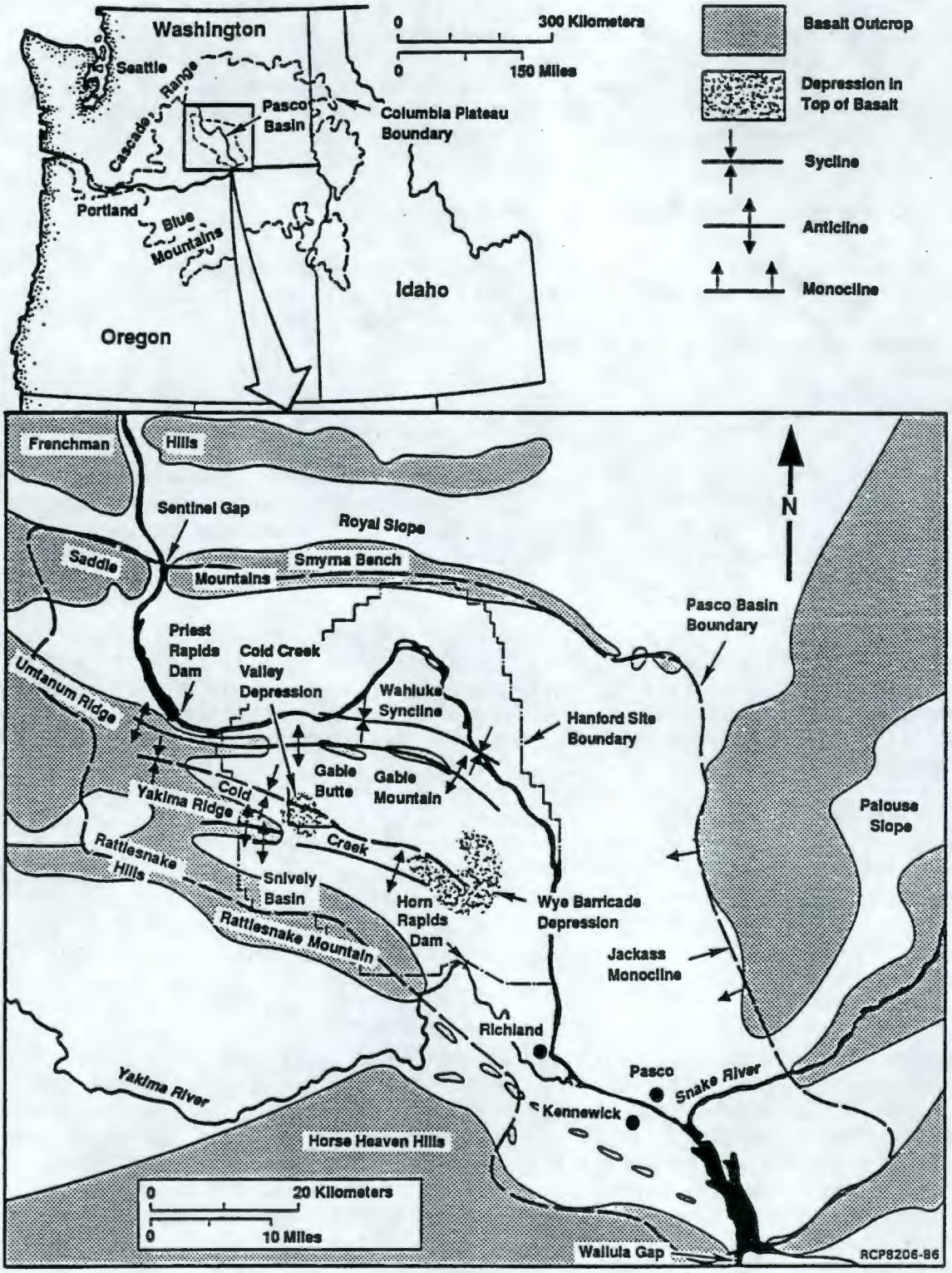

PS-90-245

Figure 1-2. Hanford Site, Washington, and Major Structural and Topographic Features.

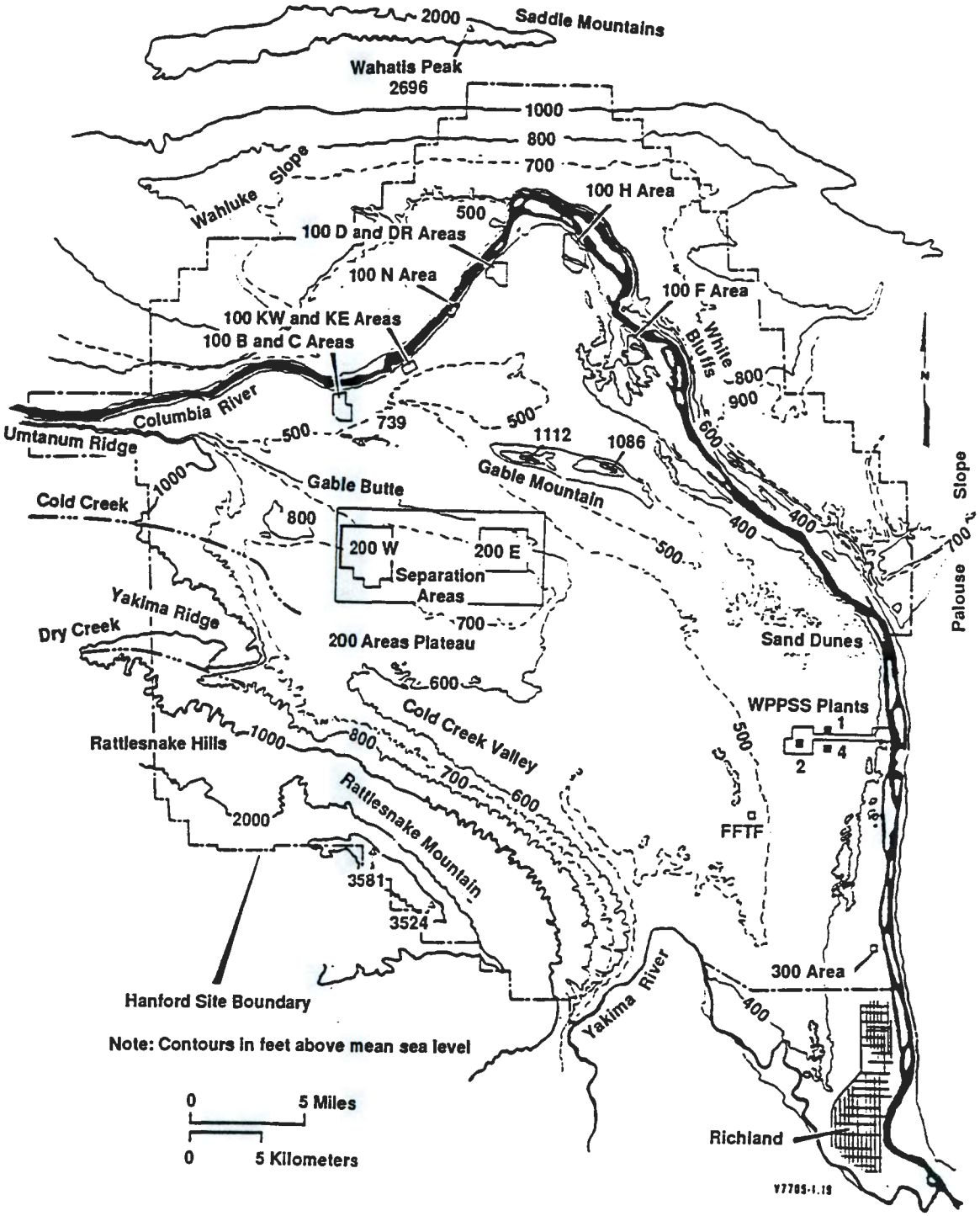

PS-90-250

Figure 1-3. Basalt and Suprabasalt Stratigraphy at the Hanford Site, Washington.

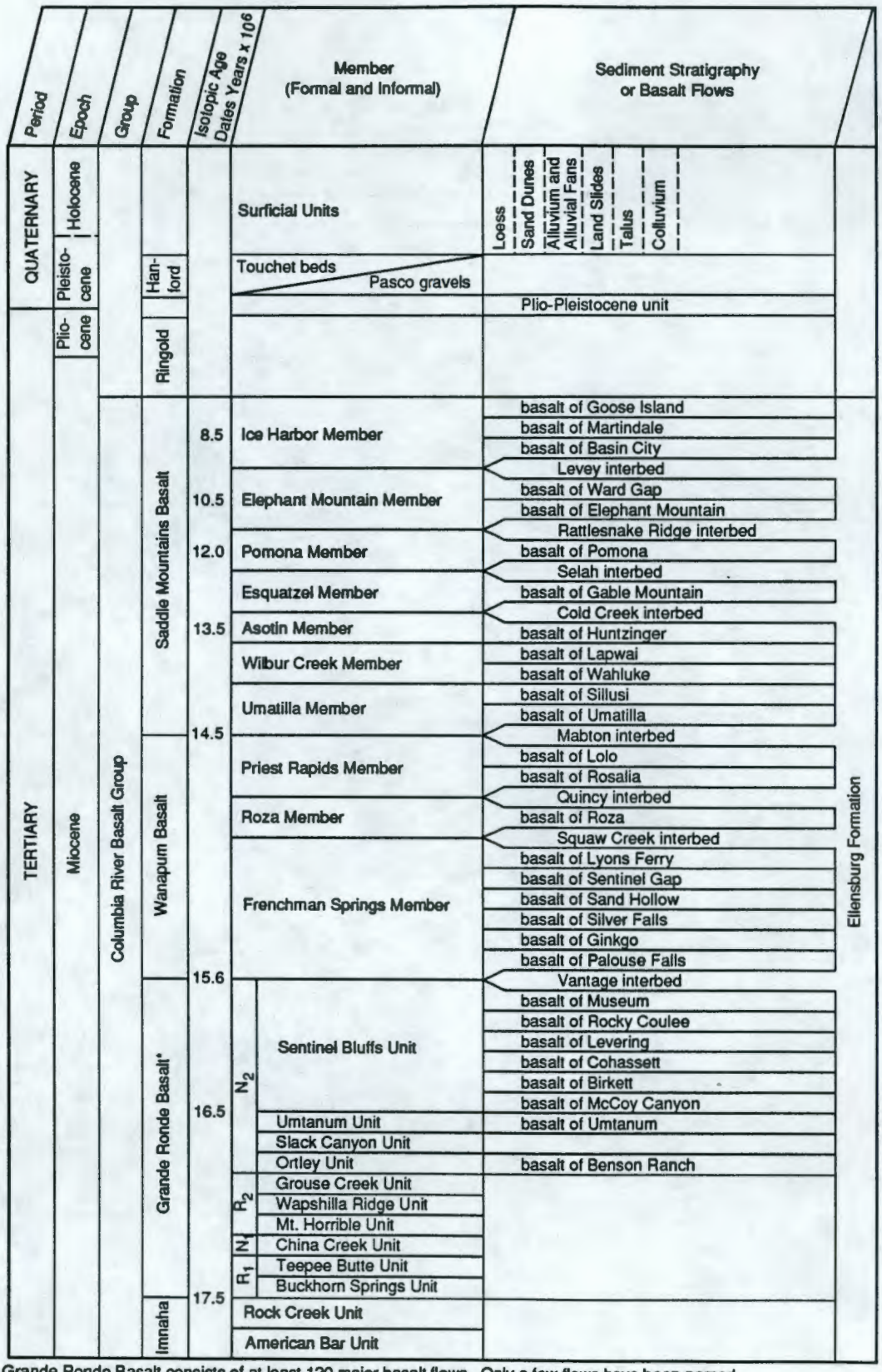

*The Grande Ronde Basalt consists of at least 120 major basalt flows. Only a few flows have been named. N_2, R_2, N_1 and R_1 are magnetostratigraphic units.

H9102029.6

Figure 1-4. Stratigraphy of Suprabasalt Strata Within and Near the 300 Area.

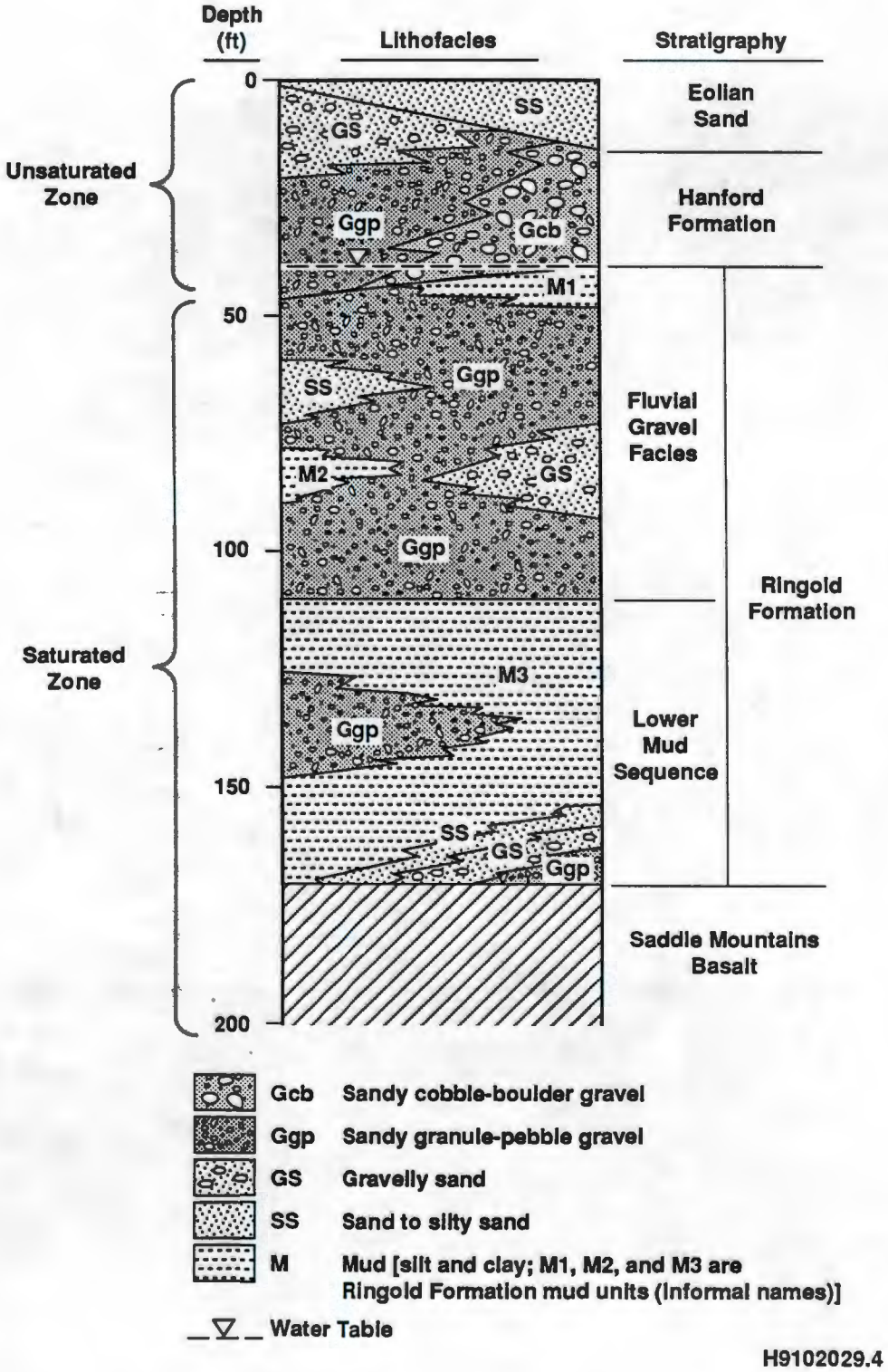

Figure 1-5. Structural Subprovinces of the Hanford Site and Surrounding Area.

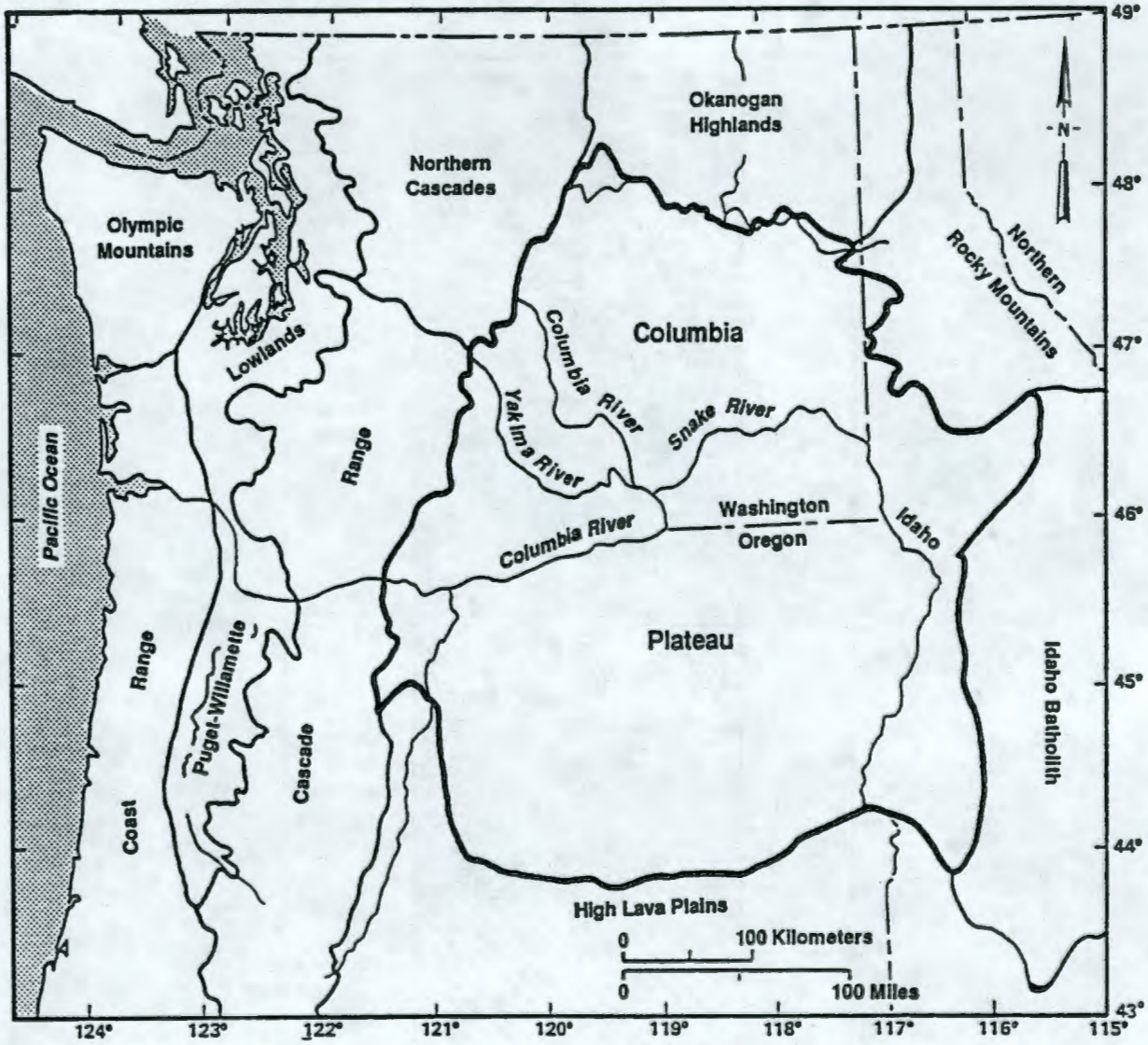

PS8609-193
PS-90-248

2.0 HANFORD SITE AND 300 AREA LITHOFACIES AND AQUIFER HETEROGENEITIES

Characterization studies of the geology and hydrogeology of the Hanford Site (including the 300 Area) have demonstrated that aquifer heterogeneities in the suprabasalt strata are best constrained using lithofacies (see also Lindsey et al. 1989; Lindsey and Gaylord 1990; Lindsey 1991). A lithofacies approach to stratigraphic characterization has been applied to the Ringold Formation offsite by Grollier and Bingham (1971; 1978) and can be applied to the Hanford formation, but has not (until recently) received very extensive acceptance or use for onsite geologic/hydrogeologic studies.

This chapter summarizes Ringold Formation lithofacies described by Lindsey et al. (1989), Lindsey and Gaylord (1990), Lindsey (1991) and Hanford formation lithofacies observed by the authors. In general, similar lithofacies occur in both the Ringold and Hanford strata, though the Hanford formation tends to be much more coarse grained. In addition, Ringold strata contain a thicker, better compacted, better cemented, and more extensive sequence of fine-grained lithofacies than Hanford formation sediments.

2.1 300 AREA STRATIGRAPHY

Suprabasalt strata in the 300 Area consist of the 95- to 145-ft (29- to 44-m) thick Miocene/Pliocene Ringold Formation, the 80- to 115-ft (24- to 35-m) thick, Pleistocene Hanford formation, and 0- to 20-ft (0- to 7-m) thick Holocene-Recent eolian deposits (Figure 1-4). Ringold strata in the 300 Area are composed of complexly interstratified, fluvially derived, fine- and coarse-grained lithofacies. Fine-grained lithofacies are composed dominantly of interstratified mud, silt, and sand, and are concentrated in a sequence of laterally variable beds and lenses. The lowermost of these deposits is a 15- to 65-ft (4.5- to 20-m) thick sequence of fine-grained lithofacies that overlap both flood basalt and granule to cobble gravel deposits that discontinuously cap the flood basalt (Figure 1-4). Deposits from this thick, fine-grained lithofacies apparently extend across the 300 Area, but are nearly absent in the vicinity of borehole 300-1-18c where mixed mud and sand deposits cap gravels. Sediments from the upper strata of the Ringold Formation within and near the 300 Area are characterized by complexly interstratified beds and lenses of sand and gravel.

Hanford formation strata within the 300 Area are composed dominantly of proglacial and fluvial sand and coarse gravel beds. These deposits were incised episodically during catastrophic, flood-induced scour and long-term, stream-induced downcutting, making individual beds difficult to trace laterally. Ringold Formation deposits are generally better cemented, calicified, and sorted than those from the Hanford formation. Ringold strata typically contain a lower percentage of angular basaltic detritus than Hanford formation deposits.

2.2 RINGOLD AND HANFORD FORMATION LITHOFACIES DESCRIPTIONS AND INTERPRETATIONS

The following sections summarize the lithofacies analysis presented by Lindsey et al. (1989) and Lindsey and Gaylord (1990) and include the recent revisions of Lindsey (1991).

The lithofacies codes used for the Ringold Formation and Hanford formation are loosely based on codes introduced by Miall (1977; 1978) and Rust (1978) for fluvial sediments. However, the limited availability of intact samples and lack of clear correlation between drill cuttings and either intact samples or analog outcrops at and near the Hanford Site did not permit differentiation of lithofacies beyond a simple texturally based system. This reliance on less-than-optimum subsurface data (the only data available) as well as the typically long distances between boreholes at the Hanford Site (often thousands of feet) limited the ability either to identify or reconstruct depositional processes or to reconstruct major depositional trends and/or large-scale architectural elements such as described by Miall (1985; 1987).

Lindsey et al. (1989) and Lindsey and Gaylord (1990) identified six lithofacies types which occur within the Hanford Site suprabasalt sequence. These lithofacies are: (1) mud (M); (2) mud and sand (MS); (3) sand (SS); (4) sandy gravel (SG); (5) granule and pebble (G); and (6) cobble and boulder (CB) lithofacies. This six-tiered group of lithofacies has since been reduced to five by Lindsey (1991) who combined the sandy gravel (SG) and granule and pebble (G) lithofacies into a single gravel (G) lithofacies.

2.2.1 Ringold Formation Lithofacies

Ringold Formation sedimentary deposits within and near the 300 Area include representatives only of the mud (M), mud and sand (MS), sand (SS), gravel (G) lithofacies. Cobble and boulder deposits occur only in post-Ringold strata in the 300 Area.

2.2.1.1 Ringold Lithofacies M: MUD. Lithofacies M (Figure 2-1) consists of massive to laminated gray, brown, olive, and blue clay and silt. Beds are a few inches (centimeters) to tens of feet (meters) thick and average <30 ft (<10 m) thick. Sand comprises up to 10% of this lithofacies and occurs as thin (<90-in. [<30-cm] thick) lenticular interbeds and as intermixed grains. Feet- (meters-) thick paleosols, thin (<25-in. [<10-cm] thick) ash beds, and partially decomposed wood fragments are common in available intact samples and analog exposures of this lithofacies in White Bluffs. Mud lithofacies tend to be discontinuous (Figure 2-1) and commonly grade down into mud-sand (MS) and sand (SS) lithofacies; they are most commonly overlain by gravel (G) lithofacies.

The fine grain size and generally good sorting indicate that this facies resulted primarily from suspension deposition in standing or slow-moving waters, probably in overbank and/or possibly backwater swamp settings such as described for texturally similar lithofacies by Miall (1977; 1978). Abundant paleosols are consistent with this interpretation and indicate episodic subaerial exposure. The laminated clay and silt of this lithofacies have been interpreted as lacustrine by Bjornstad (1985). Thin sand beds are consistent

with intermittent tractional transport of ripples and sheet sands (Miall 1977; 1978), probably during flood events. Lindsey (1991) has interpreted Ringold Formation deposits similar to lithofacies M as having both fluvial overbank and lacustrine origins.

2.2.1.2 Ringold Lithofacies MS: MUD AND SAND. Lithofacies MS (Figure 2-2) consists of massive to interlaminated gray, brown, olive, and rarely blue mud and sand. Beds generally are a few inches (centimeters) thick but combine to form sequences up to 30 ft (10 m) thick. Sand contents range from 20 to <80% and average 50%. Climbing ripples and normal grading in sets 8 to 16 in. (20 to 40 cm) thick are common in beds of analog fine-grained sands exposed along the White Bluffs. Feet- (meters-) thick paleosols, thin (<25-in. [<10-cm] thick) ash beds, and partially decomposed wood fragments are common in available intact samples and analog surface exposures; however, like in lithofacies M, they are difficult to identify in borehole cuttings. The MS lithofacies tend to be discontinuous. Deposits of lithofacies MS commonly gradationally overlie sand lithofacies are gradationally overlain by lithofacies M, and frequently are truncated and overlain by deposits of the G lithofacies.

The mixed textural character of lithofacies MS implies that it resulted from episodic input of coarse-grained detritus transported into standing or slow moving waters by intermittent traction and possibly flood currents in overbank settings. Miall (1977; 1978) and Galloway (1981) relate texturally similar, fluvially derived lithofacies to overbank deposition. The relatively high concentration of sand in this lithofacies as compared to that in the M lithofacies suggests a more proximal location to the main stream. Pedogenic modification of lithofacies MS also is consistent with a floodplain interpretation (Miall 1977; 1978). However, the ripple laminated and normally graded fine sands in the White Bluffs analog exposures probably reflect episodic and rapid accumulation of sediment in deltaic and lacustrine settings. Lithofacies MS has characteristics which closely match those described by Lindsey (1991) for Ringold lacustrine and deltaic deposits (part of his lacustrine facies association).

2.2.1.3 Ringold Lithofacies SS: SAND. Lithofacies SS (Figure 2-3) consists of gray, olive, and less commonly, tan and brown, fine- to coarse-grained, moderately to poorly sorted, subangular to subrounded, unconsolidated to weakly cemented sand. Up to 20% of this lithofacies may be composed of mud, granules, and pebbles, most commonly preserved as beds and lenses. Available intact samples and analog outcroppings of SS lithofacies display massive bedding, horizontal stratification, and planar to trough cross-stratification in 2-in. to 3-ft (5-cm to 1-m) thick tabular sets. Total thicknesses of lithofacies SS are generally <25 in. (<10 m). Deposits of the SS lithofacies commonly grade upwards into lithofacies M and MS, and grade downwards into lithofacies G. Lithofacies SS also sharply truncates lithofacies M and MS and is, in turn, truncated by lithofacies G. Sand detritus dominantly is composed of quartz, feldspar, and mica grains, with lesser granitic, basaltic, and gneissic lithic fragments.

The coarse-grain sizes, and primary sedimentary structures are consistent with migration and aggradation of ripples, sand-waves, and plane beds (Miall 1977; 1978). The discontinuous nature of SS lithofacies suggests a channel-like origin for these deposits. Deposition of the SS lithofacies is inferred to have been confined to trunk and tributary channels, probably

during normal stream flow and during the waning stages of floods when these sediments were deposited atop coarser-grained, gravel-dominated lithofacies. This lithofacies has similar characteristics to the deposits Lindsey (1991) placed within a Ringold fluvial sand facies association. Lindsey suggested that the quartzo-feldspathic sands comprising this association were deposited in wide, shallow channels incised into a muddy floodplain. The quartzo-feldspathic nature of the sand indicates these were sourced dominantly from granitic, gneissic, and quartz-rich terrains, most likely those found along the northern and eastern periphery of the Columbia Plateau. Sand-sized basaltic lithic fragments were derived from erosion of the CRBG within the plateau. These findings are consistent with those previously described by Fecht et al. (1985).

2.2.1.4 Ringold Lithofacies G: GRAVEL. Lithofacies G (Figure 2-4) consists dominantly of light to dark gray, poorly sorted, unconsolidated to poorly cemented, matrix- and clast-supported sandy, granule- to pebble-sized gravel. Gravel-sized detritus makes up >30% of lithofacies G; sand is very fine- to very coarse-grained, occurs as matrix material and in lenses and beds up to 3 ft (1 m) thick. Limited outcrops of apparently analogous lithofacies G strata (Figure 2-4) occur in 3- to 60-ft (1- to 20-m) thick beds that exhibit large-scale trough and planar cross-strata, clast imbrication, feet-(meters-) wide scours, and bar-shaped lenticular bodies. Cobble lag concentrations also are common. Gravel lithofacies deposits frequently are overlain gradationally by lithofacies M and MS and are sharply to gradationally overlain by lithofacies SS. Gravels are dominantly lithic and composed of quartzitic, basaltic, granitic, gneissic, and porphyritic volcanic clasts; sands generally are quartzo-feldspathic.

Sediments of the G lithofacies are interpreted as mixed main channel and tributary channel deposits. Deposition of cross-stratified, stratified, and imbricated gravel reflect aggradation of transverse and longitudinal gravel bars and dunes (Miall 1977; 1978). The interstratification of sand and gravel as well as the incorporation of sandy detritus in matrix material and in lenses is common to braid plain systems that experience widely fluctuating currents (Rust and Koster 1984). Episodically strong stream currents are implied by the concentrations of pebble-sized gravel within this lithofacies. Lindsey (1991) included deposits of lithofacies G within his fluvial gravel facies association. Lindsey attributed the depositional character of the often sand-rich gravels to accumulation in wide, shallow, shifting channels. The mixed quartzo-feldspathic, granitic, and volcanic lithic compositions of the gravel indicates a mixed meta-sedimentary, crystalline, volcanic provenance for the gravel as earlier suggested by Fecht et al. (1985). Gravel clasts were derived from erosion of Belt Series in eastern Washington, northern Idaho, and western Montana, granitic and gneissic terrains in eastern and northern Washington and northern Idaho, granitic and volcanic terrains in central and northern Washington (Okanogan Highlands and North Cascades) and from metasedimentary and metavolcanic terrains in west-central Idaho and northeastern Oregon (Seven Devils).

2.2.2 Hanford Formation Lithofacies

The Hanford formation on the Hanford Site consists of silt, fine- to coarse-grained sand, and pebble-to-boulder gravel. Hanford formation strata are subdivided into five principal lithofacies: (1) mud (M); (2) mud and sand

(MS); (3) sand (SS); (4) gravel (G); and (5) cobble and boulder (CB) lithofacies. The Hanford formation also is commonly divided into two informal members: the Pasco Gravels and the Touchet Beds (Myers and Price 1979; Tallman et al. 1981; Fecht et al. 1985; DOE 1988). The Pasco Gravels generally correspond with more coarse-grained lithofacies (i.e., G and CB lithofacies) while the Touchet Beds correspond with fine-grained lithofacies (i.e., M, MS, and SS lithofacies). Hanford formation deposits are thickest on the Cold Creek bar in the vicinity of 200 West and 200 East areas where it is up to 210 ft (64 m) thick (Delaney et al. 1991). Hanford deposits are absent from surfaces exceeding approximately 1,180 ft (361 m) above sea level (Delaney et al. 1991).

No significant M lithofacies were identified from either borehole geologic drill logs or outcrops within the 300 Area and thus are not included in the discussion. No significant deposits of the MS lithofacies were identified from exposures immediately within or adjacent to the 300 Area either. However, Touchet Beds within this lithofacies were described from near the Hanford Site and are described here because of their possible inclusion as thin 300 Area deposits. Note that the transport and depositional histories for the five possible Hanford formation lithofacies are generally consistent with those previously outlined for Ringold Formation lithofacies in that they largely represent fluvial transport and deposition. However, unlike the Ringold Formation deposits, the Hanford formation sequence was deposited during catastrophic floods. These flood deposits tended to accumulate in subparallel tracts reflecting: (1) main flood channel (Pasco Gravels); (2) slackwater/backwater (Touchet Beds); and (3) deposits transitional deposits between main flood channel and slackwater/backwater sediments.

2.2.2.1 Hanford Lithofacies MS: MUD AND SAND. Lithofacies MS (Figure 2-5), as noted above is either absent from or present only in thin beds within the 300 Area. If present, deposits of this lithofacies are inferred to be similar to the Touchet Beds exposed in various stream cuts and gravel pits near and adjacent to the Hanford Site (Figure 2-5). These analog MS deposits are subtly different from the Ringold Formation MS lithofacies described in the previous section. Ringold Formation MS lithofacies at the White Bluffs are generally lighter in color, better cemented and are more laterally continuous than the Hanford MS lithofacies. Paleosols, ash beds, and decomposed wood fragments are common in Ringold MS lithofacies but are less frequently observed in the Hanford formation analog MS lithofacies. Bedding thicknesses in MS lithofacies of the Ringold Formation are often much greater than in the Hanford MS lithofacies and can be from a few inches (centimeters) to a few feet (meters) thick. In spite of these differences, the Ringold and Hanford MS lithofacies do have some similarities. For instance, the range of bedding thicknesses in the Ringold MS lithofacies (1 to 12 in. [2 to 30 cm] thick) overlaps with the most common range of Hanford MS lithofacies bedding thicknesses and normally graded sets are common in both Ringold and Hanford MS lithofacies. However, set thicknesses in the Ringold range tend to be thicker (from 8 to 16 in. [20 to 40 cm]) than in the Hanford MS lithofacies (1 to 12 in. [2 to 30 cm]).

The mixed textural character of this lithofacies and assumed association with Touchet Bed deposition suggest that these are slackwater accumulations. It is also likely that these deposits later were modified by local streams and tributaries and reflect the episodic input of coarse-grained detritus and fine-grained detritus into standing or slow moving waters by intermittent

traction and possibly flood currents in overbank settings as suggested for texturally similar deposits by Miall (1977; 1978) and Rust (1978).

2.2.2.2 Hanford Lithofacies SS: SAND. Sand lithofacies comprise only a minor percentage of the 300 Area Hanford formation deposits. Interpretation of geologic and geophysical borehole logs indicate that Hanford formation SS lithofacies in the 300 Area are concentrated in the southern part of the area and are either subordinate or intermixed with coarse-grained gravel-dominated deposits. SS lithofacies exposed at the Ringold Flats gravel pit (Sec 25, T12N, R28E) are presumed analog deposits of SS lithofacies buried beneath the 300 Area (Figure 2-6). These analog sediments are fine- to coarse-grained, moderately sorted, subangular to subrounded, and unconsolidated, with plane stratification and low-angle planar cross-stratification. SS lithofacies in the Hanford formation are composed of from 30 to 70% basalt clasts with the remainder composed of quartzo-feldspathic detritus and minor volcanolithic clasts.

The sand lithofacies also consists of silt- to fine-grained sand deposited in normally graded rhythmites a few inches (centimeters) to several tens of inches (centimeters) thick (Myers and Price 1979; DOE 1988). This lithofacies corresponds to the Touchet Beds (see Baker 1973; Waitt 1980) and is found throughout the central, southern, and western Cold Creek syncline in and south of 200 East and 200 West areas. Remnants of this lithofacies are presumed to be preserved in the 300 Area, though they are so thin and/or intermixed with coarser-grained Pasco Gravels as to be equivocal.

The sand lithofacies are interpreted as either the coarse-grained portions of the slackwater deposits that followed Lake Missoula glacial flood events (as described by Waitt 1980; DOE 1988), or sediments transitional between main flood channel and slackwater deposits. Fine- and coarse-grained Missoula deposits may have been reworked by normal stream activity that followed the floods. However, present sedimentary evidence suggests that such deposits are minor.

2.2.2.3 Hanford Lithofacies G: GRAVEL. Hanford formation lithofacies G consists dominantly of poorly consolidated granule to pebble-sized gravel with intermixed minor sand and coarser-grained gravels. Gravel-sized clasts make up 70% of this lithofacies with sand and finer-grained detritus making up less than 30%. Except for the higher concentration of angular basaltic clasts and the weak consolidation, this lithofacies is similar texturally to Ringold Formation lithofacies G.

Recovery of reliable samples from this coarse-grained lithofacies using cable tool drilling techniques has been nearly nonexistent. Thus, great reliance has been placed on observations of presumed analog deposits in nearby gravel pits. At the gravel pit across the Columbia River from Washington Public Power Supply System in Richland, Washington, lithofacies SS and G commonly are interstratified. As seen in Figure 2-7, both the gravel and the sand display planar cross-stratification. Tabular sets in the gravel are approximately 3 ft (1 m) thick; sets in the sand are 0.4 to 16 in. (1 to 40 cm) thick. Hanford lithofacies G prominently exposed at the gravel pit consist of a medium to dark gray, poorly to moderately sorted, unconsolidated, clast- supported (commonly open framework) granule- to pebble-sized gravel. The gravel clasts range from 0.1 in. to 1.6 ft (2 mm to 0.5 m) in diameter and make up 90 to 95% of these coarse-grained deposits. Clast composition is

varied with basalt clasts most abundant (at least 50%); other clasts include porphyritic volcanic rocks, granite, greenstone, gneiss, mudstone, and ripped-up clasts of Ringold Formation detritus. Mudstone clasts have been incorporated into discrete pebble to cobble layers, but also are distributed throughout the gravel. Matrix material is composed of from clay to coarse sand and makes up from 5 to 10% of Hanford G lithofacies. Matrix grains include quartz, feldspar, basalt, muscovite, phlogopite and biotite detritus.

Hanford G lithofacies at the gravel pit exhibit planar stratification marked by changes in clast and matrix size, sometimes, changes in clast composition, and often by open-framework fabrics. Gravel beds range from 1 in. to 3.3 ft (2 cm to 1 m) in thickness and are traceable for tens of feet (meters). Stringers of pebbles and cobbles ranging up to 6 in. (15 cm) in diameter occur in Hanford formation G deposits and interfinger with discontinuous lenses of sand.

Hanford formation lithofacies G sediments are interpreted as main flood channel deposits or lag concentrations. The elongate trend of these sediments along inferred flood channelways, and the coarse-grained, open-framework character further supports deposition by strong, main channel currents (see Lindsey 1991). Lag concentrations of these deposits may have developed during major flood transport events when transport capacities fluctuated.

2.2.2.4 Hanford Lithofacies CB: COBBLE AND BOULDER. The Hanford cobble and boulder lithofacies is exposed in the gravel pit in Sec. 12, T10N, R28E (across the Columbia River from the 300 Area); this lithofacies is composed dominantly of medium to dark gray, poorly sorted, unconsolidated, clast-supported open- and closed-framework, pebble to large cobble and boulder gravel (Figure 2-8). The CB lithofacies displays massive bedding, plane to low-angle bedding, and large-scale cross-bedding (as seen in analog exposures). Gravel-sized clasts in these deposits comprise up to at least 70% of the sediment, and range from small, 0.1-in. (3-mm) diameter granules to 2.4-ft (0.75-m) diameter boulders. The average largest clast is 1.6 ft (0.5 m) in diameter. Clasts are of varied composition: basalt is most abundant (approximately 40%); other clasts include granite, porphyritic intermediate volcanic rocks, greenstone, gneiss, mudstone, fine- to medium-grained medium brown sandstone, and well-consolidated, matrix-supported clasts of cobble conglomerate (possibly of Ringold derivation) which occur mainly as large, 6-in. (150-mm)) diameter cobbles to 30-in. (750-mm) diameter boulders. The smaller clasts in this lithofacies tend to be subrounded, while the larger clasts are rounded to well rounded. Matrix material comprises up to 10% of the gravel and ranges from clay to large granules. The matrix consists of basalt, quartz, muscovite, and biotite, and is slightly calcified.

Pebble to large cobble deposits from the Hanford formation (as exposed at two nearby Hanford Site gravel pits) are texturally different from though structurally similar to Ringold lithofacies G deposits. Hanford lithofacies G sediments are more poorly sorted and have more cobble- and boulder-sized clasts than Ringold lithofacies G. Hanford formation gravels also characteristically display open-framework fabrics while Ringold Formation gravels fabrics are usually closed. Structurally, large-scale planar cross-strata, clast imbrication, feet- (meters-) wide channel scours, and lenticular bodies occur in both the Ringold and Hanford lithofacies G.

Hanford formation lithofacies CB sediments are interpreted as mixtures of main flood channel deposits or lags in the 300 Area and as proximal, boulder-rich deposits shed off bedrock highs such as found near Umtanum Ridge (Lindsey 1991). The parallelism between the elongate deposit trends and coarse-grained, open-framework character of the CB and G lithofacies supports a similar interpretation for both lithofacies.

Figure 2-1. Thickly Laminated to Thinly Bedded Mud Exposed Along the White Bluffs and Analogous to Ringold Lithofacies M Elsewhere.

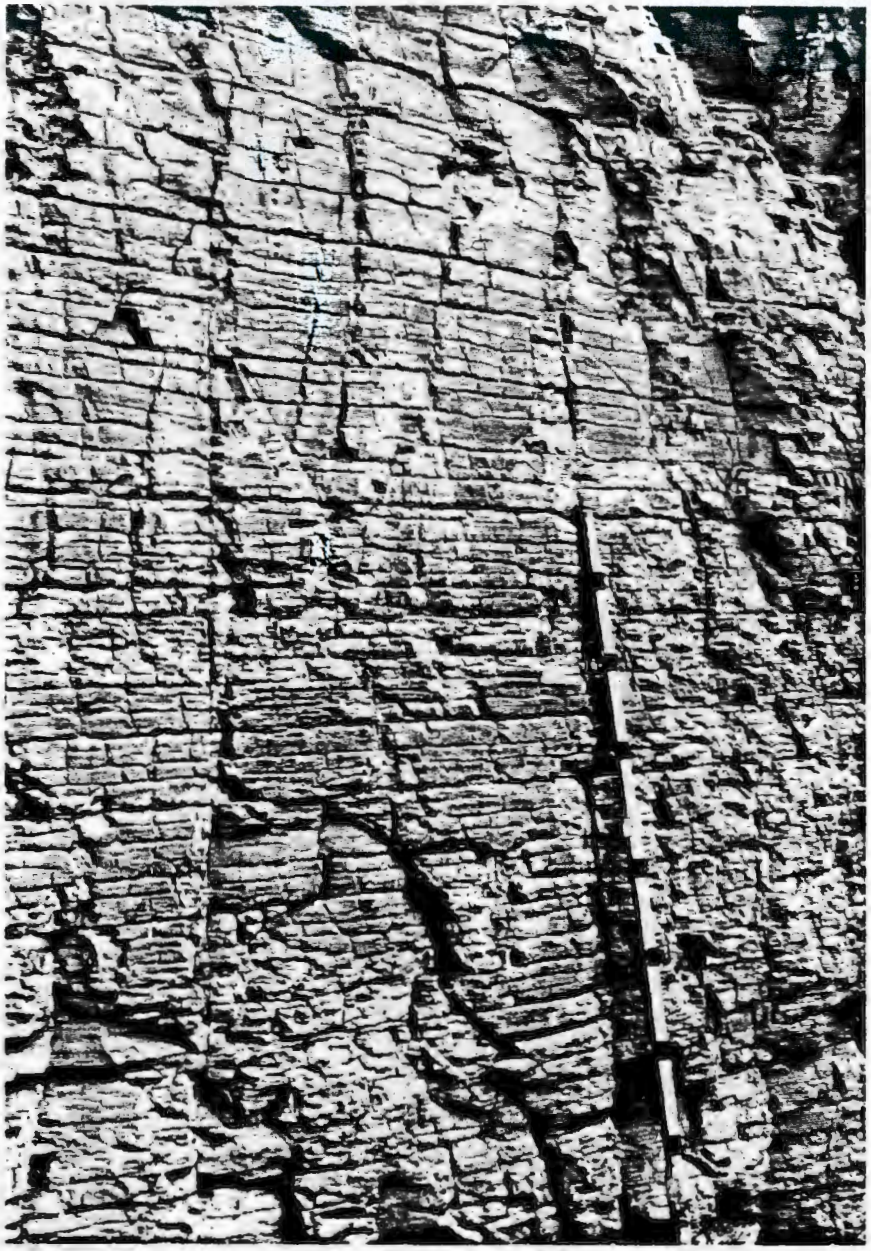

Figure 2-2. Mixed Mud (below the line) and Sand Exposed Along the White Bluffs and Analogous to Ringold Lithofacies MS Elsewhere.

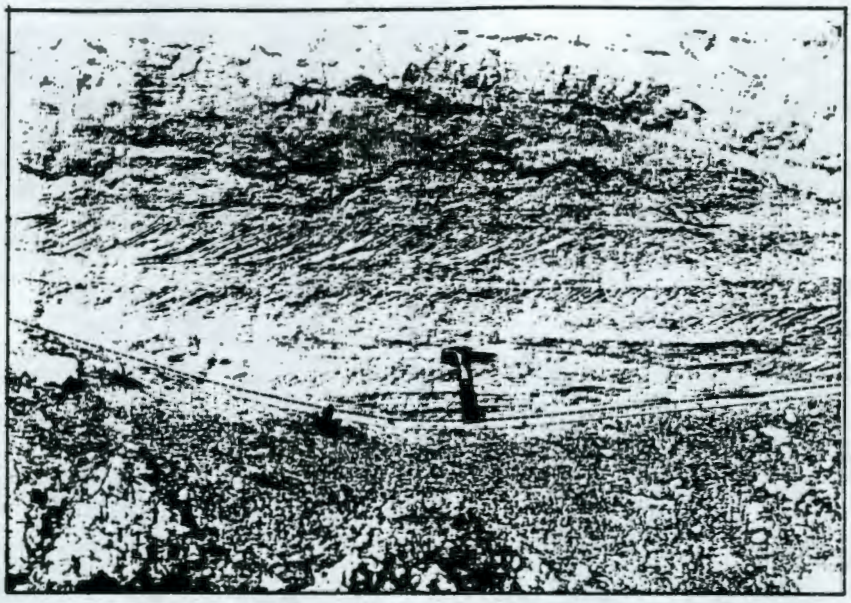

Figure 2-3. Cross Stratified Sand Exposed Along the White Bluffs and Analogous to Ringold Lithofacies SS Elsewhere.

Figure 2-4. Crudely Stratified Pebble to Cobble Conglomerate Exposed Along the White Bluffs and Analogous to Ringold Lithofacies G Elsewhere.

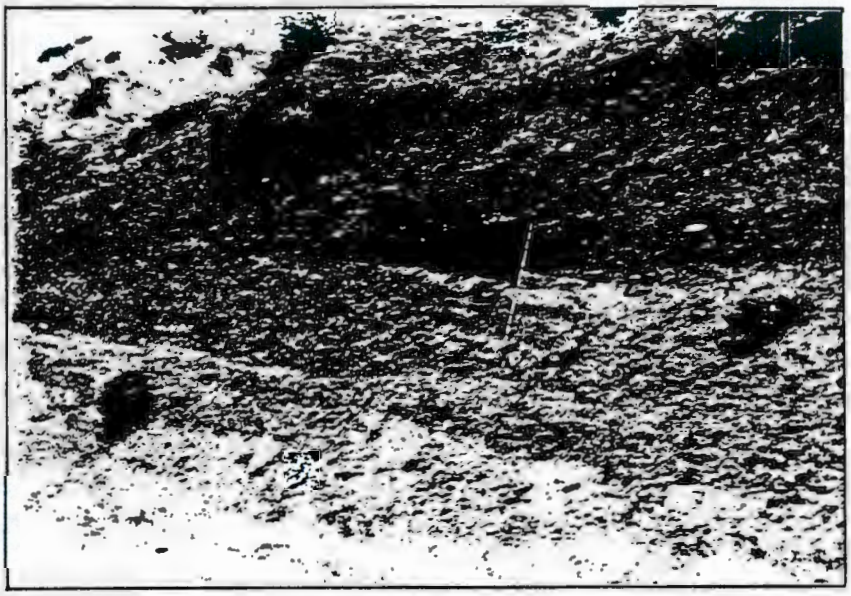

Figure 2-5. Hanford MS Lithofacies (at top of photo) Interstratified with Climbing Ripple Laminated SS and G Lithofacies Exposed in Gravel Pit in Sec. 25, T12N, R28E.

Figure 2-6. Hanford SS Lithofacies Illustrating Plane Bedding (top of photo) and Climbing Ripple Lamination (lower part of photo).

Figure 2-7. Hanford G Lithofacies of Cross-Stratified Coarse Pebble to Cobble-Sized Gravel Overlain by and Interstratified with Lithofacies SS.

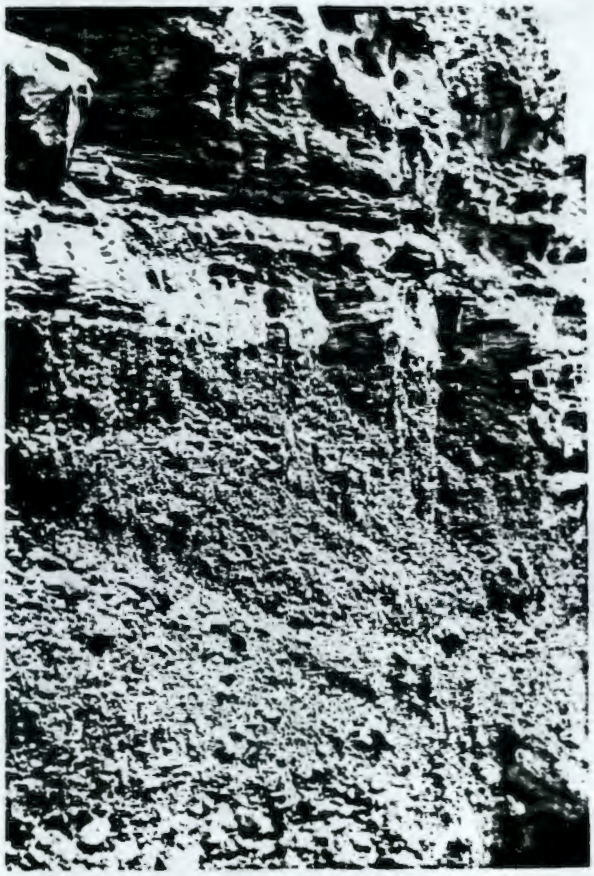

Figure 2-8. Hanford CB and G Lithofacies Displaying High-Angle Foreset Beds Dipping West-Southwest from a Gravel Pit in Sec. 25, T12N, R28E.

3.0 STRATIGRAPHIC CORRELATION AND COMPOSITIONAL ANALYSES

Stratigraphic correlation is fundamental to construction of the sedimentary architecture and reconstruction of the depositional history of suprabasalt strata in the 300 Area. Precise correlation of strata also was deemed necessary to evaluate the degree to which aggradation, erosion, and/or structural deformation have affected the area. Similarly, stratigraphic correlation was considered crucial to delineation of hydrofacies geometries. Unfortunately, the complex architectural arrangement of lithofacies within the Ringold Formation and Hanford formation made stratigraphic correlation difficult. Attempts to correlate subunits within the Hanford and Ringold strata using standard correlation techniques met with limited success. For example, the fining-upward depositional cycles that PSPL (1982) used to correlate Ringold Formation strata are not everywhere present or easily recognized. Likewise, petrologic correlation of Ringold Formation and glaciofluvial strata, while potentially valuable (Tallman et al. 1979; PSPL 1982), had not been sufficiently evaluated to determine reliability. Thus, given the need to establish the continuity of component lithofacies within (at least) the 300 Area, two geochemical tests were devised to (using available drill chips) correlate between informally defined, texturally comparable portions of the Hanford formation and Ringold Formation. The test was inspired primarily from the earlier petrologic research of Tallman et al. (1979) and PSPL (1982).

Mineralogic and bulk chemical compositions of detrital sediments can be determined using a variety of methods. Petrographic point counts provide valuable insight into the mineralogic and petrologic character of a sediment, but are also time consuming and tedious. X-ray diffraction (XRD) analysis provides a viable and more efficient way to characterize detrital composition, but still requires associated thin section point counts to determine component percentages. Composition can be more efficiently characterized using: x-ray fluorescence (XRF) spectroscopy in which the whole-rock geochemistries are determined with great accuracy and reproducibility (Johnson and Hooper 1987), and inductively coupled plasma/mass spectrometry (ICP/MS) in which concentrations of rare earth elements (REE) and certain trace elements are measured.

3.1 METHODS

Sand-sized sediments for XRF and ICP/MS analyses were selected from: (1) coarse-grained lithofacies of the upper Ringold Formation strata (upper being a relative term for shallow Ringold Formation strata in the 300 Area); (2) coarse-grained lithofacies from the glaciofluvial sediments; and (3) fine-grained lower Ringold Formation strata (lower being a relative term for deeper Ringold Formation strata in the 300 Area). Sample preparations are outlined in Appendices A and B.

3.2 XRF ANALYSES

Forty-nine samples from boreholes 399-1-16c, 1-17c, and 1-18c were analyzed for major and trace element composition using automatic XRF spectrometry (Figure 3-1, Table 3-1). Samples were taken from these boreholes because of the immediate interest to 300 Area studies, their close spacing,

and the completeness of their stratigraphic sections (all drilled to basalt). The 23 elements analyzed for each of these samples are listed in Table 3-1. Sample preparations are outlined in Appendix A.

3.3 DISCUSSION OF XRF ANALYSES

Elemental data were compared from three lithostratigraphic units divided on the basis of texture. These three units were the glaciofluvial strata, the coarse-grained upper (shallow) Ringold Formation strata, and fine-grained lower (deeper) Ringold Formation strata. The glaciofluvial and upper (Ringold strata are characterized by a wide range of sand grain size (from very fine to very coarse). The lower Ringold Formation strata are characterized by a smaller range of sand grain sized (from very fine to medium). The analyses demonstrate that certain major and trace elements provide a potentially reliable method of correlating between strata (Figure 3-2). Graphical plots of major element concentrations (SiO_2 versus Al_2O_3, SiO_2 versus MgO, SiO_2 versus MnO, Al_2O_3 versus TiO_2, Al_2O_3 versus K_2O, Al_2O_3 versus MnO, Al_2O_3 versus MgO, Al_2O_3 versus P_2O_5, and Al_2O_3 versus CaO) all demonstrate that there are distinct fields that permit differentiation of the informal lithostratigraphic units. Plots of selected trace element concentrations (i.e., niobium versus zirconium, niobium versus scandium, niobium versus chromium, and niobium versus copper) allow more precise discrimination between the strata. More detailed research must be conducted to explain the mineralogical and petrological basis for these correlative variations.

3.4 ICP/MS--REE ANALYSES

Inductively coupled plasma/mass spectrometry was used to quantitatively measure the concentrations of 14 REE and the trace elements yttrium, thorium, hafnium, and tantalum in selected sediment samples to further explore the possibilities of geochemical analysis for stratigraphic correlations. The results are presented in Table 3-2. Factors affecting the concentration and relative distribution of the REE in sediments include mineralogical composition, modal distribution, grain size, and clay content. REE analysis has an advantage over conventional petrographic correlation methods in that the REE concentrations and relative distributions are not significantly changed during weathering (Taylor and McLennan 1985), and only a small sample is necessary for analysis. Fifteen sediment samples from 300 Area boreholes 399-1-16c and 399-1-17c were analyzed. Sample preparations were performed as described in Appendix B.

To graphically compare the REE content of different rocks, it is necessary to eliminate the Oddo-Harkins effect, which is the occurrence of greater concentrations of elements with even atomic numbers as compared to those with odd atomic numbers. This is accomplished by normalizing the REE analyses to those of chondritic meteorites (i.e., concentration of each REE in the rock was divided by the concentration of that element in chondritic meteorites). These data then plot as a smooth curve (Figure 3-2, sheets 7-9).

Chondrite normalized patterns for the Hanford formation sediments, upper Ringold Formation, and lower Ringold Formation are presented in Figure 3-2. The general shape of the patterns are similar to typical continental sediments (Taylor and McLennan 1985), but lack appreciable europium anomaly and show

differing degrees of enrichment with respect to chondrite values. The steepness of a REE pattern can conveniently be represented by the lanthanum/ytterbium ratio. Larger lanthanum/ytterbium ratios represent greater relative enrichment of light to heavy REE, hence, steeper normalized curves. The average lanthanum/ytterbium of the glaciofluvial sediments, upper Ringold and lower Ringold Formations are 6.12, 7.91, and 10.44, respectively. The lower Ringold Formation has the steepest pattern, with light REE (LREE) more than 100 times chondrite, dropping to heavy REE (HREE) values of approximately 10 times chondrite. Hanford formation sediments have a flatter REE pattern ranging from 75 times chondrite for the LREE to 13 times chondrite for the HREE. In summary, the chondrite normalized lanthanum/ytterbium ratio appears to be a valid method of distinguishing between the units tested.

The thorium content of the Hanford sediments and upper Ringold Formation also are significantly different (Table 3-2), thus offering another potential method of stratigraphic differentiation. The thorium content of the lower Ringold Formation appears to be distinct from the other units, but more samples will need to be analyzed to verify this finding conclusively.

Figure 3-1. Location map of the 300 Area and Borehole Locations.

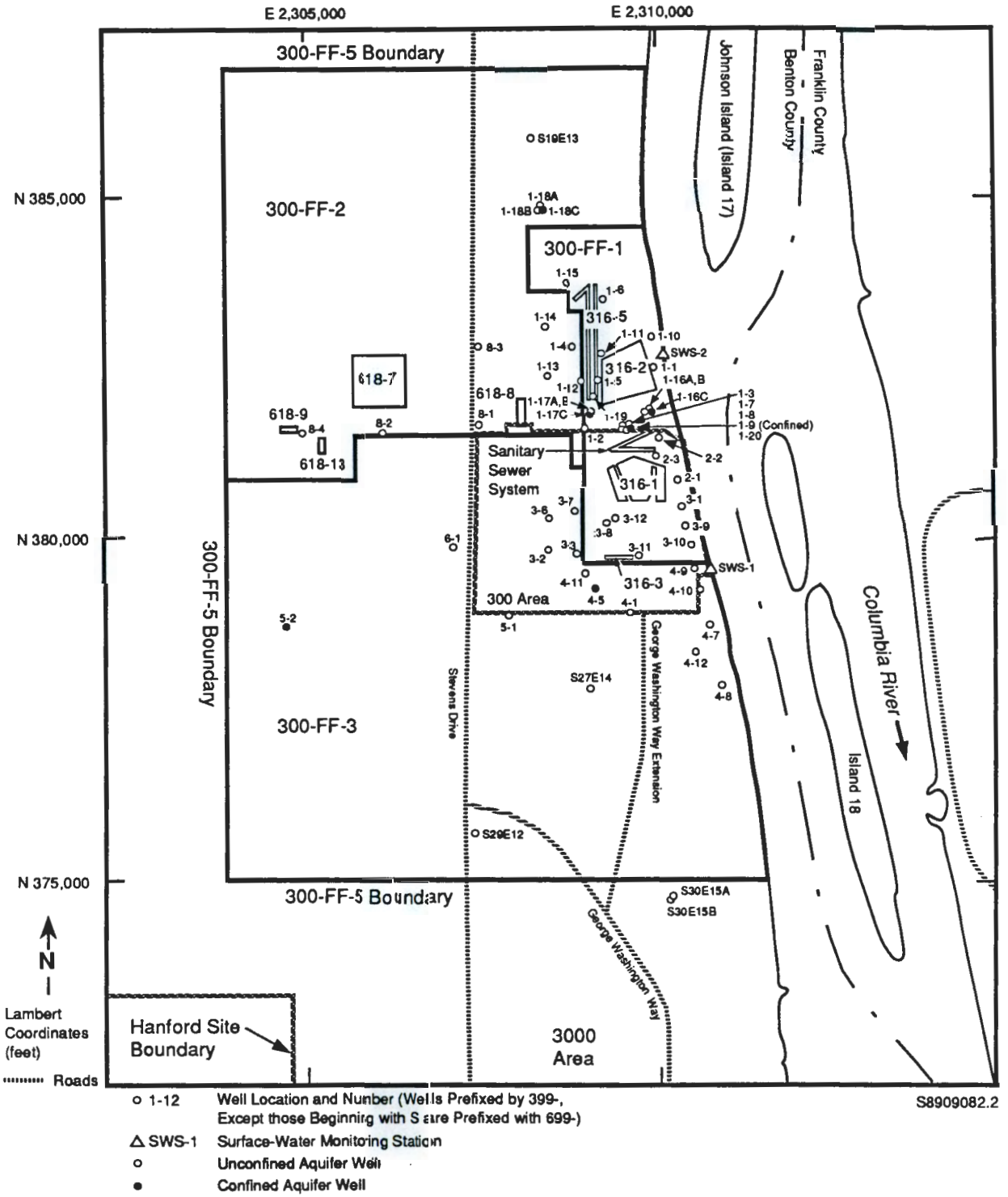

Figure 3-2. Scatter Diagrams of XRF Data from Glaciofluvial, Upper, and Lower Ringold Formation Strata. (Sheet 1 of 9)

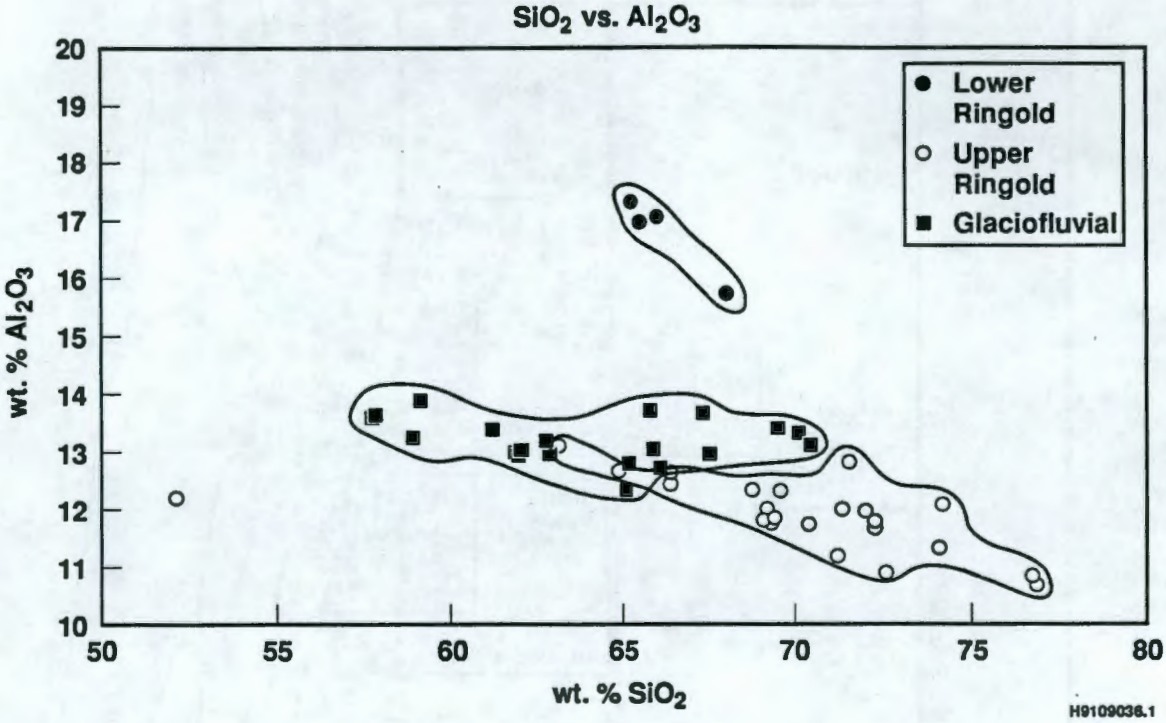

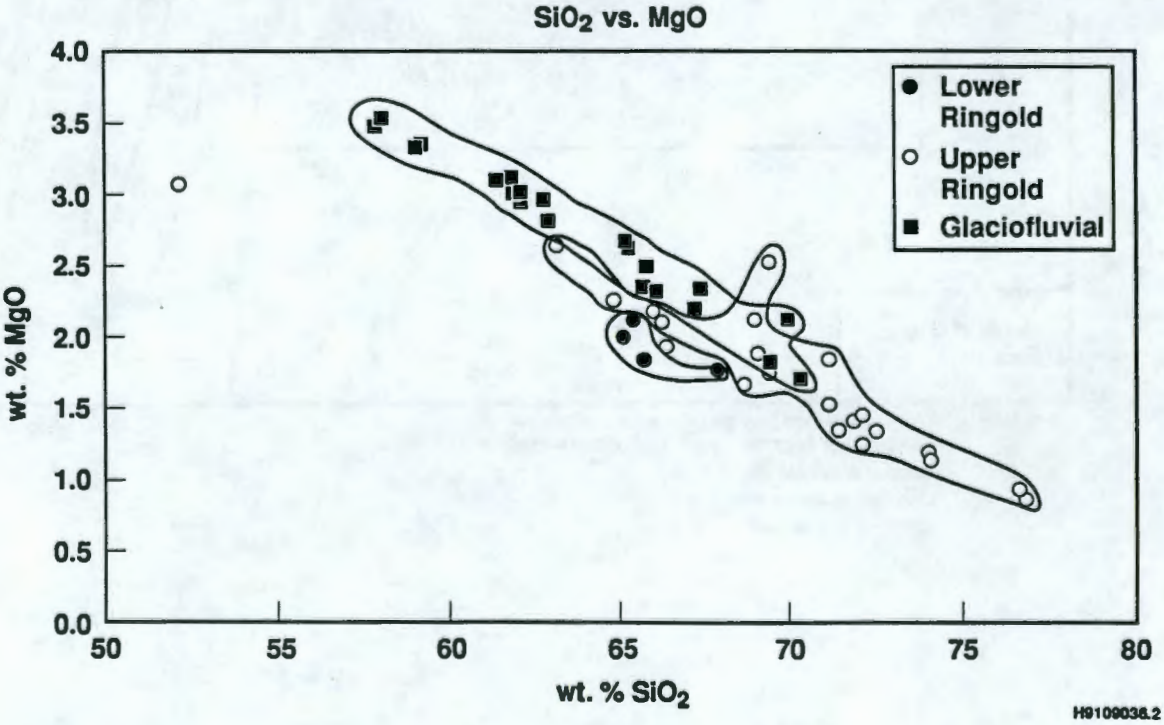

Figure 3-2. Scatter Diagrams of XRF Data from Glaciofluvial, Upper, and Lower Ringold Formation Strata. (Sheet 2 of 9)

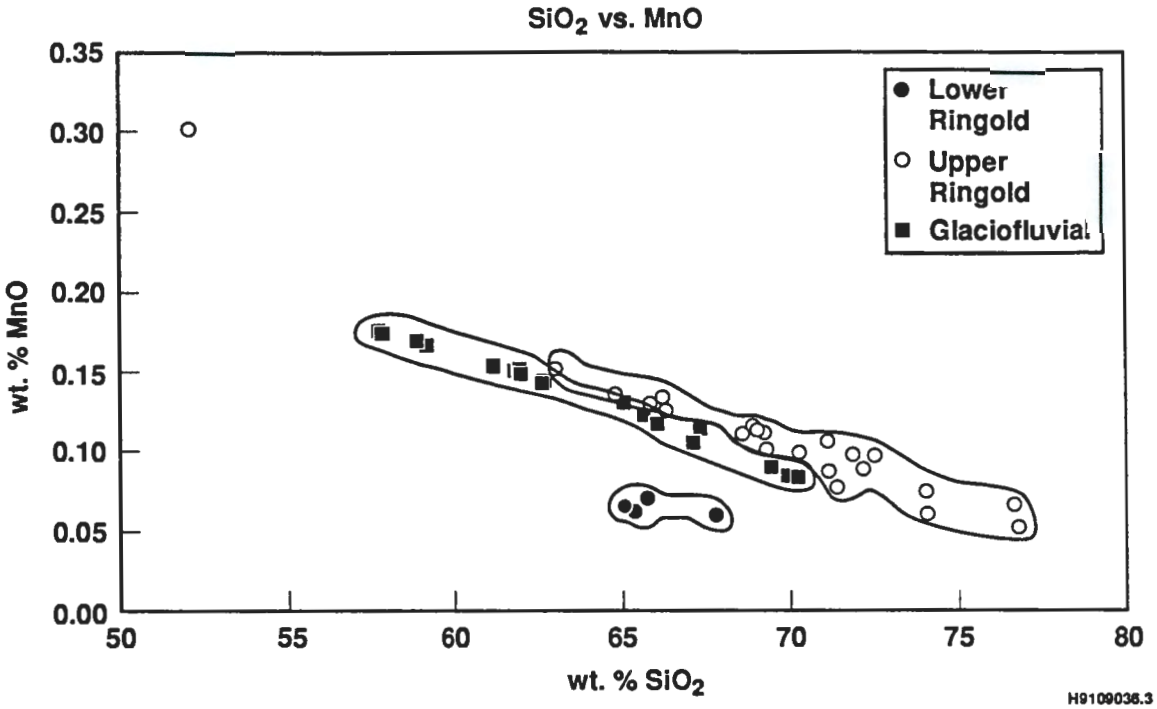

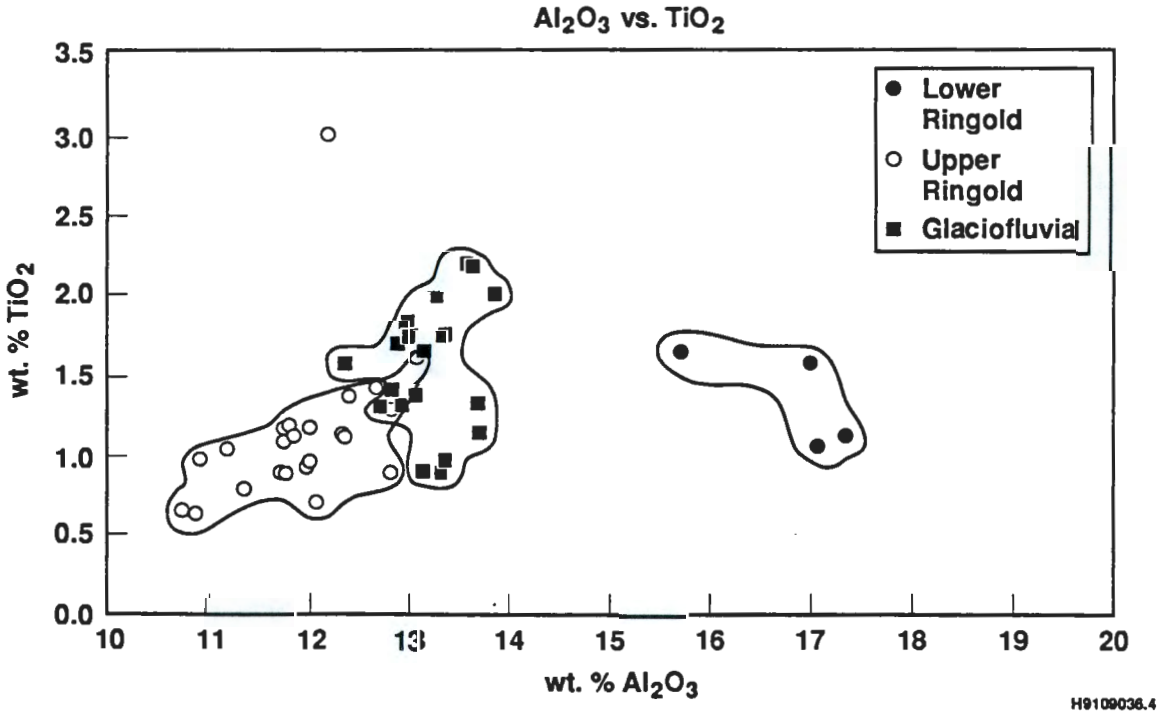

Figure 3-2. Scatter Diagrams of XRF Data from Glaciofluvial, Upper, and Lower Ringold Formation Strata. (Sheet 3 of 9)

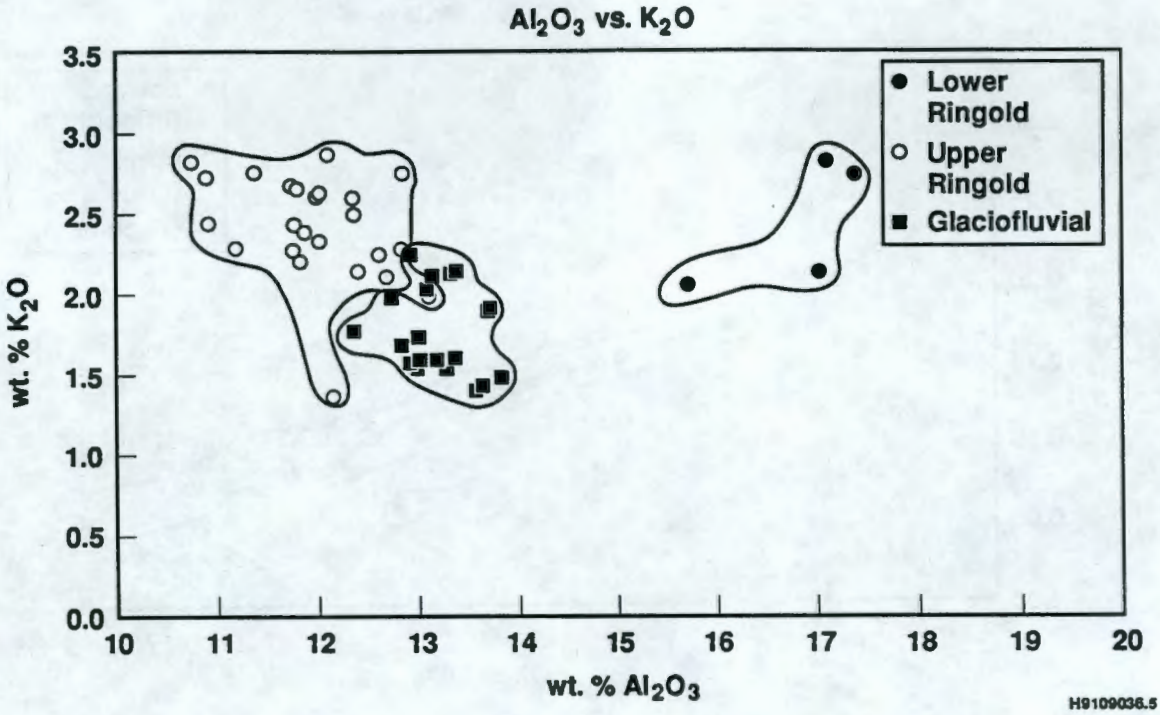

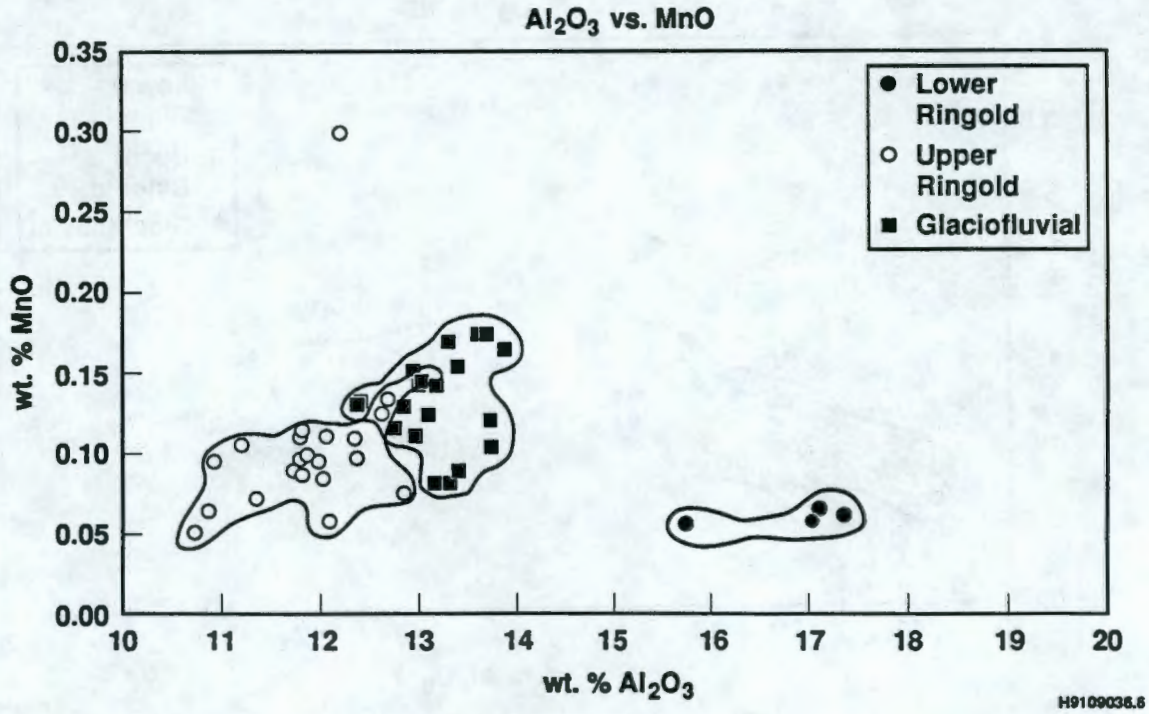

Figure 3-2. Scatter Diagrams of XRF Data from Glaciofluvial, Upper, and Lower Ringold Formation Strata. (Sheet 4 of 9)

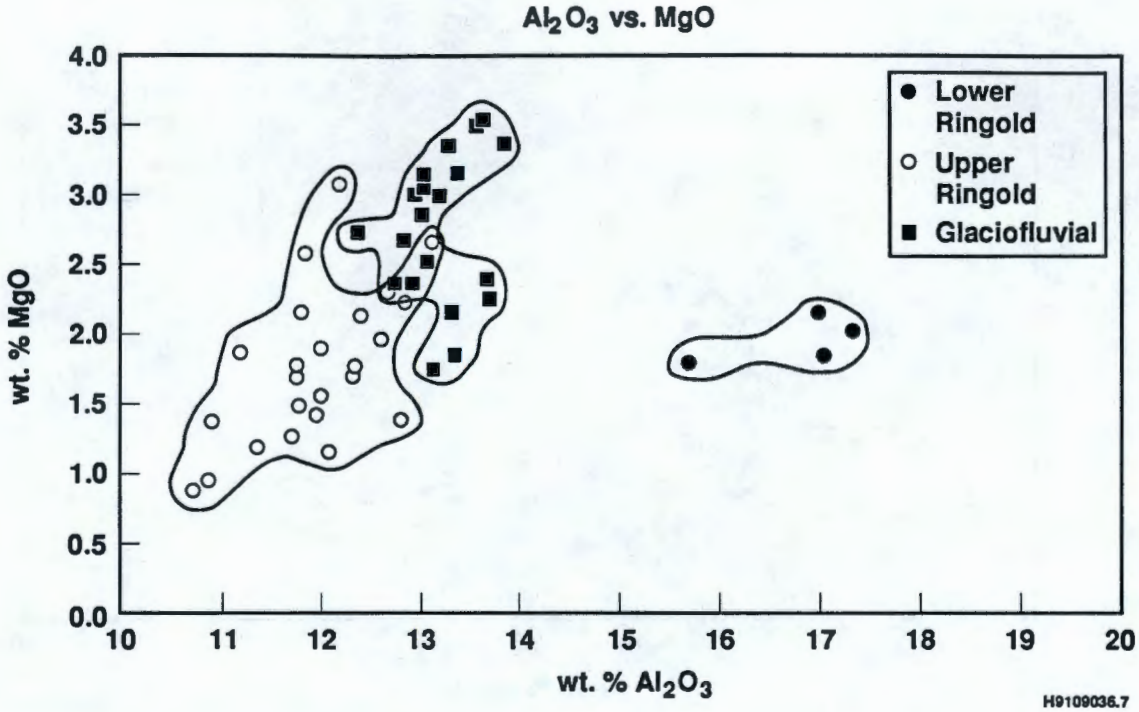

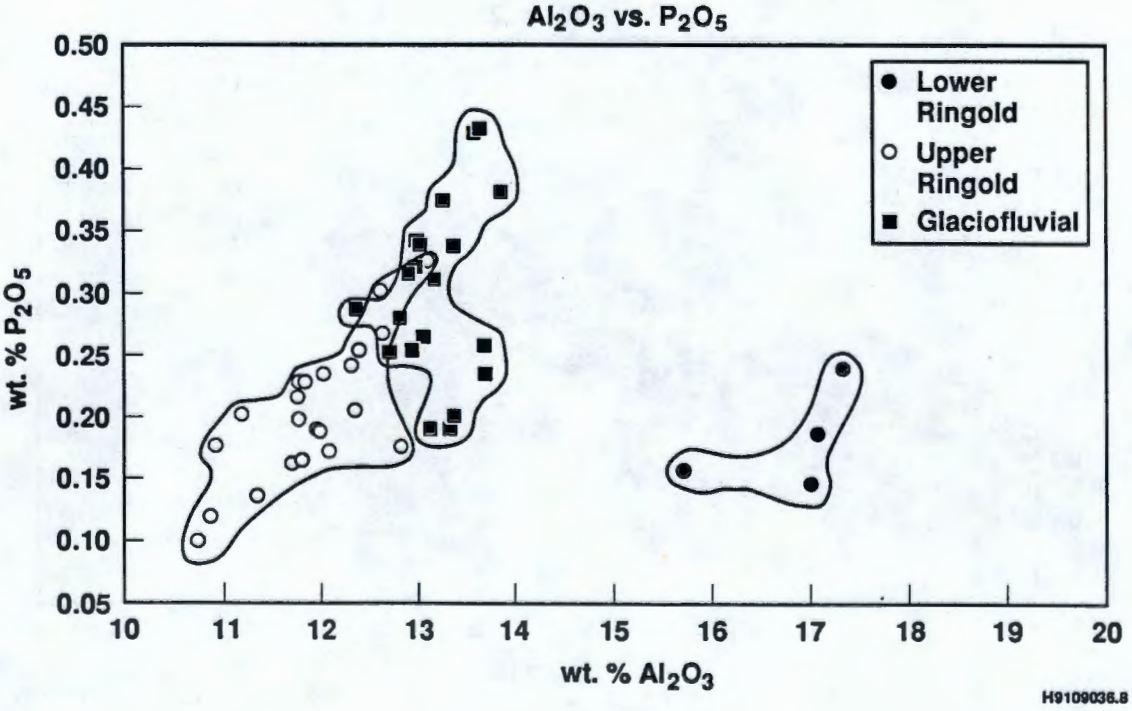

Figure 3-2. Scatter Diagrams of XRF Data from Glaciofluvial, Upper, and Lower Ringold Formation Strata. (Sheet 5 of 9)

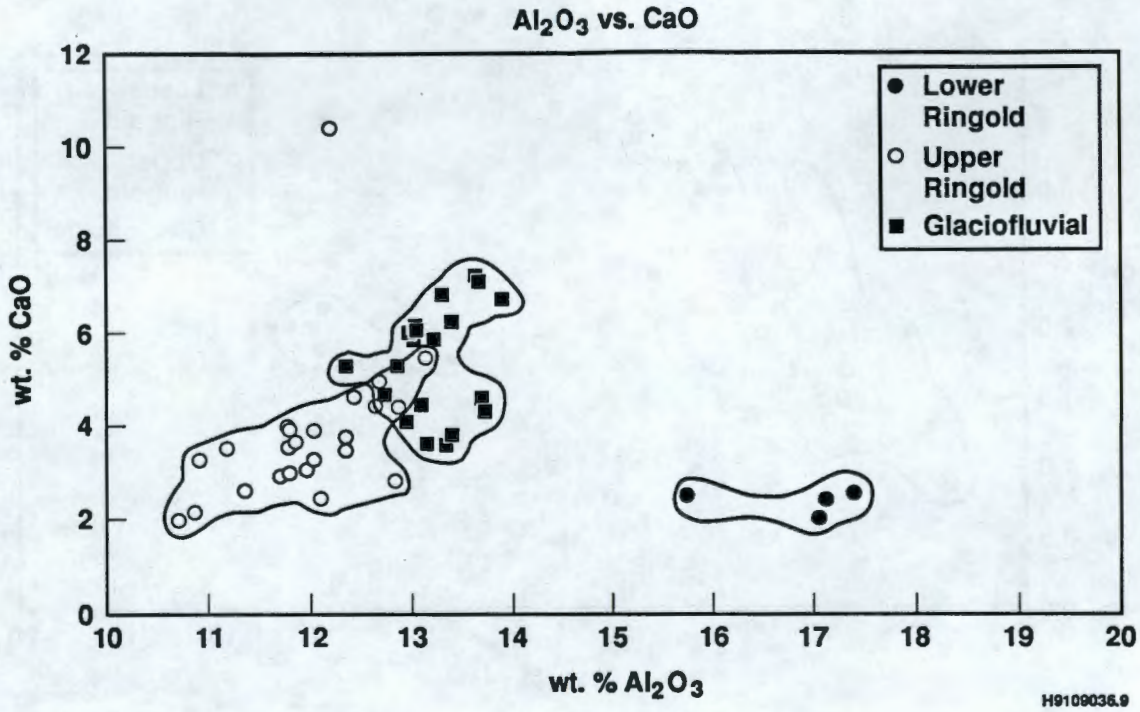

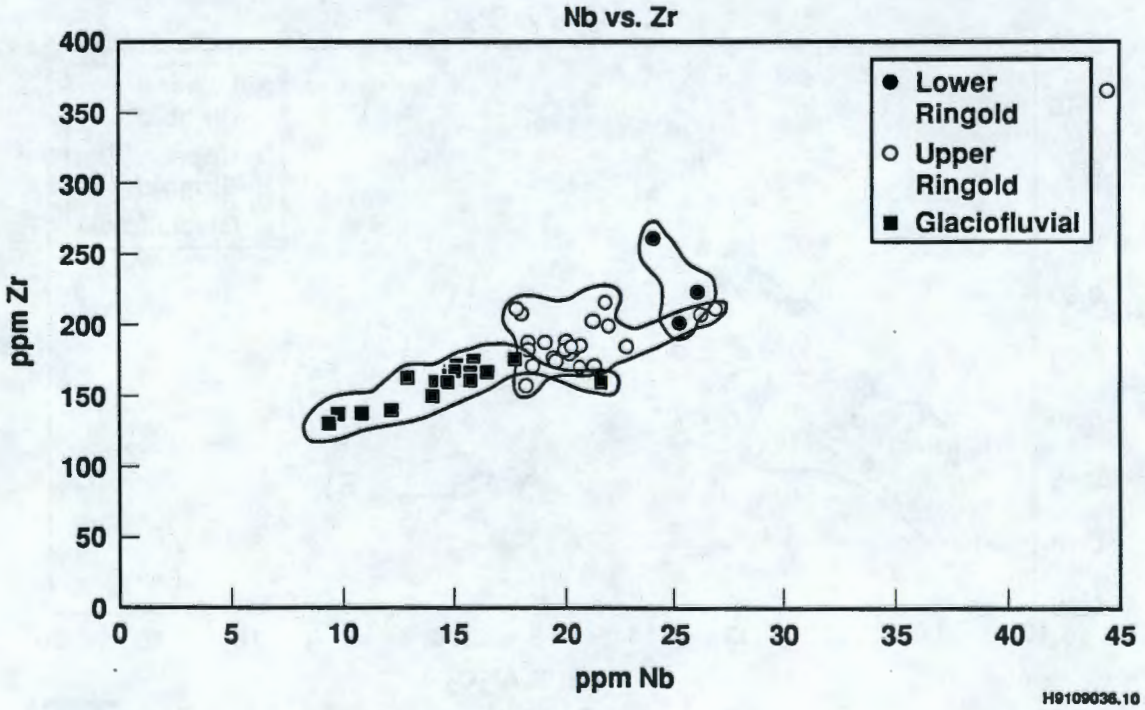

Figure 3-2. Scatter Diagrams of XRF Data from Glaciofluvial, Upper, and Lower Ringold Formation Strata. (Sheet 6 of 9)

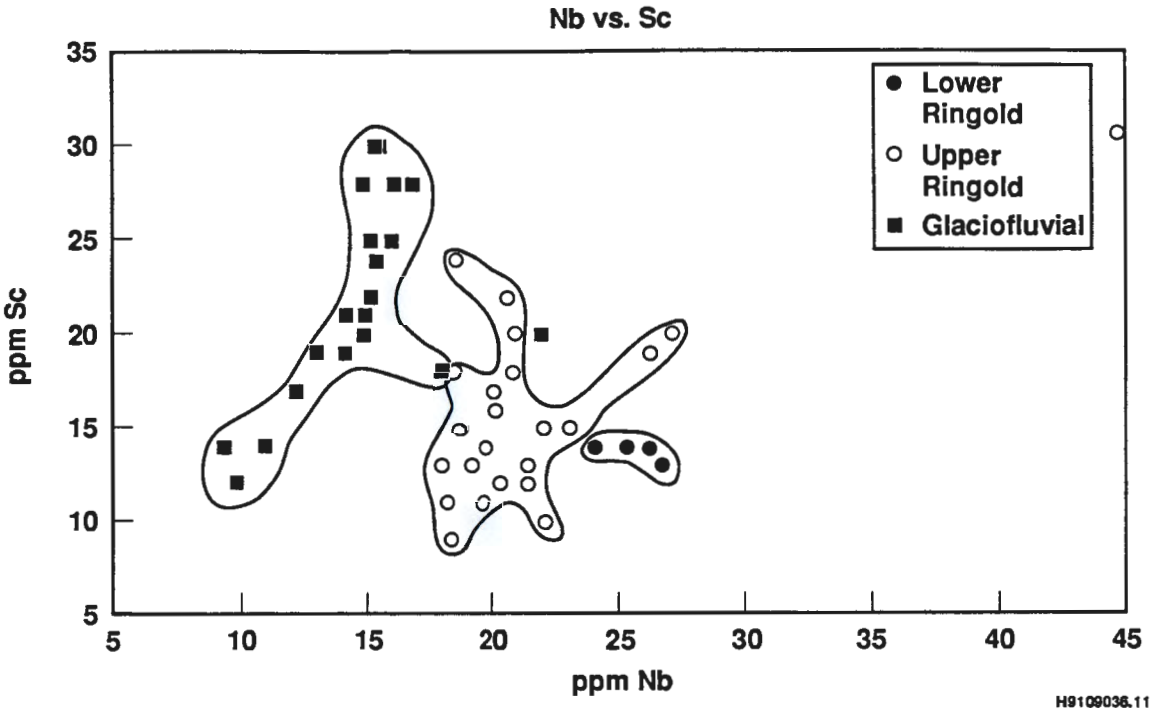

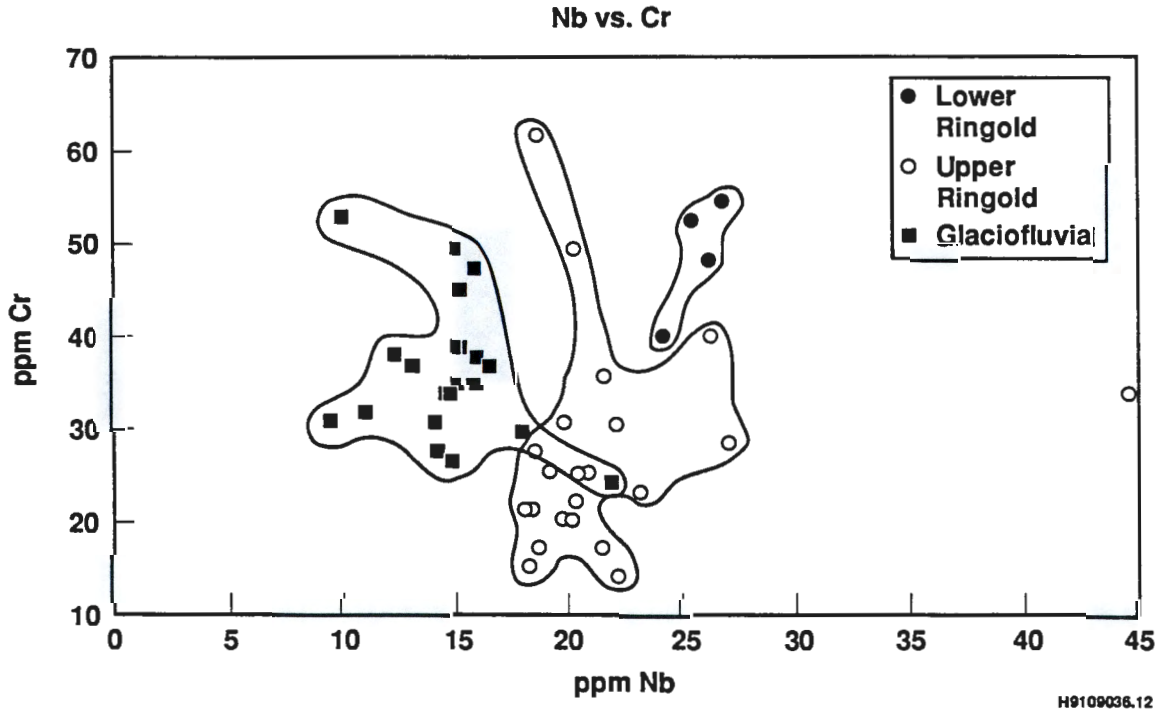

Figure 3-2. Scatter Diagrams of XRF Data from Glaciofluvial, Upper, and Lower Ringold Formation Strata. (Sheet 7 of 9)

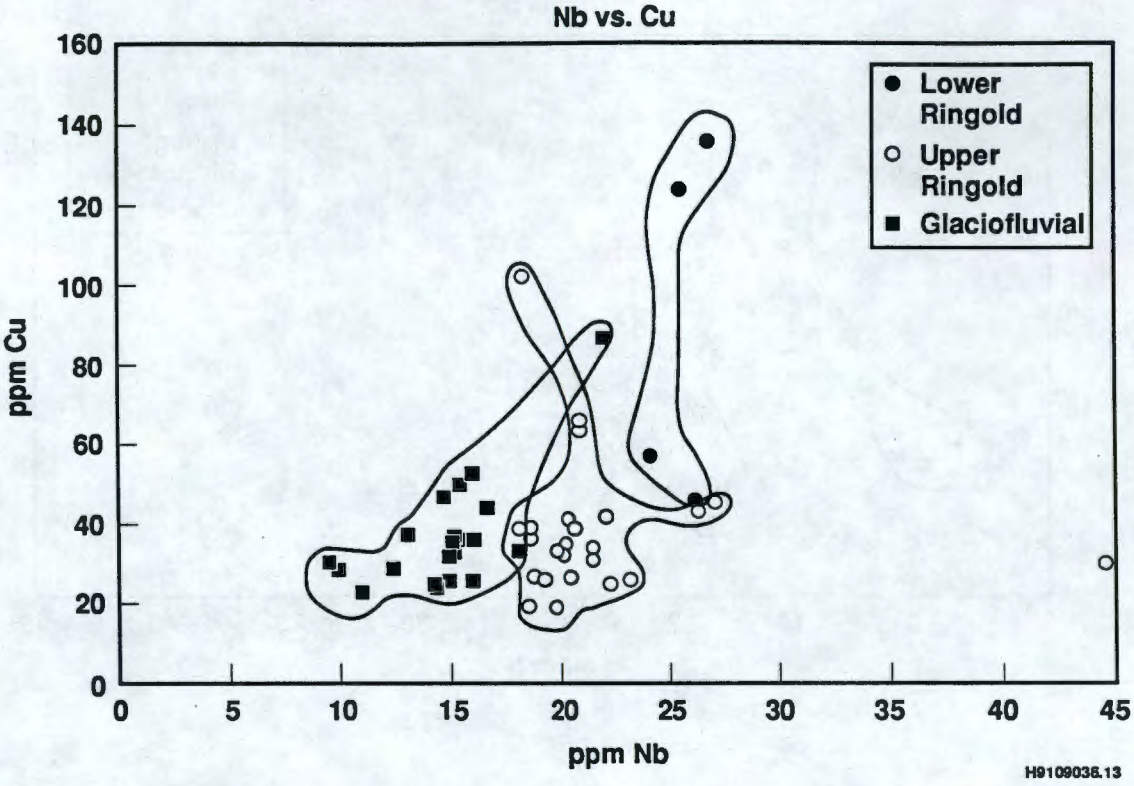

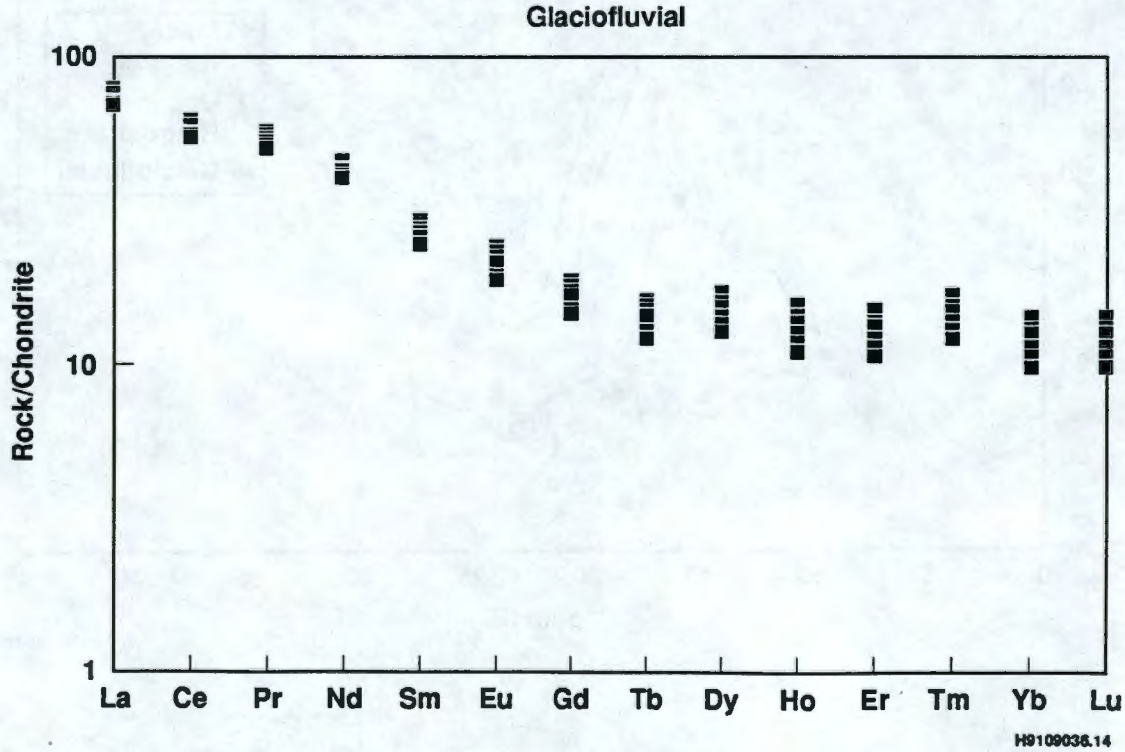

Figure 3-2. Scatter Diagrams of XRF Data from Glaciofluvial, Upper, and Lower Ringold Formation Strata. (Sheet 8 of 9)

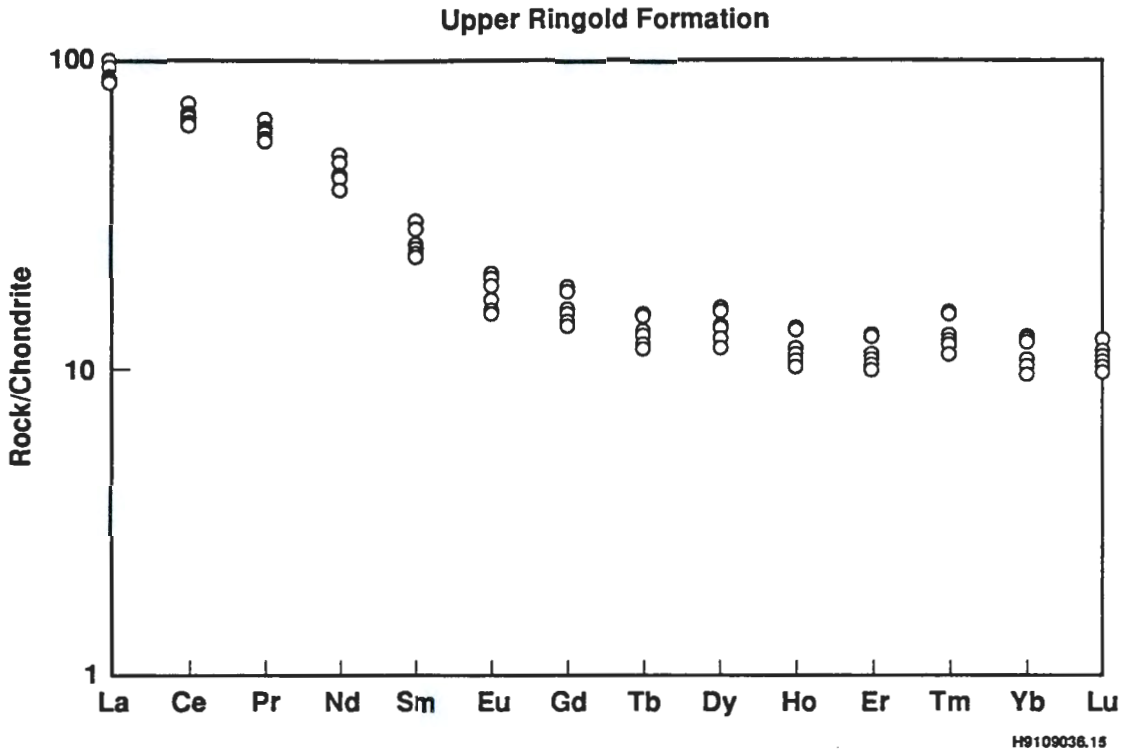

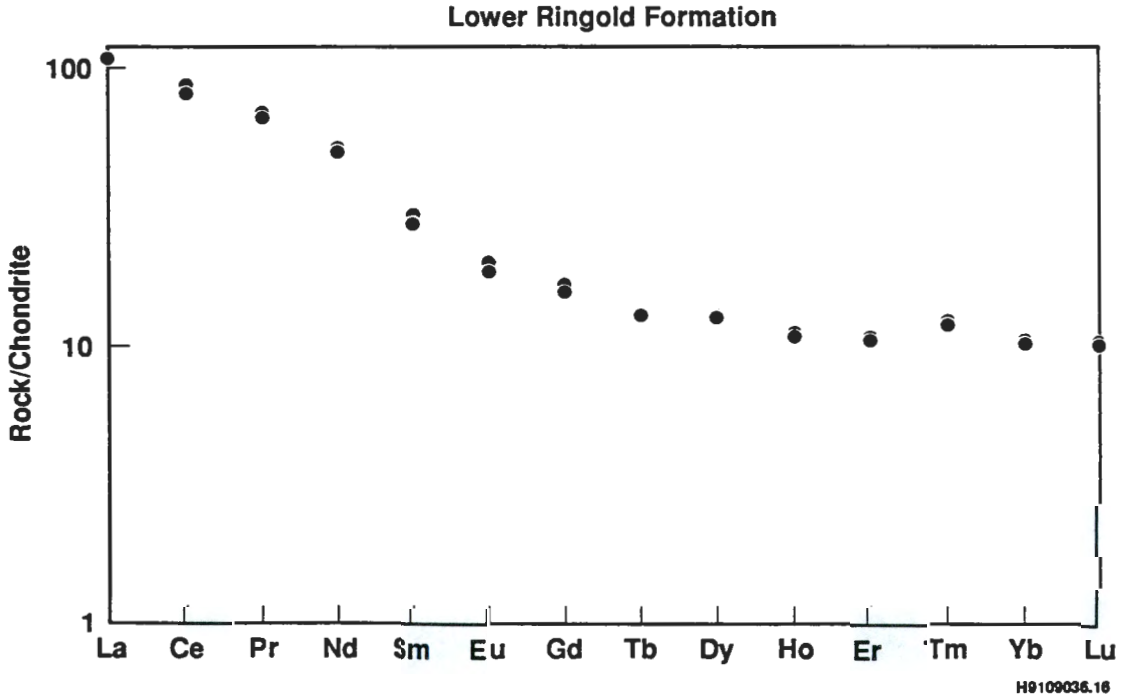

Figure 3-2. Scatter Diagrams of XRF Data from Glaciofluvial, Upper, and Lower Ringold Formation Strata. (Sheet 9 of 9)

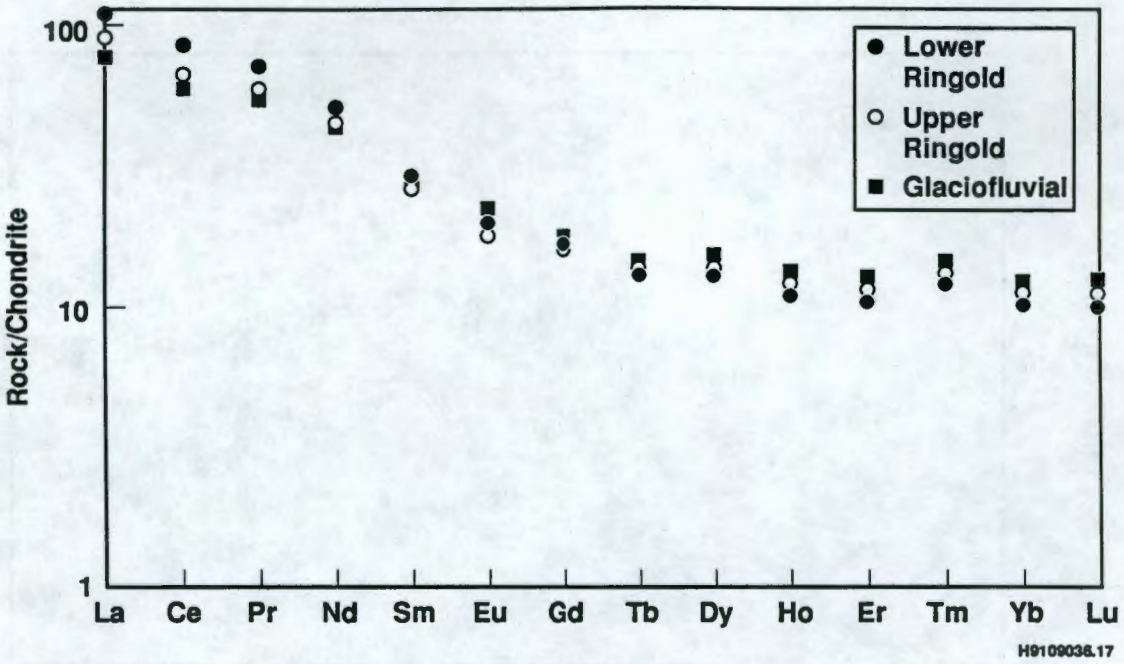

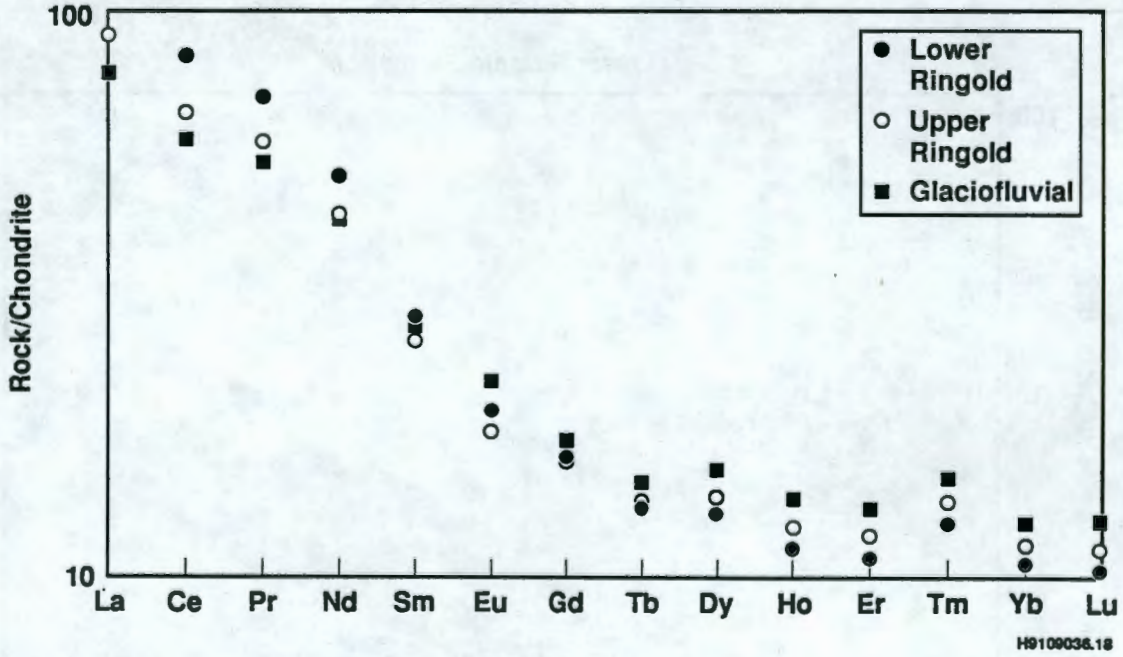

Table 3-1. XRF Data from Glaciofluvial, Upper Ringold Formation, and Lower Ringold Formation Samples.

Well	Depth (ft)	SIO2	AL2O3	TIO2	FEO*	MNO	CAO	MGO	K2O	NA2O	P2O5
		GF	GF	GF	GF	GF	GF	GF	GF	GF	GF
399-1-16C	4	57.68	13.59	2.20	10.92	0.18	7.31	3.49	1.42	2.79	0.42
399-1-16C	14	59.12	13.86	2.00	10.16	0.17	6.76	3.36	1.51	2.69	0.38
399-1-16C	24	61.76	13.02	1.70	9.19	0.15	5.22	3.13	1.57	2.94	0.32
399-1-16C	29	65.83	13.07	1.38	7.82	0.13	4.51	2.53	2.07	2.41	0.26
399-1-16C	34	67.42	12.94	1.32	6.79	0.12	4.15	2.36	2.28	2.37	0.25
399-1-16C	45	61.84	13.00	1.84	9.32	0.15	6.07	3.04	1.55	2.86	0.34
399-1-16C	48	65.70	13.70	1.33	7.06	0.12	4.65	2.39	1.91	2.89	0.25
399-1-16C	54	66.07	12.73	1.30	7.39	0.12	4.68	2.35	1.99	3.10	0.25
399-1-17C	10	57.84	13.65	2.18	10.69	0.18	7.18	3.54	1.45	2.87	0.43
399-1-17C	20	58.89	13.28	1.99	10.60	0.17	6.87	3.35	1.55	2.94	0.37
399-1-17C	30	62.83	13.00	1.68	8.76	0.15	5.86	2.84	1.76	2.81	0.32
399-1-17C	35	61.99	12.94	1.69	9.43	0.15	6.05	2.98	1.60	2.87	0.31
399-1-17C	44	62.04	13.04	1.74	9.00	0.15	6.14	3.04	1.61	2.92	0.34
399-1-18C	4	70.04	13.32	0.88	4.75	0.08	3.59	2.16	2.16	2.62	0.19
399-1-18C	9	69.46	13.37	0.96	5.13	0.09	3.83	1.87	2.18	2.91	0.20
399-1-18C	14	67.22	13.71	1.13	6.08	0.11	4.35	2.24	1.95	2.99	0.23
399-1-18C	20	70.39	13.13	0.90	4.75	0.08	3.62	1.75	2.15	3.04	0.19
399-1-18C	29	65.16	12.83	1.40	7.58	0.13	5.32	2.65	1.70	2.94	0.28
399-1-18C	39	61.24	13.38	1.75	9.26	0.16	6.25	3.14	1.92	2.86	0.33
399-1-18C	44	62.68	13.19	1.65	8.65	0.14	5.91	2.99	1.81	2.88	0.31
399-1-18C	49	65.12	12.35	1.58	8.04	0.13	5.31	2.72	1.79	2.67	0.28
		Up. Ring	Up. Ring	Up. Ring	Up. Ring	Up. Ring	Up. Ring	Up. Ring	Up. Ring	Up. Ring	Up. Ring
399-1-16C	59	70.33	11.76	1.09	5.98	0.10	3.59	1.71	2.45	2.78	0.20
399-1-16C	69	76.84	10.71	0.63	3.60	0.05	2.02	0.91	2.83	2.31	0.10
399-1-16C	80	72.20	11.70	0.88	5.42	0.09	2.92	1.29	2.71	2.63	0.16
399-1-16C	90	74.08	11.34	0.78	4.38	0.07	2.66	1.22	2.77	2.57	0.13
399-1-16C	99	66.28	12.40	1.38	7.72	0.13	4.66	2.12	2.17	2.90	0.25
399-1-16C	104	71.93	11.95	0.93	5.20	0.10	3.10	1.45	2.61	2.54	0.19
399-1-16C	109	71.48	12.63	0.88	4.99	0.08	2.83	1.40	2.77	2.57	0.17
399-1-16C	114	76.67	10.85	0.62	3.41	0.07	2.20	0.98	2.75	2.32	0.12
399-1-17C	55	69.34	11.78	1.18	6.54	0.11	4.02	1.78	2.30	2.75	0.22
399-1-17C	65	72.58	10.90	0.97	5.52	0.10	3.27	1.40	2.45	2.65	0.18
399-1-17C	75	68.71	12.34	1.13	6.48	0.11	3.76	1.71	2.62	2.91	0.24
399-1-17C	85	64.88	12.67	1.42	8.19	0.14	4.97	2.28	2.13	3.07	0.26
399-1-17C	94	69.49	12.35	1.11	6.48	0.10	3.49	1.79	2.52	2.48	0.20
399-1-17C	104	66.40	12.61	1.29	7.55	0.13	4.49	1.96	2.26	3.01	0.30
399-1-18C	58	69.00	11.80	1.18	6.75	0.12	3.93	2.15	2.22	2.82	0.23
399-1-18C	69	69.13	12.02	1.18	6.34	0.11	3.94	1.90	2.35	2.78	0.23
399-1-18C	80	65.98	12.83	1.30	7.66	0.13	4.43	2.22	2.31	2.89	0.25
399-1-18C	89	71.20	11.18	1.04	6.12	0.11	3.52	1.87	2.31	2.45	0.20
399-1-18C	99	71.23	12.02	0.96	5.21	0.09	3.31	1.57	2.65	2.78	0.19
399-1-18C	109	72.21	11.79	0.87	5.01	0.09	3.04	1.51	2.66	2.65	0.16
399-1-18C	119	74.16	12.09	0.70	3.71	0.06	2.48	1.17	2.89	2.58	0.17
399-1-18C	129	69.40	11.84	1.12	6.08	0.10	3.67	2.57	2.40	2.58	0.23
399-1-18C	139	63.08	13.12	1.61	8.80	0.15	5.45	2.66	2.00	2.80	0.32
399-1-18C	149	52.05	12.17	3.01	13.99	0.30	10.40	3.07	1.37	2.14	1.50
		Low .Rin	Low .Rin	Low .Rin	Low .Rin	Low .Rin	Low .Rin	Low .Rin	Low .Rin	Low .Rin	Low .Rin
399-1-16C	144	65.81	17.09	1.03	6.41	0.07	2.44	1.86	2.87	2.22	0.18
399-1-16C	169	65.40	17.02	1.56	8.12	0.08	2.11	2.16	2.18	1.25	0.14
399-1-17C	134	65.14	17.35	1.09	6.58	0.08	2.60	2.02	2.79	2.12	0.24
399-1-17C	159	67.89	15.72	1.63	6.48	0.08	2.54	1.81	2.09	1.83	0.15

Well	Depth (ft)	NI	CR	SC	V	BA	RB	SR	ZR	Y	NB	GA	Cu	Zn
		GF	GF	GF	GF	GF	GF	GF	GF	GF	GF	GF	GF	GF
399-1-16C	4	17	37	28	302	577	40	329	175	36	16	20	36	111
399-1-16C	14	15	36	28	284	617	50	336	167	34	16.6	17	44	106
399-1-16C	24	15	33	28	240	628	41	325	161	30	14.6	18	47	93
399-1-16C	29	15	27	21	184	686	69	315	159	29	14.2	15	24	78
399-1-16C	34	15	26	20	167	660	79	316	158	29	14.8	19	26	75
399-1-16C	45	10	34	22	258	634	45	321	165	31	15.1	17	33	93
399-1-16C	48	17	36	19	188	701	60	385	162	27	13	18	37	81
399-1-16C	54	15	24	20	192	587	67	251	161	28	21.9	15	87	90
399-1-17C	10	17	38	30	301	608	40	339	171	35	15.3	22	36	110
399-1-17C	20	17	36	30	269	586	41	328	168	32	15.1	19	37	105
399-1-17C	30	18	48	25	230	645	50	346	165	30	15	15	36	90
399-1-17C	35	19	44	24	242	623	46	333	167	29	15.3	17	50	95
399-1-17C	44	23	46	28	247	635	43	318	168	32	15.9	22	53	96
399-1-18C	4	29	51	12	117	747	67	404	135	21	9.8	14	29	70
399-1-18C	9	19	31	14	125	756	66	401	137	22	10.9	16	23	59
399-1-18C	14	19	37	17	173	745	60	399	139	25	12.2	15	29	75
399-1-18C	20	20	30	14	128	774	64	407	128	22	9.4	14	31	54
399-1-18C	29	18	30	19	212	618	46	336	150	26	14.1	19	25	82
399-1-18C	39	14	34	25	241	627	43	323	163	29	15.9	22	26	97
399-1-18C	44	13	33	21	227	652	45	312	159	29	14.8	19	32	94
399-1-18C	49	15	29	18	226	638	49	294	176	30	17.9	17	33	86
		Up. Rin	Up. Rin	Up. Rin	Up. Rin	Up. Rin	Up. Rin	Up. Rin	Up. Rin	Up. Rin	Up. Rin	Up. Rin	Up. Rin	Up. Rin
399-1-16C	59	15	17	15	161	647	81	235	171	27	18.7	15	27	67
399-1-16C	69	15	14	10	74	827	88	257	199	21	22.2	11	25	42
399-1-16C	80	14	23	15	115	674	91	240	184	29	23.1	13	26	60
399-1-16C	90	16	20	11	108	812	87	260	177	23	19.7	15	19	50
399-1-16C	99	14	60	24	207	669	66	269	198	30	18.5	16	36	76
399-1-16C	104	16	26	13	110	798	83	280	186	26	19.2	18	26	59
399-1-16C	109	21	35	13	97	890	91	307	203	27	21.5	16	31	62
399-1-16C	114	15	21	9	86	825	87	264	158	19	18.4	17	19	44
399-1-17C	55	14	22	18	162	689	71	254	180	28	20.3	17	41	76
399-1-17C	65	28	48	18	133	605	80	219	189	29	20.2	16	35	63
399-1-17C	75	19	28	20	157	653	89	242	210	32	27.1	21	45	74
399-1-17C	85	15	25	22	199	601	69	252	182	32	20.6	20	39	83
399-1-17C	94	19	30	15	137	703	87	256	216	30	22.1	16	42	72
399-1-17C	104	25	39	19	176	623	74	243	208	31	26.3	16	43	80
399-1-18C	58	23	25	20	163	691	68	246	171	28	20.9	16	64	82
399-1-18C	69	11	20	17	177	624	75	236	182	30	20.1	16	32	74
399-1-18C	80	13	25	18	186	636	75	250	186	31	20.9	20	66	81
399-1-18C	89	20	30	14	139	665	73	229	174	28	19.6	12	33	72
399-1-18C	99	15	17	12	120	668	86	239	171	25	21.5	17	34	63
399-1-18C	109	16	25	12	104	723	87	258	184	25	20.4	15	27	60
399-1-18C	119	15	15	11	84	885	87	308	207	25	18.2	12	102	60
399-1-18C	129	65	21	13	143	777	71	282	211	28	18	14	39	68
399-1-18C	139	13	27	18	223	719	69	278	192	32	18.5	20	39	100
399-1-18C	149	14	33	31	190	793	39	258	367	76	44.6	25	30	166
		Low .F	Low .F	Low .F	Low .F	Low .F	Low .F	Low .F	Low .F	Low .F	Low .F	Low .F	Low .F	Low .F
399-1-16C	144	30	51	14	125	1046	111	330	200	31	25.4	24	124	110
399-1-16C	169	29	47	14	144	573	92	212	222	35	28.2	25	46	96
399-1-17C	134	27	53	13	125	1014	112	326	210	33	26.7	23	136	118
399-1-17C	159	25	39	14	144	801	82	262	260	31	24.1	20	57	88

Table 3-2. Quantitative Results of ICP/MS Analyses.

Rare Earth and trace element values (ppm)

Well	Depth (ft)	La	Ce	Pr	Nd	Sm	Eu	Gd	Tb	Dy	Ho	Er	Tm	Yb	Lu	ΣREEs	Th	Y	Hf	Ta
Glaciofluvial																				
399-1-16C	4	25.40	51.50	6.34	25.45	4.90	1.45	4.02	0.63	4.35	0.84	2.43	0.40	2.19	0.34	130.2	5.46	25.33	2.35	1.11
399-1-16C	14	24.95	52.24	6.92	28.74	5.96	1.89	5.24	0.85	5.93	1.18	3.38	0.55	3.17	0.49	141.5	5.12	34.35	3.85	1.33
399-1-16C	29	25.13	51.18	6.47	25.94	5.16	1.54	4.22	0.68	4.67	0.92	2.60	0.43	2.47	0.38	131.8	5.51	26.92	2.96	1.28
399-1-16C	45	25.59	52.38	6.77	27.15	5.80	1.77	5.18	0.82	5.48	1.08	3.10	0.51	2.83	0.45	138.9	5.51	32.11	3.60	1.26
399-1-17C	20	23.56	48.78	6.34	26.52	5.59	1.78	4.99	0.82	5.59	1.12	3.12	0.49	2.91	0.46	132.1	4.53	35.66	3.63	0.93
399-1-17C	30	25.40	51.47	6.62	26.91	5.42	1.67	4.61	0.75	5.04	1.01	2.85	0.46	2.69	0.42	135.3	5.61	31.69	3.21	1.02
399-1-17C	44	23.07	47.53	6.21	25.72	5.43	1.72	4.84	0.79	5.39	1.07	3.05	0.49	2.87	0.45	128.6	4.76	33.93	3.59	1.12
	average:	24.73	50.73	6.52	26.63	5.46	1.69	4.73	0.76	5.21	1.03	2.93	0.47	2.73	0.43	134.06	5.21	31.43	3.31	1.15
	σ:	1.00	1.84	0.26	1.12	0.36	0.15	0.47	0.08	0.55	0.12	0.33	0.05	0.32	0.05	4.71	0.42	3.89	0.52	0.15
Upper Ringold Formation																				
399-1-16C	59	28.57	54.84	6.79	26.36	4.96	1.30	4.06	0.66	4.53	0.88	2.54	0.43	2.45	0.39	138.8	8.71	26.92	3.51	1.82
399-1-16C	80	30.73	58.52	7.07	26.14	4.81	1.19	3.92	0.63	4.24	0.82	2.43	0.40	2.32	0.35	143.6	9.70	26.65	3.37	1.96
399-1-16C	99	27.26	53.18	6.76	26.43	5.10	1.43	4.35	0.68	4.60	0.92	2.66	0.41	2.45	0.37	136.6	6.99	31.64	3.44	1.49
399-1-17C	65	27.99	53.34	6.53	24.36	4.67	1.17	3.83	0.61	4.07	0.79	2.28	0.36	2.14	0.34	132.5	8.15	27.69	3.12	1.77
399-1-17C	85	28.84	56.04	7.22	28.54	5.53	1.54	4.88	0.78	5.21	1.03	2.93	0.49	2.77	0.43	146.2	7.24	34.73	3.77	1.41
399-1-17C	104	32.68	62.69	7.83	30.60	5.91	1.57	5.11	0.79	5.37	1.05	2.90	0.49	2.80	0.42	160.2	7.65	35.59	3.33	1.50
	average:	29.34	56.43	7.03	27.07	5.16	1.36	4.36	0.69	4.67	0.92	2.62	0.43	2.49	0.38	142.96	8.07	30.54	3.42	1.66
	σ:	2.00	3.64	0.46	2.18	0.47	0.17	0.53	0.08	0.52	0.11	0.26	0.05	0.25	0.04	9.77	1.01	4.02	0.22	0.22
Lower Ringold Formation																				
399-1-16C	144	35.14	69.18	8.38	31.48	5.54	1.45	4.33	0.67	4.33	0.83	2.39	0.40	2.27	0.34	166.7	9.14	27.22	3.10	1.58
399-1-17C	134	36.54	73.53	8.62	32.01	5.84	1.53	4.55	0.68	4.37	0.84	2.36	0.39	2.30	0.35	173.9	9.05	29.98	2.97	1.30
	average:	35.84	71.35	8.50	31.75	5.69	1.49	4.44	0.68	4.35	0.84	2.38	0.40	2.29	0.35	170.33	9.10	28.60	3.03	1.44

Chondrite Normalized Values

Well	Depth (ft)	La	Ce	Pr	Nd	Sm	Eu	Gd	Tb	Dy	Ho	Er	Tm	Yb	Lu	La/Yb
Glaciofluvial																
399-1-16C	4	76.98	59.54	51.96	40.40	24.50	18.86	14.61	12.04	12.73	11.10	10.78	12.38	9.95	10.10	7.74
399-1-16C	14	75.60	60.39	56.71	45.62	29.79	24.51	19.07	16.38	17.33	15.56	15.03	17.06	14.42	14.35	5.24
399-1-16C	29	76.16	59.17	53.04	41.17	25.82	19.94	15.33	13.11	13.66	12.05	11.57	13.37	11.24	11.07	6.78
399-1-16C	45	77.55	60.56	55.52	43.09	28.98	23.04	18.83	15.81	16.01	14.17	13.78	15.82	12.86	13.17	6.03
399-1-17C	20	71.40	56.39	51.95	42.10	27.95	23.08	18.16	15.68	16.36	14.67	13.89	15.43	13.24	13.43	5.39
399-1-17C	30	76.98	59.50	54.29	42.71	27.10	21.62	16.75	14.41	14.73	13.32	12.66	14.34	12.22	12.24	6.30
399-1-17C	44	69.91	54.95	50.89	40.82	27.14	22.35	17.62	15.17	15.76	14.12	13.57	15.24	13.03	13.19	5.36
	average:	74.94	58.64	53.48	42.27	27.32	21.91	17.19	14.66	15.23	13.57	13.04	14.81	12.42	12.51	6.12
	σ:	3.02	2.13	2.11	1.78	1.80	1.95	1.71	1.58	1.61	1.54	1.47	1.57	1.46	1.48	0.91
Upper Ringold Formation																
399-1-16C	59	86.59	63.40	55.62	41.84	24.78	16.82	14.78	12.76	13.24	11.64	11.31	13.33	11.12	11.35	7.79
399-1-16C	80	93.11	67.65	57.96	41.50	24.05	15.40	14.25	12.09	12.38	10.85	10.80	12.40	10.53	10.18	8.84
399-1-16C	99	82.61	61.48	55.41	41.95	25.49	18.60	15.81	13.16	13.44	12.07	11.81	12.91	11.16	10.83	7.40
399-1-17C	65	84.61	61.66	53.48	38.66	23.34	15.19	13.92	11.75	11.89	10.37	10.12	11.35	9.73	9.86	8.71
399-1-17C	85	87.39	64.78	59.14	45.30	27.65	20.00	17.74	15.05	15.23	13.56	13.04	15.20	12.58	12.62	6.95
399-1-17C	104	99.04	72.47	64.21	48.57	29.56	20.33	18.58	15.18	15.71	13.80	12.88	15.27	12.71	12.48	7.79
	average:	88.92	65.24	57.64	42.97	25.81	17.72	15.84	13.33	13.65	12.05	11.66	13.41	11.30	11.22	7.91
	σ:	6.07	4.21	3.79	3.46	2.36	2.25	1.92	1.47	1.53	1.40	1.15	1.56	1.16	1.15	0.74
Lower Ringold Formation																
399-1-16C	144	106.48	79.97	68.72	49.97	27.71	18.80	15.74	12.96	12.67	10.91	10.64	12.44	10.33	10.14	10.31
399-1-17C	134	110.73	85.00	70.64	50.81	29.18	19.92	16.56	13.02	12.78	11.09	10.47	12.27	10.47	10.26	10.58
	average:	108.60	82.49	69.68	50.39	28.44	19.36	16.15	12.99	12.73	11.00	10.56	12.36	10.40	10.20	10.44
Chondrite Normalizing values (Nakamura, 1974)		0.330	0.865	0.122	0.630	0.200	0.077	0.275	0.052	0.342	0.076	0.225	0.032	0.220	0.034	

4.0 PRELIMINARY HYDROFACIES DEFINITION IN THE 300 AREA

New methodologies for sampling and monitoring contaminant movement have been developed and ground water modeling codes have become more robust with regard to dimensionality, size, speed of computation, and treatment of flow and transport processes during the past decade (IGWMC 1989; NRC 1990). To maximize usage of these methodologies and modeling codes, it was necessary to document aquifer heterogeneities in a hydraulically meaningful fashion. The technique used by the project team was to identify fundamental, three-dimensional aquifer elements termed hydrofacies. Identification of such aquifer heterogeneities are basic to all hydrogeologic studies and must be undertaken in association with the sampling, monitoring, analysis, and numerical modeling of contaminant movement in ground water systems to obtain the best results.

Results from our work indicate that hydrofacies maps can be used to guide the placement, monitoring, and testing of future boreholes. However, monitoring of contaminant concentrations and hydraulic testing must be designed so that only one hydrofacies is sampled or tested via a single open interval. If samples are obtained across hydrofacies, the resulting averaged, bulk, or integrated values of contaminant concentrations and hydraulic properties cannot be used in numerical models that treat the hydrofacies as discrete units.

Hydrofacies maps also can aid the interpretation of contaminant concentration data by providing the hydrogeologist with information regarding the relative position of contaminant source, hydrofacies, and open intervals. For example, if a contaminant plume is not of an ideal shape, hydrofacies distributions can assist in determining whether an anomalously high concentration in one area is due to a stagnation zone behind a fine-grained lens or to convergence of flow into a small but continuous high conductivity zone. On the other hand, if an open interval spans a variety of hydrofacies, anomalously low values may be due to relatively fresh water from some uncontaminated, highly conductive zone diluting the sample. The various ways that the combination of hydrofacies and open intervals can be used to understand the concentration data are as numerous as the possible combinations of hydrofacies, open intervals, and relative concentrations.

The hydrofacies delineated on the maps are not simplified block representations of well-defined sediment bodies that occur in the field. Rather, definition of hydrofacies is a way of defining sediment packages (which are variable at a small scale) into units that can be simulated with one representative set of hydraulic parameter distributions at a larger scale. This process of establishing the overall character of a unit is a common procedure for defining units in numerical models. The particular definition of hydrofacies in the 300 Area is unique because macro-scale heterogeneities are derived by building up from small-scale textural data. The blocky nature of the hydrofacies is due to the process of constructing the hydrofacies. Smooth transitions that describe the thinning of units can easily be incorporated into the process.

4.1 DEFINITION OF HYDROLOGIC UNITS (HYDROFACIES)

Hydrofacies are three-dimensional sediment bodies displaying distinct hydraulic properties and, as noted above, will not always clearly overlap with geologically defined lithofacies. One factor that is crucial in controlling the hydraulic performance of a sedimentary unit, though, is the percentage of fine-grained material. Lambe and Whitman (1969) recognized this hydraulic control and noted that "logic and experimental data suggest that the finer particles in a soil have the most influence on permeability." In addition, a number of empirical relationships have been developed that associate the grain size of unconsolidated material to hydraulic conductivity. Perhaps the best known is the Hazen (1910) relationship which states that the hydraulic conductivity is proportional to the square of the grain size larger than the finest 10% of the sample.

Recognizing the importance of the fine-grained sedimentary component to hydraulic behavior, as well as recognizing the: (1) complex nature of sedimentary units in the 300 Area; (2) need to limit the number of hydrofacies (for modelling purposes); and (3) generally poor quality of the grain-size data resulting from use of cable-tool drilling to obtain samples and lack of consistencey of geologic descriptions, we subdivided the 300 Area suprabasalt sediments into four general hydrofacies. These hydrofacies are defined on the basis of grain size and sorting and have some degree of overlap with the lithofacies described earlier in this report.

1. Gravel Hydrofacies (G) - Consists of >80% gravel-sized particles including granules, pebbles, cobbles, and boulders. This hydrofacies includes most of the gravel-rich lithofacies G and CB.

2. Sand Hydrofacies (S) - Consists of >75% sand-sized particles. This hydrofacies corresponds with the sand-rich portions of lithofacies SS.

3. Silt and Clay Hydrofacies (MZ) - Consists of >25% silt- and clay-sized particles. This hydrofacies includes portions of lithofacies G, where silt and clay make up >25% of the sediment; lithofacies SS, where silt and clay make up >25% of the sediment; and lithofacies MZ and MZS.

4. Sandy Gravel Hydrofacies (SG) - Consists of any zone not defined by hydrofacies G, S, MZ. This broad definition of the SG hydrofacies is a weakness of the method used to delineate hydrofacies and includes sediments with the following textural threshold values: units composed of <80% gravel, <75% sand, and <25% silt and clay. Using the above threshold values, a sandy gravel hydrofacies includes units composed of: 70% gravel and 30% sand, 50% gravel and 50% sand, and 30% gravel and 70% sand (note that in all of these cases, it is likely that the hydraulic conductivity of the sand component is most representative of the unit). Alternatively, a SG hydrofacies also could include units composed of 76% sand and 24% clays and silt, which obviously could be described as a silty or clayey sand. We did not find any significant sedimentary material of this nature in the 300 Area deposits and only found two small zones where the definition was inappropriate. This hydrofacies includes portions of all lithofacies described from and near the 300 Area.

Definition of hydrofacies should also be based on the degree of cementation and the nature of sediment packing. However, at present, the data required to incorporate these factors into the hydrofacies definition are not available. Future work should use grain shape, cementation data, and intact samples to compile estimates of these important parameters.

4.2 CONSTRUCTION OF HYDROFACIES AND HYDROFACIES MAPS

Hydrofacies and hydrofacies maps were constructed using geologic data from 42 of the 53 drill logs available from the 300 Area. Drill logs from the remaining 11 boreholes were either unavailable or contained inadequate sediment descriptions for hydrofacies delineation. Of the 42 boreholes used for hydrofacies delineation, 10 extended deeper than 290 ft (89 m) above mean sea level while seven of the boreholes were shallower than 330 ft (101 m).

The percentages of gravel, sand, silt, and clay from each of the 42 boreholes examined were calculated for the following intervals in feet above mean sea level: 200 to 250, 250 to 270, 270 to 290, 290 to 310, 310 to 320, 320 to 330, 330 to 340, and 340 to 350. These intervals reflect data density and sedimentary variability. Subsequently, these sediment percentages were used to determine the three-dimensional extent of the included hydrofacies by: (1) constructing maps of the percentage of each grain size (i.e., G, S, MZ) for each of the above intervals; (2) constructing slice maps that illustrate the lateral distribution of each hydrofacies for each interval; and (3) overlaying successive slice maps to construct the hydrofacies vertically. The final product of step 3 depicts the spatial distribution of hydrofacies (Figures 4-1 through 4-8).

4.3 INTERPRETATION OF HYDROFACIES MAPS

The following example uses the gravel hydrofacies map (Figure 4-1) to illustrate how the hydrofacies maps depicted in Appendix B are to be interpreted. Starting at the 350-ft (107-m) contour line that intersects the west edge of the map and working northward from that contour line, one observes hydrofacies zones labeled 10, 20, and 30, respectively. These zones delineate gravel bodies that extend below the 350-ft (107-m) datum and are 10, 20, and 30 ft (3, 6, 9 m) thick, respectively. The 350-ft (107-m) contour identifies the bounds of a horizontal datum (a plateau) from which the thick-ness of the gravel hydrofacies can be measured. Changes in hydrofacies thickness are defined by dashed lines representing elevation contours on the bottoms of hydrofacies bodies. Dashed elevation contours merge locally where hydrofacies are stacked vertically. For example, in the case described above, the 10- and the 30-ft (3- and the 9-m) thicknesses are adjacent to one another. In such areas, the change in thickness is so abrupt that, at the scale of the map, the transition is essentially vertical. Elevation contour lines defining the tops of hydrofacies also merge locally; therefore, contour labels are always written with the top of the label oriented in the direction of the plateau for the indicated elevation. This convention is intended to prevent confusion concerning which labels are associated with which plateaus.

The thickness of the tongues and interbeds not vertically connected to the main body of the hydrofacies cannot be presented on the primary hydrofacies map due to intervening thicknesses of different hydrofacies.

[NOTE: The main body of the hydrofacies is the largest portion of the hydrofacies that can be shown on one map.] Therefore, where tongues or interbeds are present and vertically separated from the main body by an intervening facies, an accessory map is required (Figure 4-2). Accessory maps are made in the same manner as the primary maps. Vertical continuity between the hydrofacies on the accessory map and the main hydrofacies body on the primary are indicated with a stipple pattern. For example, on the gravel hydrofacies accessory #1 (Figure 4-2), the northernmost gravel body is connected to the main gravel hydrofacies in stippled regions. Examination of other hydrofacies maps reveals that the easternmost portion of the gravel hydrofacies is a tongue overlain by a sandy gravel hydrofacies. The sandy gravel hydrofacies is, in turn, overlain by the gravel hydrofacies represented on the primary map. In addition, the stippled portion indicates an additional 10 ft (3 m) of gravel is connected to the overlying 30-ft (9-m) thick main gravel body, producing a total gravel thickness of 40 ft (12 m).

Checks for internal consistency of hydrofacies were conducted during construction of the hydrofacies maps. These checks entailed overlaying separate hydrofacies to verify that specific regions had not been defined by two hydrofacies. Primary and accessory hydrofacies maps depict a number of interconnected bodies of similar sediment sizes. These maps portray the vertical and lateral distribution of zones having similar hydraulic properties and can be input into numerical models.

4.4 APPLICATION OF HYDROFACIES AND HYDROFACIES MAPS TO NUMERICAL MODELING

Hydrofacies can readily be input into numerical models. This should be done sequentially as follows. First, the maximum number of layers to be included at any location in the numerical model is established from inspection of the hydrofacies maps (examination of Figure 4-9 suggests a minimum of four layers for the section presented). The number of layers also depends on the memory capacity of the computer. Next, the modeler works from one side of the area of interest to the other with the hydrofacies map in hand and defines grid elements of reasonable size based on the detail required to simulate the flow system. In addition to the nature of the hydrofacies, the steepness of the hydraulic gradient, location of aquifer stresses (e.g., pumping, waste discharge), and purpose of the study are considered when defining element size. If the hydrofacies are thick and uniform over a portion of the simulated area but a number of aquifer stresses are present, a high density of elements would be defined. In areas of the mesh that are peripheral to the area of interest and stresses are not present, only a few elements would be required both laterally and vertically, even if the hydrofacies are complex. In areas where the hydrofacies are complex and near the zone of interest, numerous elements may be defined, even if the imposed stresses are few. A dense mesh in the area of interest allows a more realistic simulation of the influence of the aquifer heterogeneities on the character of the flow field. Such gridding of elements would be appropriate in areas where contaminant transport is being simulated. Finally, if the hydrofacies are complex and in a zone where stresses are being applied, the most detailed definition of elements would be required.

4.5 ESTIMATION OF HYDRAULIC CONDUCTIVITY OF THE HYDROFACIES

Estimating the values of hydraulic parameters of geologically derived lithofacies is a necessary prerequisite during development of an accurate hydrogeologic model. Two sources of data have been utilized to estimate storage coefficients and hydraulic conductivities for the hydrofacies. These two data sources are aquifer tests and grain size analyses.

4.5.1 Hydraulic Conductivity Values Obtained from Aquifer Testing for Hydrofacies

The results of 10 of 14 aquifer tests in the 300 Area were not deemed suitable to define parameter values for the hydrofacies either because of inadequate documentation of the test conditions or because the open interval spanned more than one hydrofacies. The remaining four tests (from boreholes 399-1-18A, 399-1-13, 399-1-16A, and 399-1-16C) yielded the most representative data available for the 300 Area hydrofacies. The open intervals tested in these wells occurred within gravel (G), sandy-gravel (SG), sand (S), and silt and clay (MZ) hydrofacies, respectively. Table 4-1 lists best estimates of the hydraulic conductivities of the sediments near each of the four wells. Given the limited data on which Table 4-1 is based, each of these values was considered as one value in a range of characteristic hydraulic conductivity values for the tested hydrofacies.

Saturated thickness must be defined before hydraulic conductivity can be calculated. Three values of hydraulic conductivity calculated from each open interval are presented in Table 4-1. These values were calculated by assuming that the saturated thickness: (1) is represented by the open interval; (2) corresponds with the interpreted hydrofacies thickness plus the thickness of adjacent hydrofacies of higher hydraulic conductivity; and (3) is the difference between the pre-test static water level and the top of the deepest silt and clay hydrofacies. The hydraulic conductivities based on hydrofacies thickness appear most appropriate since: (1) they account for the hydraulic conductivity of adjacent conductive hydrofacies; (2) they are within the expected range for their respective grain sizes (Freeze and Cherry 1979); and (3) hydraulic conductivity in general decreases from gravel to sandy gravel to sand to silt. The expected hydraulic conductivity ranges for sediment sizes overlap because (in addition to grain size variations) sorting, packing, and the degree of cementation also influence hydraulic conductivity. Hydraulic conductivities reported for each hydrofacies (Table 4-1) are first approximations because of the limited hydraulic data available and the inherent variability of grain size distribution, sorting, packing, and lithification within each hydrofacies. Further laboratory and (particularly) field testing must be conducted to better establish the range of hydraulic conductivities that are representative of each hydrofacies.

4.5.2 Specific Yield and Hydraulic Conductivity Values Obtained from Hydrofacies Grain Size Analysis

Estimates of specific yield and hydraulic conductivity from sediment samples require that the samples be intact. However, because of the nature of the sediments at Hanford, it often is difficult to acquire intact samples during drilling. In the absence of intact samples, it may be possible to use

grain size data from disaggregated samples to stimate specific yield and hydraulic conductivity. This section outlines efforts made in estimating these hydraulic parameters from grain size data.

Hydraulic conductivity determined from grain size distributions and permeameter tests must be used with caution because it does not reflect the interconnectedness of high hydraulic conductivity zones at field scales and so is typically more applicable to small-scale hydraulic properties than to large-scale aquifer characteristics. As a result, efforts were made to determine the relationships between grain size-derived hydraulic conductivities and hydraulic conductivities derived from field-scale aquifer tests. The successful correlation between grain size- and field test-derived hydraulic conductivities permits the use of grain size-derived hydraulic parameters as an alternative to expensive field testing.

Grain size textural data were derived from documents and from laboratory analyses of selected borehole samples at WSU's sedimentology laboratory. Grain size distributions from these sources were entered into empirical equations that estimate hydraulic conductivity (Hazen 1910; Masch and Denny 1966; McKee 1979 [Attachment 1]). Originally, the values obtained from these empirical relationships were to have been compared with permeameter-derived values (from both intact and remolded samples), and aquifer test-derived hydraulic conductivities. In this manner, correlable relationships would have been established. Suspension of drilling activities prohibited completion of these tests.

Results presented in Sections 4.5.3 and 4.5.4 reveal that the relationships between small-scale sedimentary textural data and larger-scale parameters cannot be developed from existing samples. This failure largely reflects the weaknesses of cable-tool drilling as a method of geologic and hydrogeologic data acquisition in coarse-grained (i.e., sand- and gravel-sized) sediments and sedimentary rocks. First, samples had been contaminated by sediments eroded from the borehole wall during the drilling and sampling process; thus, specific borehole depths for the sediment samples often were in doubt. In addition, the grains often were fragmented in the drilling process (especially when hard tools were employed) resulting in grain size distributions with lower than in situ mean grain diameters. Although some relative textural and compositional aspects of the sediments may have been retained, absolute values of hydraulic properties from these analyses could not be considered reliable. The acquisition of intact samples is vital to study of the 300 Area hydrogeology (and of hydrogeologic studies across the Hanford Site). Procedures used to estimate the hydraulic parameters from sedimentary textural data are discussed in Appendix C. The values obtained from these low quality samples for each hydrofacies are provided.

4.5.3 Specific Yield

Specific yield cannot be determined from available field-scale tests in the 300 Area suprabasalt strata because the tests were single hole tests. Therefore, the specific yield data derived from grain size analyses cannot be verified. The three methods used to estimate specific yields are provided by: Piper et al. (1939), Eckis (1934), and CWRB (1957).

The average specific yield for the silt and clay (MZ) hydrofacies was (unexpectedly) higher than the specific yield of coarse-grained materials for all the estimation methods. Estimated specific yields using Piper et al. (1939) method were consistently higher than estimated specific yields derived from the Eckis (1934) and CWRB (1957) method. This may partially be due to the use of different representative grain sizes as the basis for the estimate or the limited number of samples considered by Piper et al. (1939).

Specific yield estimates from boreholes 399-1-16C, 399-1-17C, and 399-1-18C were compared with the interpreted hydrofacies and are presented in Table 4-2. A preferred method for estimating specific yield from grain size data cannot be recommended because specific yield has not been measured at either the laboratory or field scale at Hanford. Values of specific yield calculated from grain size distributions do not vary substantially across the spectrum of facies. Neither are there consistent trends in specific yield of the facies within or between the methods. It was concluded that the fragmented nature of the samples caused loss of both the absolute and relative textural nature of the sediments, thus rendering them of little use in estimations of specific yield. Again, collection of unfragmented samples is imperative to correct this problem.

4.5.4 Hydraulic Conductivity

Hydraulic conductivity values based on methods developed by Hazen (1910), Masch and Denny (1966), and McKee (1979 [Attachment 1]) were estimated from grain size analysis of sediment samples from wells 399-1-16C, 399-1-17C, and 399-1-18C. These samples suffer the same shortcomings as those discussed in the previous section (i.e., fragmentation of original detrital particles and contamination of samples by grains from shallower depths in the hole). Values of hydraulic conductivity were calculated for each sample and grouped by the hydrofacies which occurs at the depth interval where the sample was taken (Table 4-3). The hydraulic conductivities estimated from grain size data were compared with expected ranges of hydraulic conductivity for individual grain size classes reported by Freeze and Cherry (1979). This comparison demonstrates that: (1) estimated values for gravel are below the expected range (probably due to the bias toward small or broken grains in the sample); (2) estimated values for sandy gravel are in the lower to intermediate part of the expected range; (3) values for sand are on the low end of the expected range; and (4) values for silt and clay are on the high end of the expected range. Estimated values for gravel, sandy gravel, and sand hydrofacies are lower than those from aquifer tests; whereas, the estimated values for silt and clay hydrofacies are higher (see Tables 4-1 and 4-3).

The discrepancy between hydraulic conductivities estimated from grain size data and those from aquifer tests and published field-scale tests is probably due to differences not only in the nature, but also in the scale, of the sampling. The grain size estimates are based on small, disturbed samples, whereas the aquifer test values and published ranges represent field-scale values. Bias of the sediment sampling process to smaller grain sizes may explain why hydraulic conductivities for the coarser-grained hydrofacies (G, SG, S) are lower than the field values. For example, during drilling, an unknown portion of larger-sized clasts: (1) are broken into smaller fragments; (2) are lost in the recovery process; or (3) may not fit into sample containers. Subsequent drilling should require intact sediment samples

be obtained. In addition, the very fine grains (i.e., fine silt and clay) may be lost in the bailing and collection process, or as the result of incomplete disaggregation before sieving. This may be the cause of the elevated values of hydraulic conductivity associated with the silt and clay (MZ) lithofacies.

In addition to sampling and scale problems, estimates of hydraulic conductivity based on grain size data do not account for the influences of cementation, grain shape, or packing. During field scale tests, these factors are incorporated into the measurement of hydraulic conductivity.

All of the methods for estimating hydraulic properties from grain size data have inherent limitations due to the general lack of consideration of fine-grained silt and clay when the techniques were being developed. Nevertheless, it appears that the McKee (1979) method (provided as Attachment 1), or an expanded version of the Masch and Denny (1966) method have the most flexibility; and, hence, are better suited for application to the Hanford Site sediments. Lack of calibration of these equations with aquifer tests and permeameter tests has greatly hindered the ability to assess the accuracy of these relationships for reliable estimations of the hydraulic conductivity for the 300 Area sediments.

Figure 4-1. Contoured Isopach Map for Gravel Hydrofacies Bodies in the 300 Area (Main).

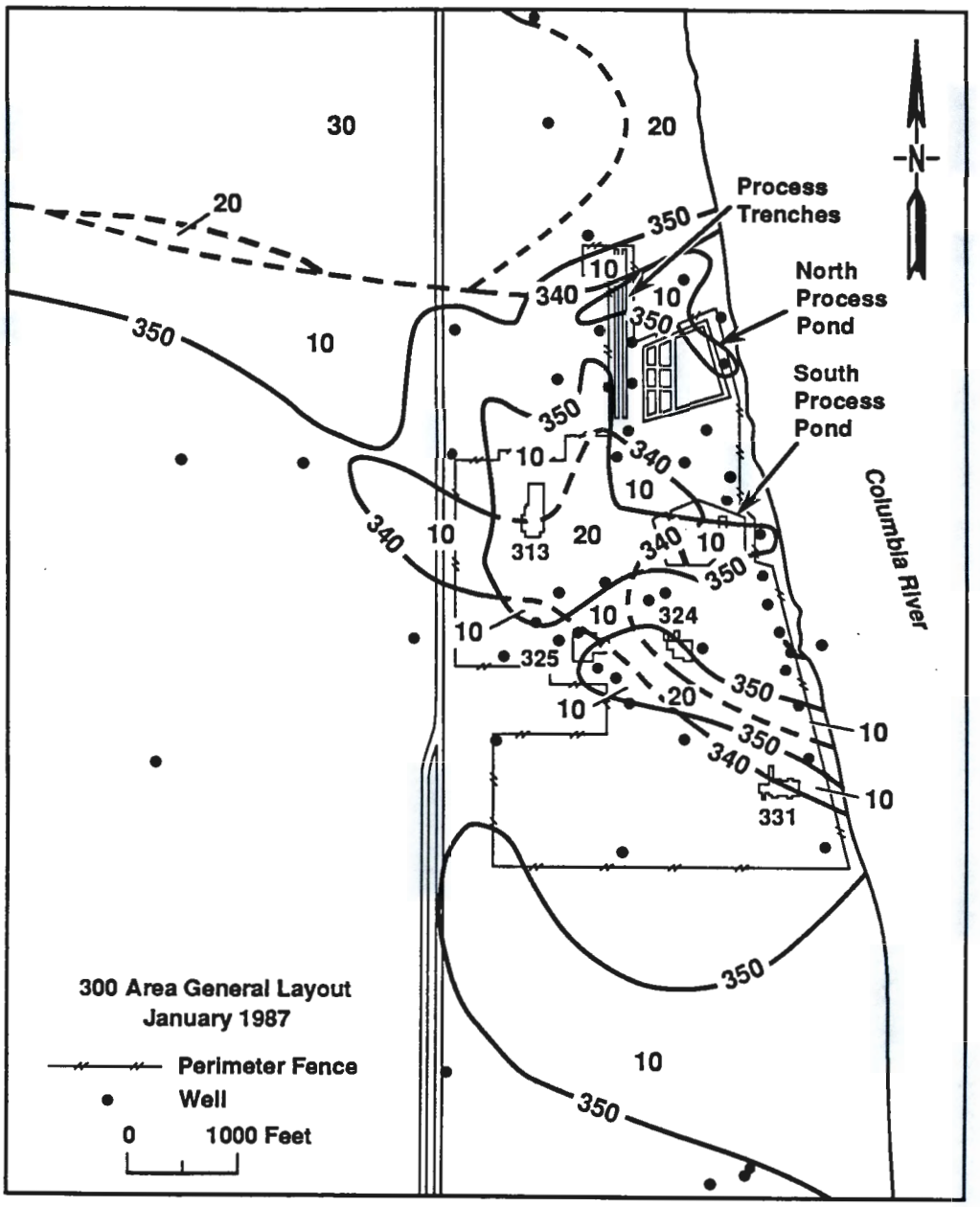

Figure 4-2. Contoured Isopach Map for Gravel Hydrofacies Bodies in the 300 Area (Accessory #1).

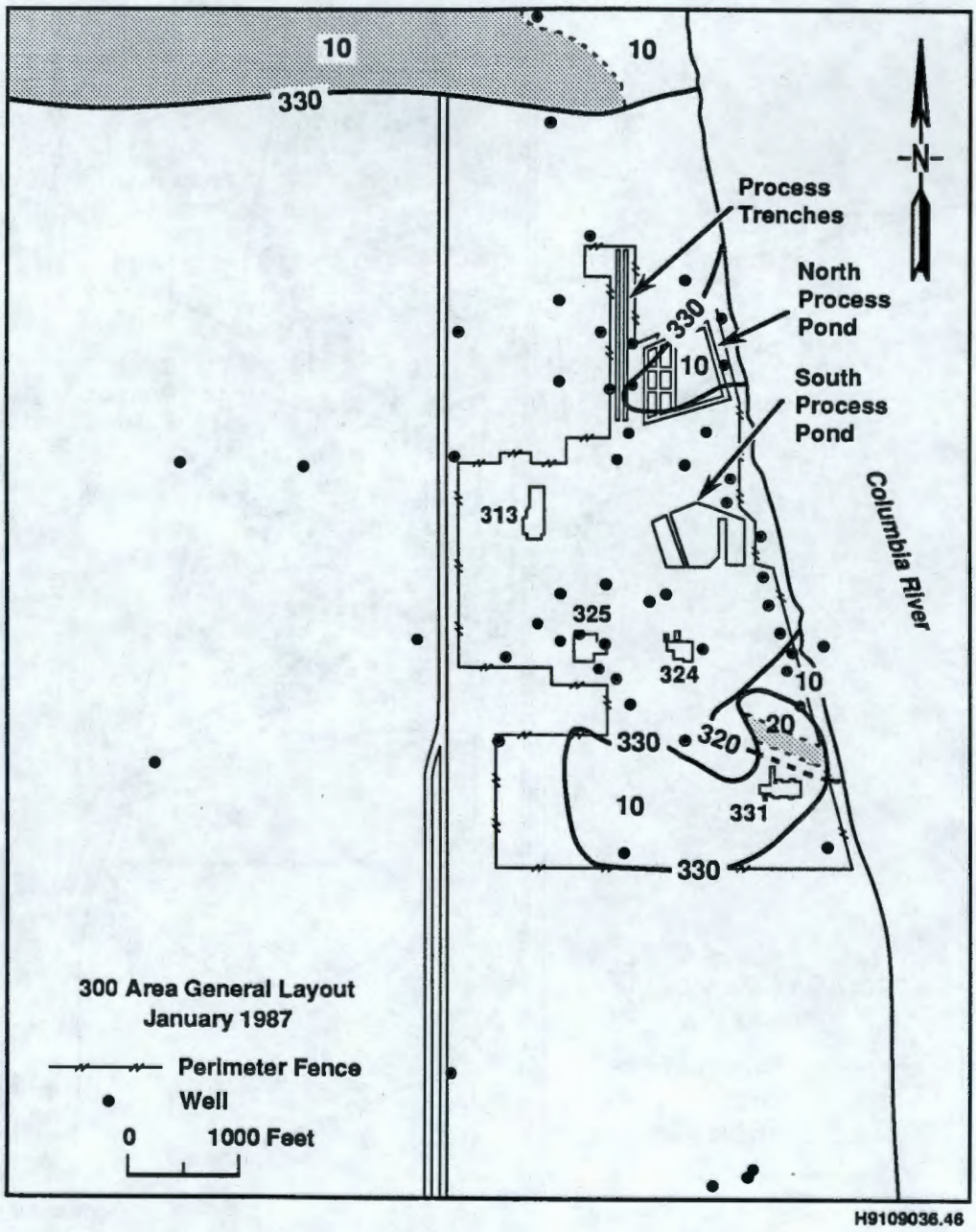

Figure 4-3. Contoured Isopach Map for Gravel Hydrofacies Bodies in the 300 Area (Accessory #2).

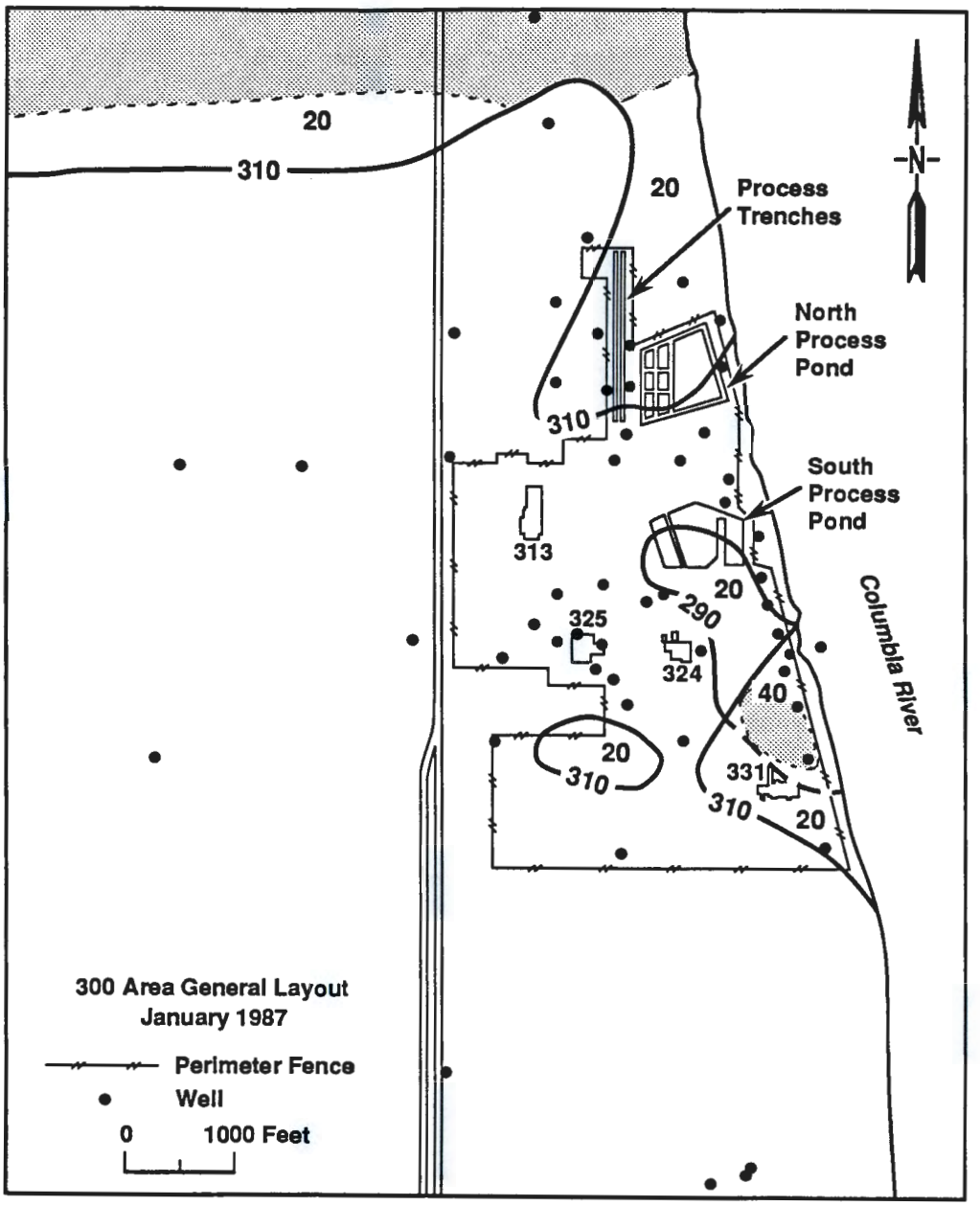

H9109036.39

Figure 4-4. Contoured Isopach Map for Sand Hydrofacies in the 300 Area (Main).

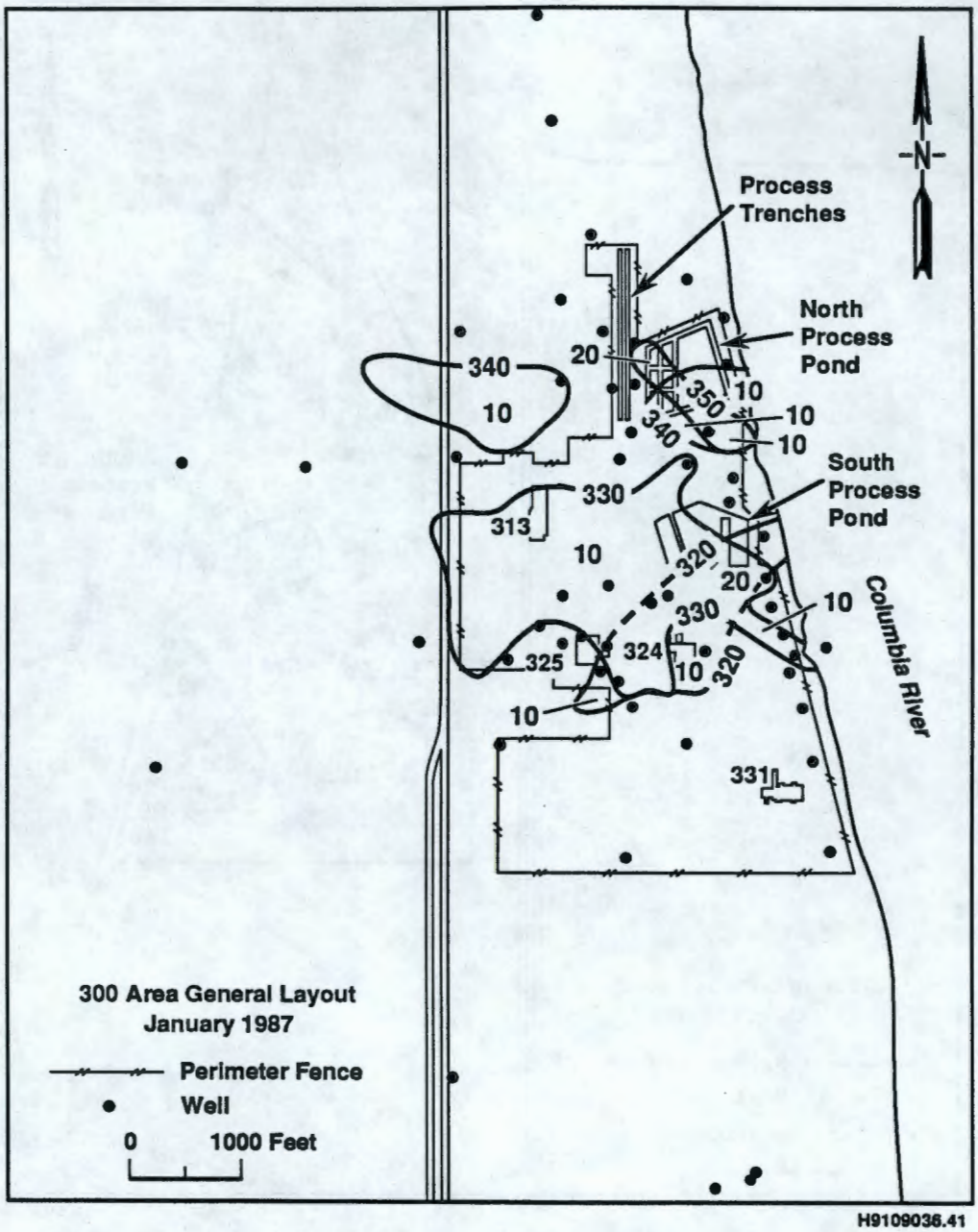

Figure 4-5. Contoured Isopach Map for Sand Hydrofacies in the 300 Area (Accessory #1).

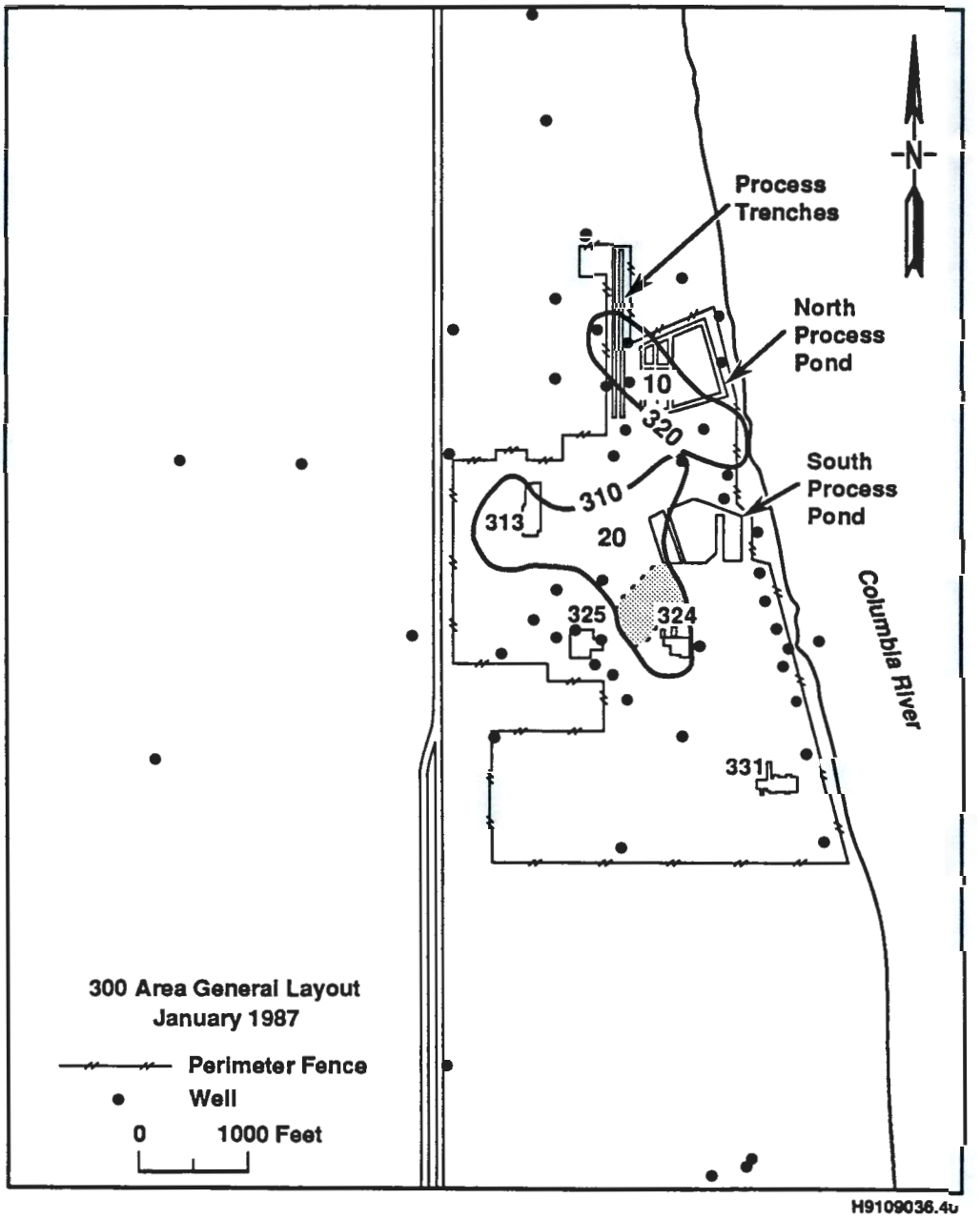

Figure 4-6. Contoured Isopach Map for Mud/Silt Hydrofacies in the 300 Area (Main).

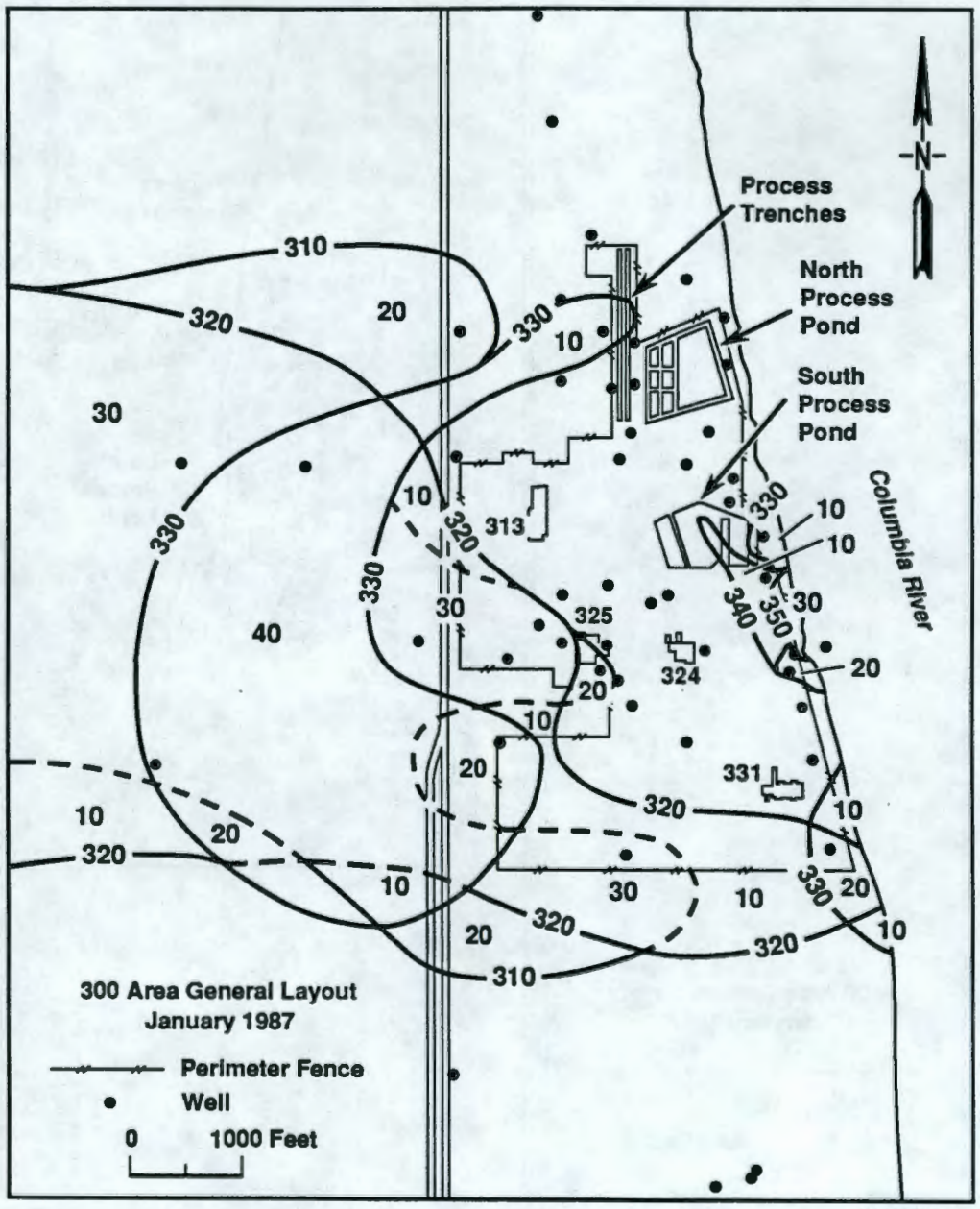

H9109036.42

Figure 4-7. Contoured Isopach Map for Mud/Silt Hydrofacies in the 300 Area (Accessory #1).

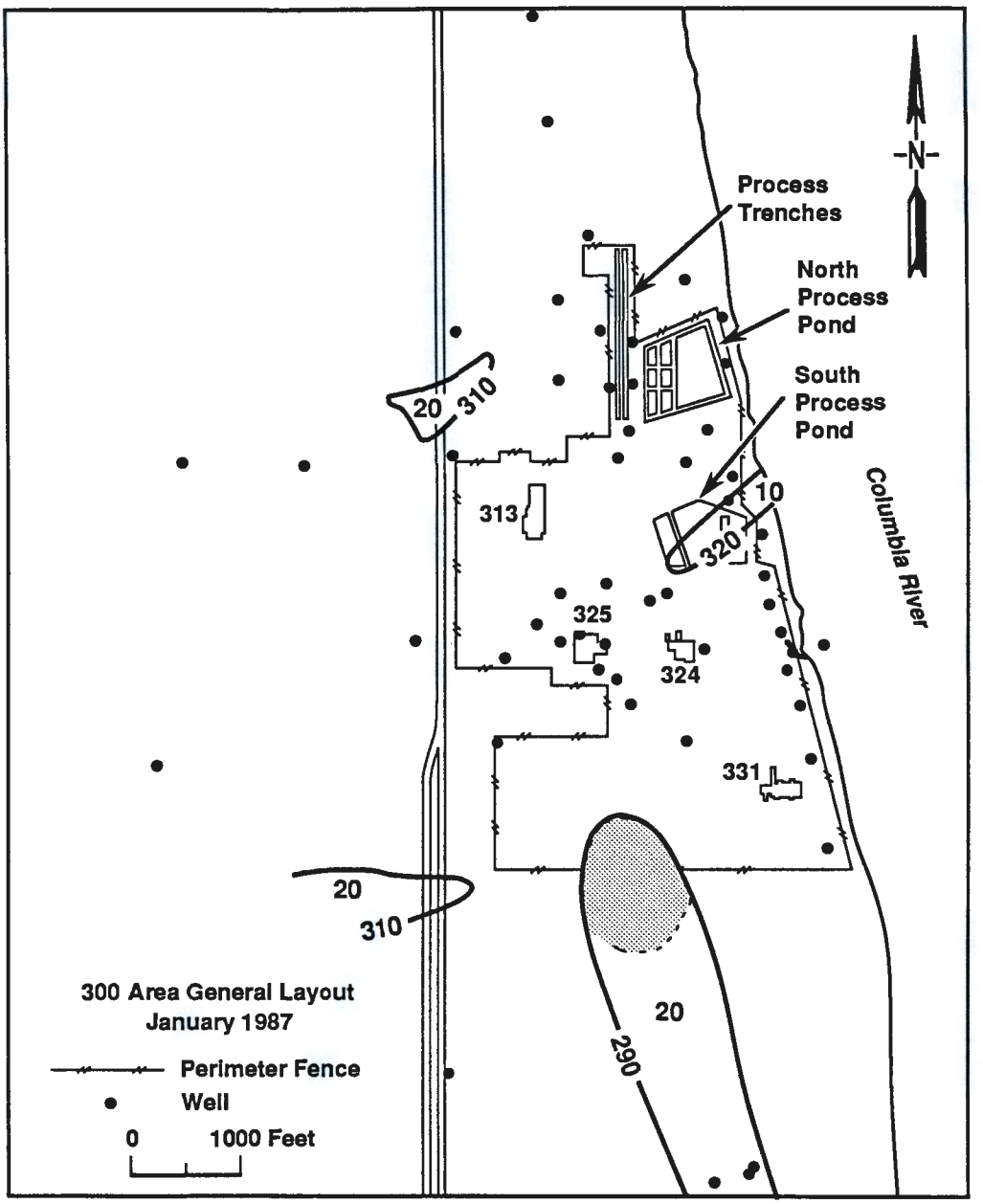

H9109036.43

Figure 4-8. Contoured Isopach Map for Mud/Silt Hydrofacies in the 300 Area (Accessory #2).

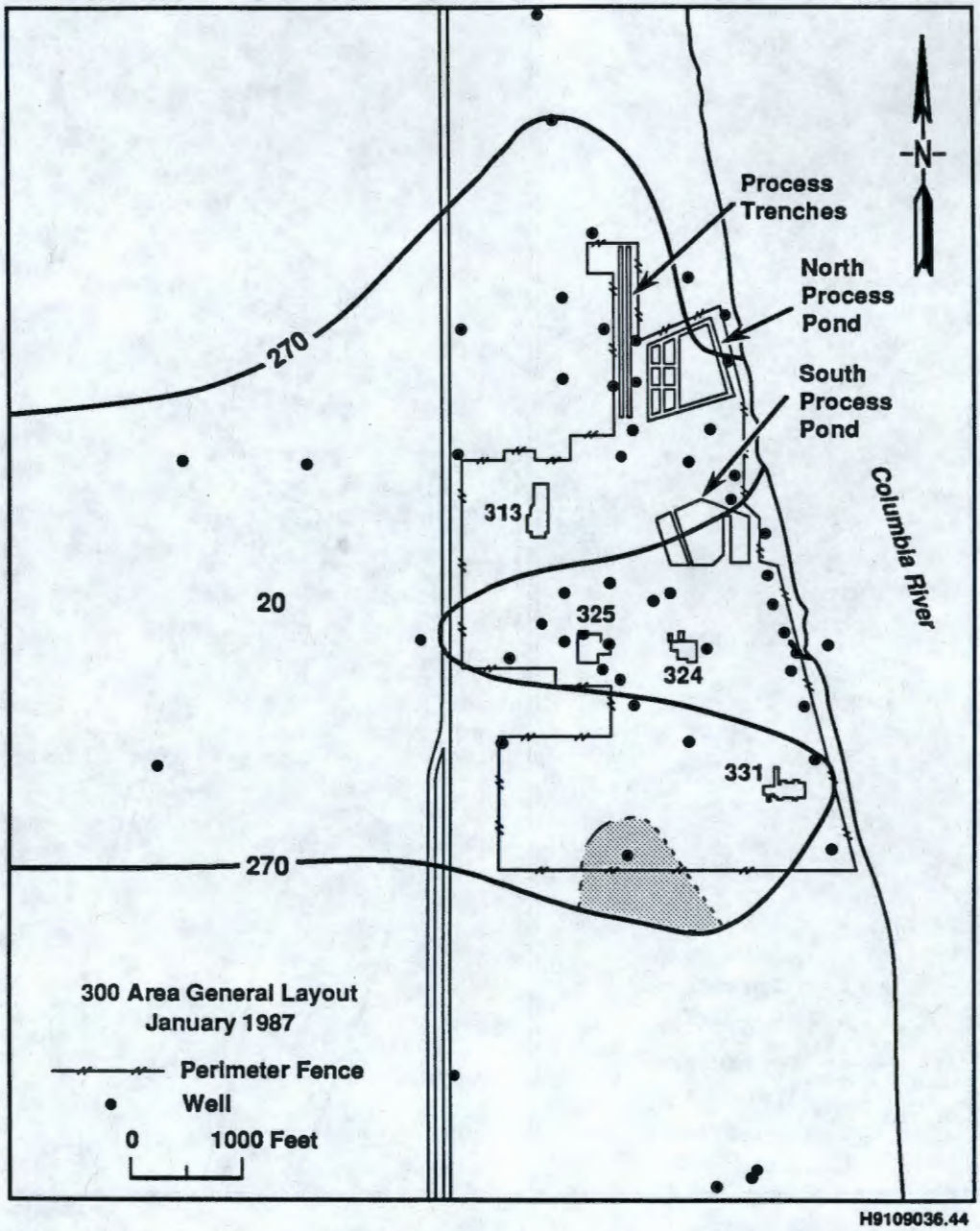

Figure 4-9. Hydrofacies Representative for Numerical Modeling.

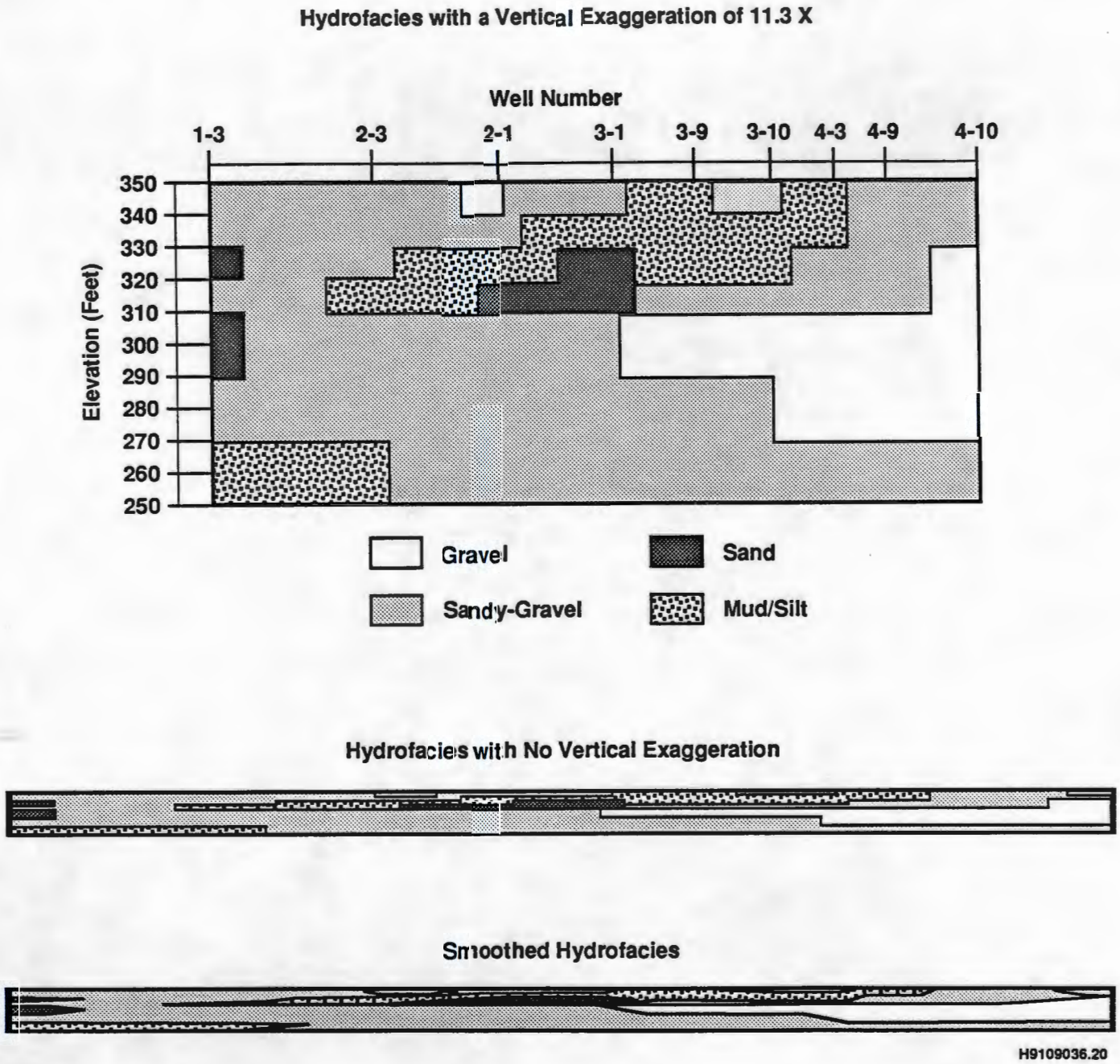

Table 4-1. Hydraulic Conductivities for the Interpreted Hydrofacies as Estimated from Aquifer Tests.

Well	Hydrofacies	Open Interval	Facies	Saturated Thickness	'Typical' Range
3-1-18A	Gravel	8×10^4	4×10^4	2×10^4	10^3 - 10^6
3-1-13	Sandy Gravel	8×10^3	1×10^4	2×10^3	10^1 - 10^5
3-1-16A	Sand	1×10^3	2×10^2	2×10^2	10^0 - 10^4
3-1-16C	Mud/Silt	9×10^0	6×10^{-1}	6×10^{-1}	10^{-3} - 10^1

NOTES:

All values in ft/d.

Transmissivity values are estimated from aquifer test data.

Hydraulic conductivity is calculated by dividing the transmissivity by the aquifer thickness. The appropriate aquifer thickness isnot obvious, hence, three different thicknesses are used.

Open interval values are based on the length of the screened interval.

Facies values are based on the thickness of the corresponding hydrofacies and includes the thickness of adjacent hydrofacies that have a hydraulic conductivity equal to or greater than the tested hydrofacies.

Saturated thickness values are based on the distance between the pre-test, static water level, and the interpreted location of the basal mud-silt hydrofacies.

Typical range values are as reported by Freeze and Cherry (1979, p. 29).

Table 4-2. Hydrofacies Specific Yield Values Estimated from Grain Size Data for Samples from Three Wells.

	Gravel			Sandy Gravel			Sand			Mud/Silt		
	Eckis	Piper	CWRB	Eckis	Piper	CWRB	Eckis	Piper	CWRB	Eckis	Piper	CWRB
	0.28	0.35	0.25	0.18	0.35	0.25	0.26	0.23	0.27	0.26	0.24	0.27
	0.28	0.35	0.25	0.28	0.35	0.25	0.31	0.32	0.28	0.26	0.24	0.27
	0.28	0.35	0.25	0.32	0.33	0.28	0.30	0.35	0.25	0.32	0.27	0.29
	0.29	0.34	0.25	0.27	0.35	0.25	0.25	0.29	0.24	0.30	0.32	0.29
	0.28	0.35	0.25	0.30	0.34	0.26	0.32	0.35	0.34	0.27	0.17	0.27
	0.27	0.35	0.25	0.29	0.35	0.25	0.32	0.32	0.33	0.11	0.13	0.11
	0.28	0.35	0.25	0.31	0.31	0.28	0.28	0.31	0.28	0.18	0.16	0.18
	0.31	0.35	0.28	0.29	0.35	0.25	0.26	0.30	0.26	0.22	0.16	0.23
	0.27	0.35	0.23	0.28	0.35	0.25				0.28	0.17	0.25
				0.32	0.35	0.32				0.31	0.22	0.29
				0.33	0.35	0.32						
				0.28	0.35	0.31						
				0.31	0.35	0.27						
arith	0.2822	0.3489	0.2511	0.2977	0.3446	0.2723	0.2875	0.3087	0.2813	0.2510	0.2080	0.2450
max	0.3100	0.3500	0.2800	0.3300	0.3500	0.3200	0.3200	0.3500	0.3400	0.3200	0.3200	0.2900
min	0.2700	0.3400	0.2300	0.2700	0.3100	0.2500	0.2500	0.2300	0.2400	0.1100	0.1300	0.1100
var	1.3E-04	9.9E-06	1.4E-04	3.3E-04	1.3E-04	7.1E-04	7.2E-04	1.3E-03	1.1E-03	3.8E-03	3.2E-03	3.1E-03
std	0.0113	0.0031	0.0120	0.0180	0.0115	0.0266	0.0268	0.0359	0.0337	0.0616	0.0567	0.0554
n	9	9	9	13	13	13	8	8	8	10	10	10

arith = arithmetic mean
max = maximum value
min = minimum value
var = variance of data
std = standard deviation of data
n = number of samples.

Table 4-3. Hydrofacies Hydraulic Conductivity Values Estimated from Grain Size Data.

	Gravel			Sandy Gravel			Sand			Mud/Silt		
	Hazen	Denny	McKee	Hazen	Denny	McKee	Hazen	Denny	McKee	Hazen	Denny	McKee
	2.4	10	18.4	190.0	12	165.9	1.8	11	19.7	1.4	10	7.7
	4.2	10	33.2	154.0	10	127.0	2.8	18	9.8	1.6	10	17.3
	19.3	10	83.5	7.3	10	23.7	7.8	18	19.3	1.1	11	17.5
	1.6	10	21.1	33.6	12	54.0	8.4	16	13.1	2.8	9	8.7
	6.8	10	118.0	11.1	9	36.5	7.8	9	11.0	1.1	9	11.9
	11.1	10	51.9	102.0	6	79.8	25.4	10	17.4	0.7	9	20.0
	102.0	15	59.6	88.6	16	65.1	1.2	22	11.0	41.2	35	7.7
	125.0	19	59.6	30.0	9	55.3	25.4	28	5.9			5.9
	1,417.0	19	607.0	5.5	9	41.4	44.3	28	33.5			6.8
	354.0	260	306.0	8.4	9	26.6						22.6
				16,035.0	24	3,233.0						26.8
				8.72	400	386.0						
geom	26.26	16.40	73.09	70.05	15.75	92.38	7.64	17.21	13.97	2.16	11.59	12.21
max	1,417.0	260	607.0	16,035.0	400	3,233.0	44.3	22	33.5	41.3	35.	26.8
min	1.6	10	18.4	5.5	9	23.7	1.2	9	5.9	0.7	9	5.9
adev	282.46	44.54	128.27	2,428.92	59.22	483.91	11.8	7.11	6.08	9.76	6.20	6.31
n	10	10	10	12	12	12	9	9	9	7	7	11

geom = geometric mean
max = maximum value
min = minimum values
adev = average deviation (mean absolute deviation) (Press et al. 1986)
n = number of samples

Typical range of hydraulic conductivity values (Freeze and Cherry 1979)

Gravel	10^3 - 10^6
Sandy gravel	10^1 - 10^5
Sand	10^0 - 10^4
Mud/Silt	10^{-3} - 10^1

5.0 PRELIMINARY MODELING OF GROUND WATER FLOW IN THE HANFORD 300 AREA

This chapter presents a preliminary model for ground water flow in the 300 Area using the existing steady-state version of the coupled fluid, energy, and solute transport (CFEST) computer code (Gupta et al. 1987) and the inverse version of the same code, CFEST-INV. The modeling presented here estimates hydraulic conductivities for hydrofacies using projected hydrofacies geometries and preexisting hydraulic head data.

By definition, a deterministic or forward model is one in which the material properties and boundary conditions are specified by the user and the resulting head distribution is calculated. In the process of deterministic modeling, the modeler first calibrates the model. Calibration is the process of adjusting material properties and, if necessary, boundary conditions until the heads calculated by the model match those measured in the field. Calibration yields more representative values for the estimated parameters because the calibration process integrates data which describe the system. Individual field measurements are more sensitive to local conditions than to system conditions. Calibration is a tedious and time-consuming process and often is concluded at an arbitrary time based on a qualitative assessment of the match between modeled and measured head and flow rates.

In this study, an inverse model of the 300 Area was executed to estimate the value of hydraulic conductivities of hydrofacies. An inverse model, in essence, is an automated calibration process. In an inverse model, estimates of the material properties and boundary conditions, and information on the certainty the modeler has in those estimates are input to the code along with the values of heads measured in the field. The code adjusts the material properties and boundary conditions until the difference between the calculated heads and the field measured heads are minimized.

5.1 HYDROGEOLOGIC UNITS USED IN THE MODEL

For the purpose of simulating ground water flow in the 300 Area, it is most useful to describe the glaciofluvial sediments in the 300 Area as hydrofacies rather than formations because hydrofacies are defined by sedimentary textural parameters which influence hydraulic properties. Hydrofacies maps showing the distribution of units of different grained-sized materials in the 300 Area (Chapter 4) were used as the framework for the model. These maps are more convenient for defining material zones for input into computer model meshes (Figures 5-1a through 5-1j) than isopach maps or cross-sections (Figure 5-2). The hydrofacies maps are based on limited subsurface well data and outcrop observation, and represent one of many alternative interpretations of interwell connectedness of the hydrofacies. The hydrofacies maps utilized here do not reflect variations in cementation, sorting, grain shape, or packing which may affect hydraulic properties. This shortcoming of the data may have resulted in the grouping of hydraulically different sediments into one hydrofacies. Hydraulic understanding of the hydrofacies could have been greatly improved if intact samples had been available.

5.2 BOUNDARY CONDITIONS USED IN THE MODEL

The 300 Area borders the Columbia River, which has a variable stage of several feet over a period of days to weeks and significantly affects the water table in the area (Lindberg and Bond 1979, Figures 5-3a and 5-3c). Consequently, the ground water flow field in the 300 Area is unusually dynamic. Because of the dynamic nature of the 300 Area ground water flow system, modeling of the Area should be conducted in the transient mode. However, in this preliminary modeling exercise, the 300 Area was modeled assuming steady-state conditions to obtain a "first cut" estimate of hydraulic properties of the hydrofacies. Steady-state conditions were assumed in this preliminary model for several reasons:

- The spatial variations of parameter values could be preliminarily determined without the additional complexity of transient data and calculations.
- There were minimal transient data for calibration; only seven wells in the area have continuous monitors.
- The results provide preliminary information for comparison with a transient solution.
- The steady-state and steady-state inverse version of CFEST had to be converted to a MS-DOS 80386/87 environment before they could be used and before the inverse transient code could be developed.
- The inverse transient code was under development but not available at the time that the work was conducted.

Aquifer head conditions mapped by Lindberg and Bond (1979) were assumed to represent an average condition of the 300 Area water table (Figure 5-4). These maps were used to define model boundary conditions, to provide prior estimates of head for inverse-modeling, and for comparison with heads predicted by the ground water flow simulations. Boundary conditions for this preliminary steady-state model included fixed heads around the perimeter of the model and were taken to be equal to heads illustrated on Lindberg and Bond's maps. The top and bottom of the model were no-flow boundaries except in one case where fixed flux was defined over the process trenches. In this case, it was assumed 4×10^5 ft^3/d ($\sim 1.1 \times 10^4$ m^3/d) of water was leaking to the aquifer (Figure 5-1b).

5.3 MATERIAL PROPERTIES USED IN THE MODEL

Zones of homogeneous hydraulic properties had to be delineated for modeling purposes. Hydraulic conductivity zones, based on hydrofacies maps were transferred to the CFEST and CFEST-INV model grid (Figures 5-1c through 5-1j) to define the zonation of parameters spatially. As defined in Table 4-1, horizontal hydraulic conductivity estimated from a field test for each hydrofacies is: G 4×10^4 ft/d ($\sim 1.2 \times 10^4$ m/d); SG, 1×10^4 ft/d ($\sim 3 \times 10^3$ m/d); S, 2×10^2 ft/d (~ 6.1 m/d); and MS, 6×10^{-1} ft/d ($\sim 2 \times 10^{-1}$ m/d) and these values were used as starting values for the inverse solution. The units were assumed to be isotropic. These hydraulic conductivities were the only values available for each hydrofacies in the 300 Area.

It is not known if the values estimated for each hydrofacies are at the top, bottom, or middle, of the range of actual values.

5.4 MODEL RESULTS

The 300 Area was modeled to simulate the aquifer flow field as mapped by Lindberg and Bond (1979) on February 16, 1977. This map represents the head distribution at one point in time of a transient flow field, but was assumed to represent steady state to facilitate setup of the model.

When the estimated hydraulic conductivity of the hydrofacies presented in Table 4-1 were input to a forward model of the 300 Area using CFEST, the simulated aquifer heads (Figure 5-4) did not correspond as well as was desired with mea-sured heads (Figure 5-5). The mounding of the water table under the process trenches did not approach the magnitude found in the field by Lindberg and Bond (1979). However, the flow field over the rest of the model area did approximate the flow field observed in the 300 Area.

The hydraulic conductivity estimated by the inverse model for each zone was:

Hydrofacies	Hydraulic Conductivity (ft/d)		
	x	y	z
Gravel	8.6×10^4 (4.5×10^4)	8.6×10^4 (4.5×10^4)	4.55×10^4 (4.5×10^4)
Sandy-Gravel	3.7×10^3 (1×10^4)	3.7×10^3 (1×10^4)	1.39×10^4 (1×10^4)
Sand	1.95×10^2 (2×10^2)	1.95×10^2 (2×10^2)	1.85×10^2 (2×10^2)
Mud-Silt	6×10^{-1} (6×10^{-1})	6×10^{-1} (6×10^{-1})	5.3×10^{-1} (6×10^{-1})

NOTE: Original estimates from field tests are in parentheses.

The above values are preliminary estimates because the model must be continually refined to incorporate additional field data. During subsequent modeling, conditions which result in the more pronounced mounding must be determined, storage parameters estimated, and the transient nature of the flow field incorporated before the predicted values of hydraulic conductivity could be considered reliable and recharge estimated. To assess the probability that this configuration (or one very similar) will occur in the field and to assess confidence in the estimated parameter values an uncertainty assessment should be undertaken.

Use of hydraulic conductivities estimated by the inverse model as input to a forward model yields head distributions (Figure 5-5) more similar to the distribution presented by Lindberg and Bond (1979) than the forward solution

(Figure 5-6) based on estimates of hydraulic conductivity based on field tests. This is expected because the inverse modeling (i.e., calibration process) integrates more of the system than individual field tests. The trough-shaped depression of heads in the central portion of the 300 Area is slightly more pronounced in the simulations which use the inverse model parameter estimates than in the simulations using the parameters obtained from aquifer testing. The trough produced by the simulation using estimates of hydraulic conductivity from the inverse modeling is more similar to the map produced by Lindberg and Bond (1979) than the trough produced by the simulation using hydraulic conductivities interpreted from aquifer tests.

5.5 SUMMARY

Hydrofacies mapping based on grain size analysis has been used to define zones which are likely to have similar hydraulic character. This method produces nonunique geometries because of the inherent complexity of the subsurface geology. Zonation based on grain size variations was found to be a good initial approach for defining zones of different hydraulic characteristics even though zones may need to be further modified when consideration is given to sorting, cementation, grain shape, and other physical properties. An initial estimate of hydraulic conductivity of the hydrofacies was made using a steady-state, inverse flow model of the 300 Area. Estimates of hydraulic conducitivity can be improved and storage parameters estimated once more data are available and transient inverse modeling is conducted.

Figure 5-1. Hanford 300 Area Model Hydrofacies Maps/Grids. (Sheet 1 of 5)

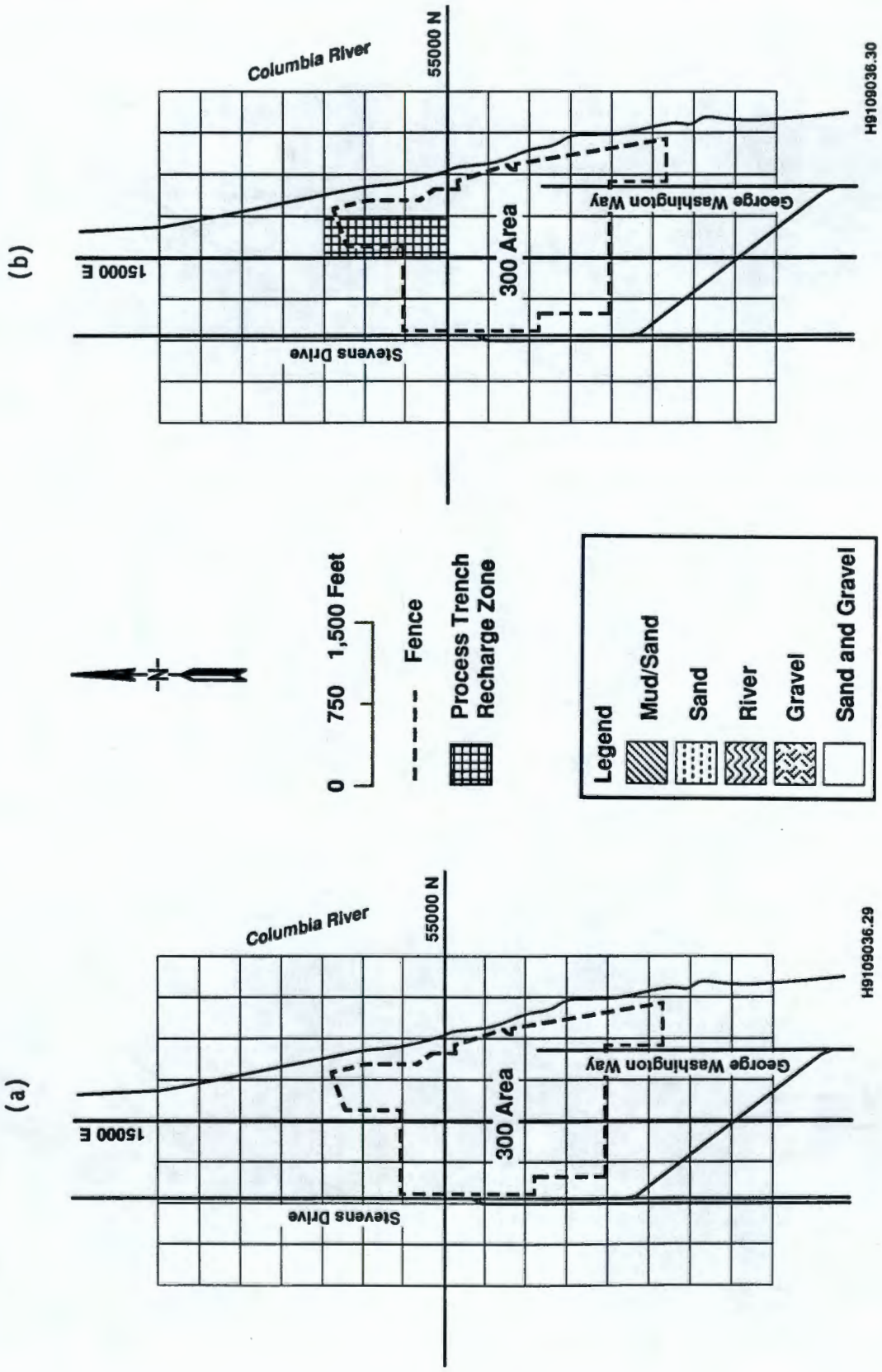

Figure 5-1. Hanford 300 Area Model Hydrofacies Maps/Grids. (Sheet 2 of 5)

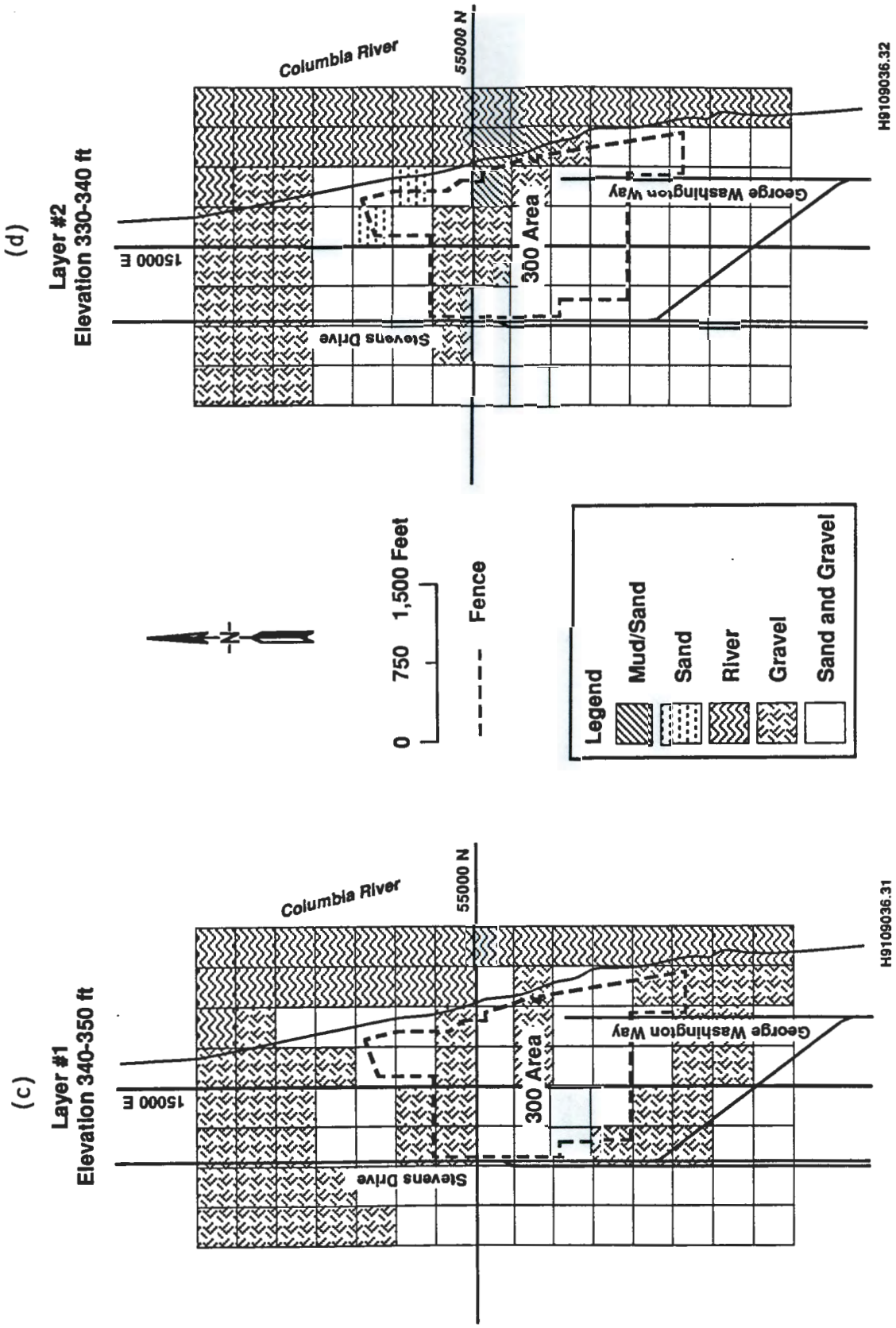

Figure 5-1. Hanford 300 Area Model Hydrofacies Maps/Grids. (Sheet 3 of 5)

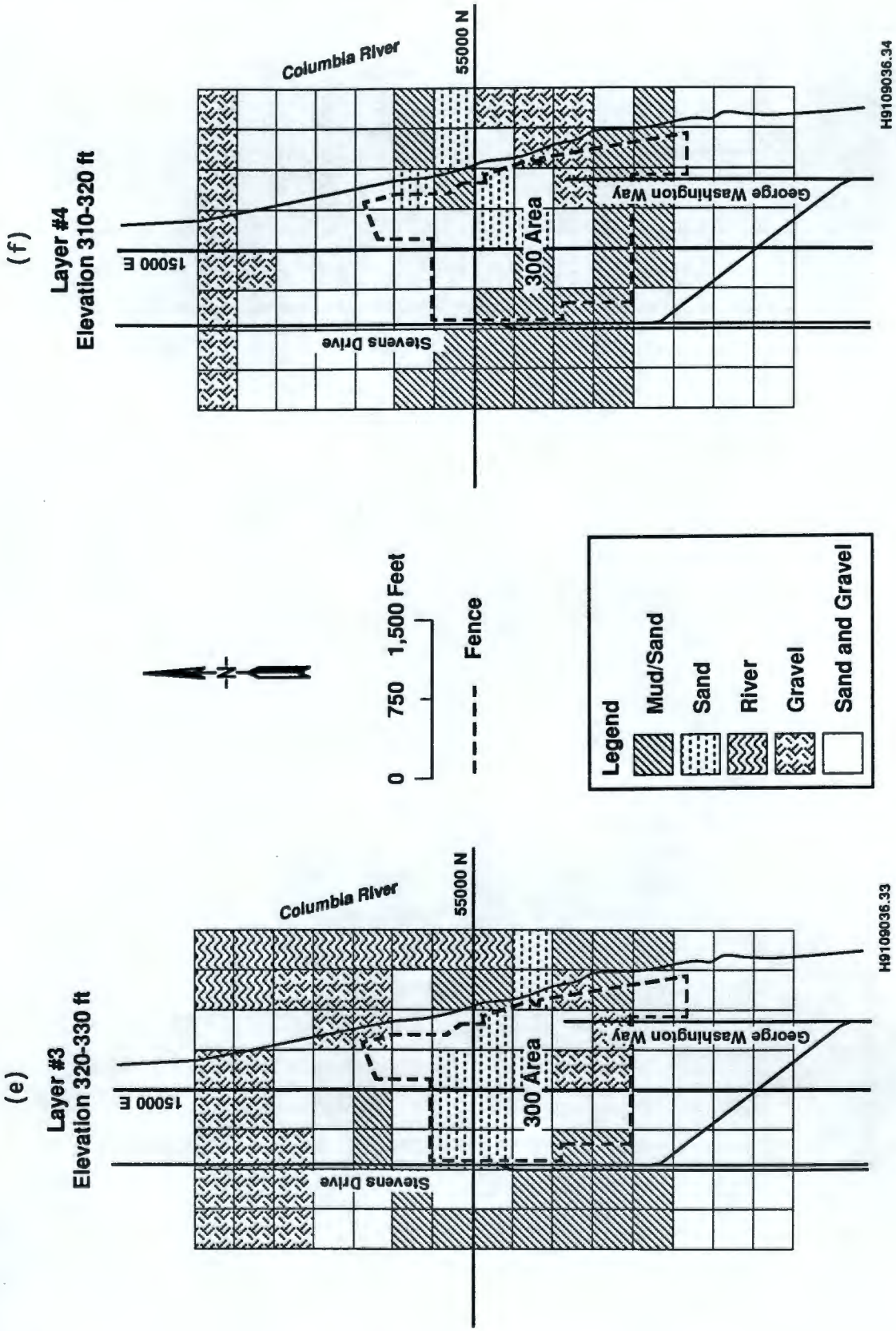

Figure 5-1. Hanford 300 Area Model Hydrofacies Maps/Grids. (Sheet 4 of 5)

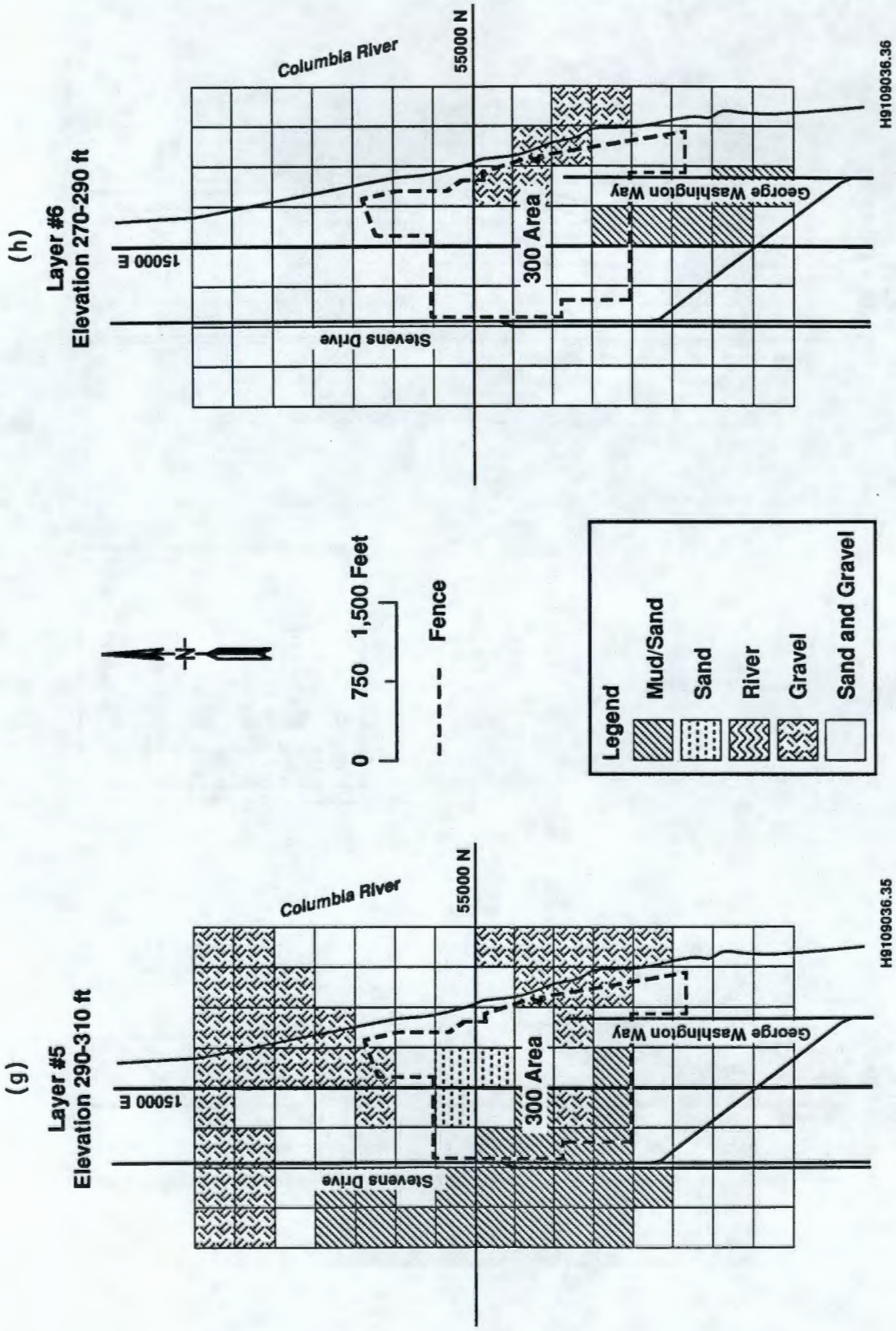

Figure 5-1. Hanford 300 Area Model Hydrofacies Maps/Grids. (Sheet 5 of 5)

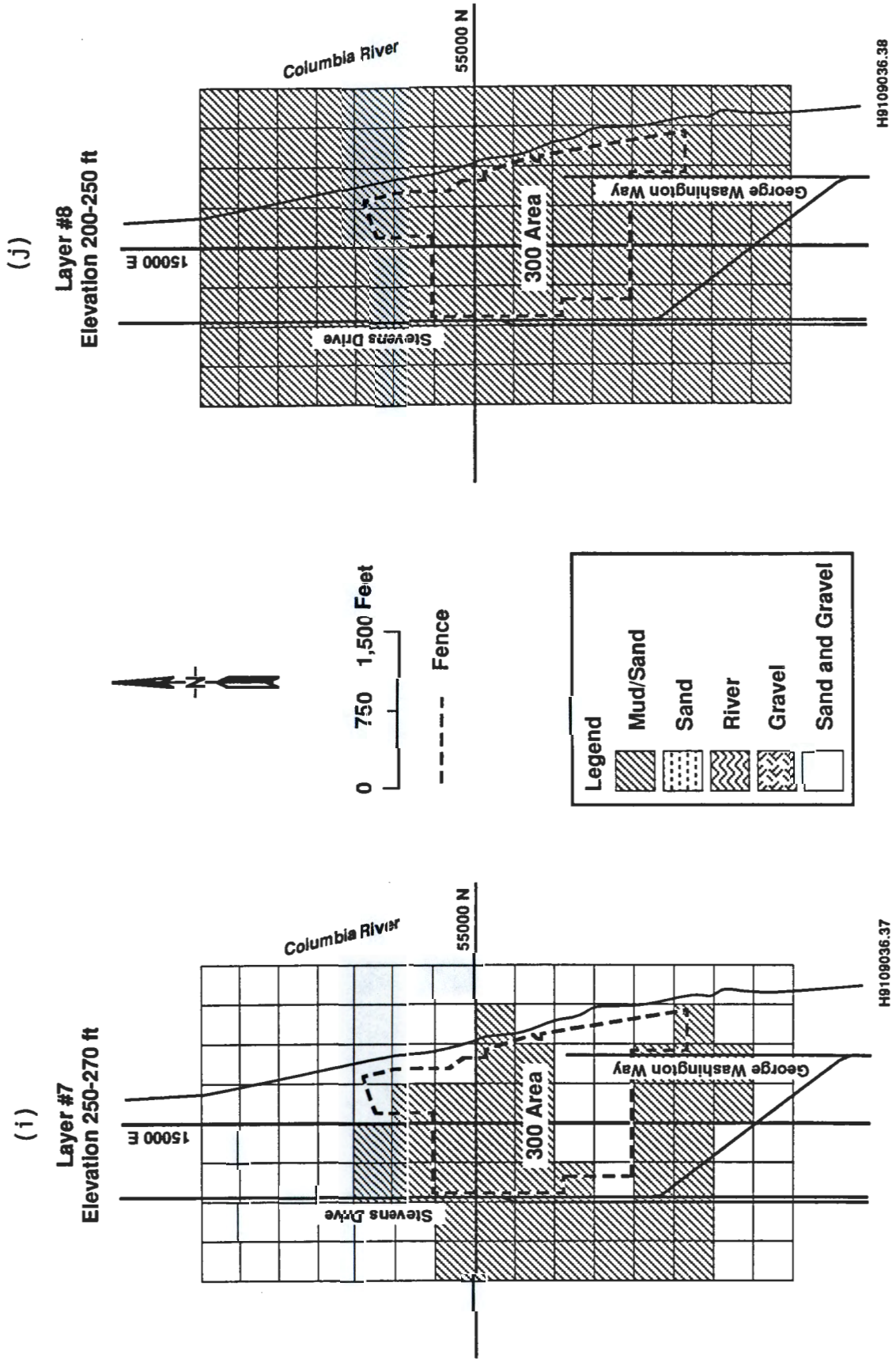

Figure 5-2. Example Geologic Cross Section of 300 Area. (Lindberg and Bond 1979)

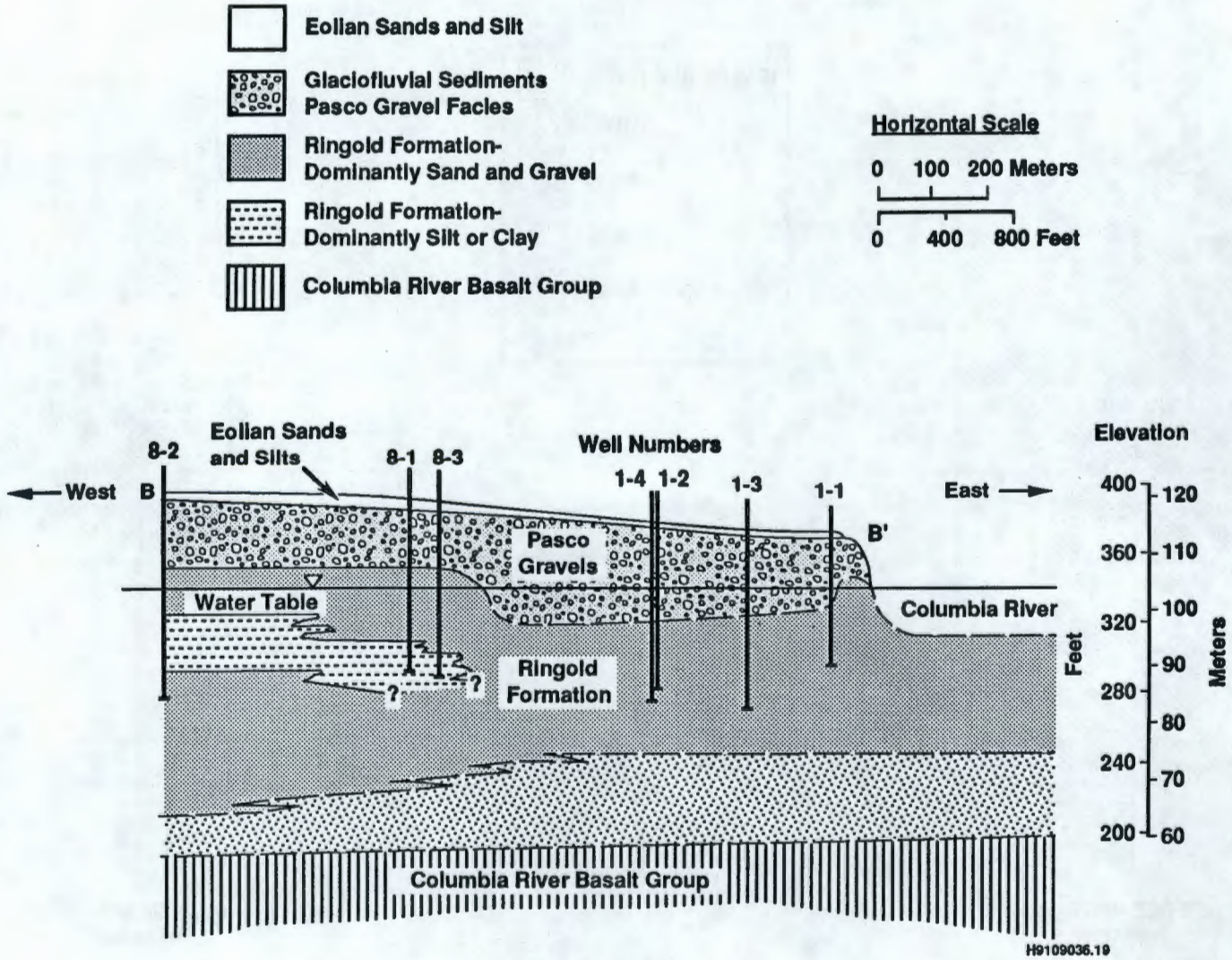

Figure 5-3a. Example Water Table Map Used to Model 300 Area - February 16, 1977 (Lindberg and Bond 1979)

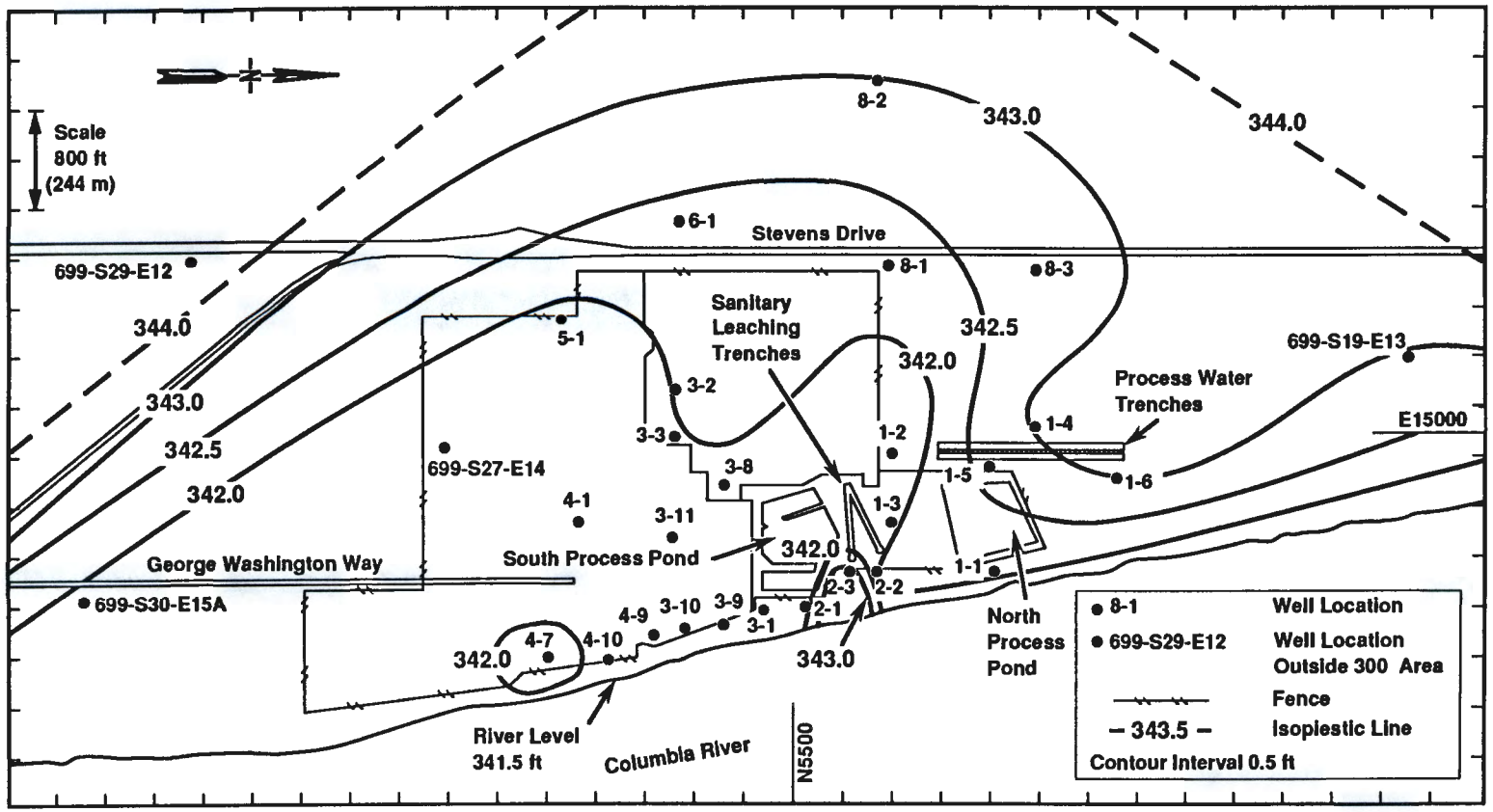

Figure 5-3b. Example Water Table Map Used to Model 300 Area - May 20, 1977 (Lindberg and Bond 1979)

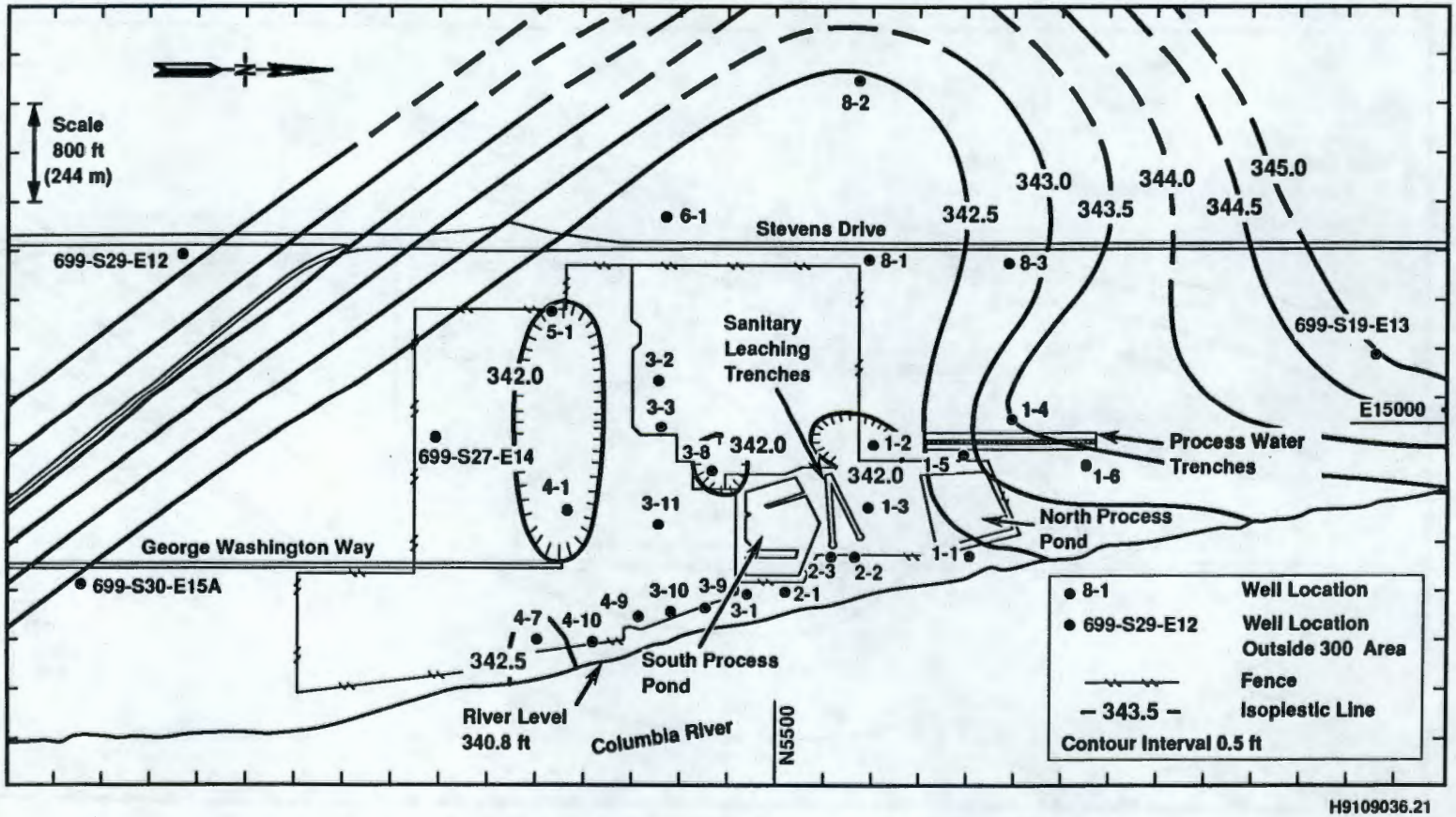

Figure 5-3c. Example Water Table Map Used to Model 300 Area - May 27, 1977 (Lindberg and Bond 1979)

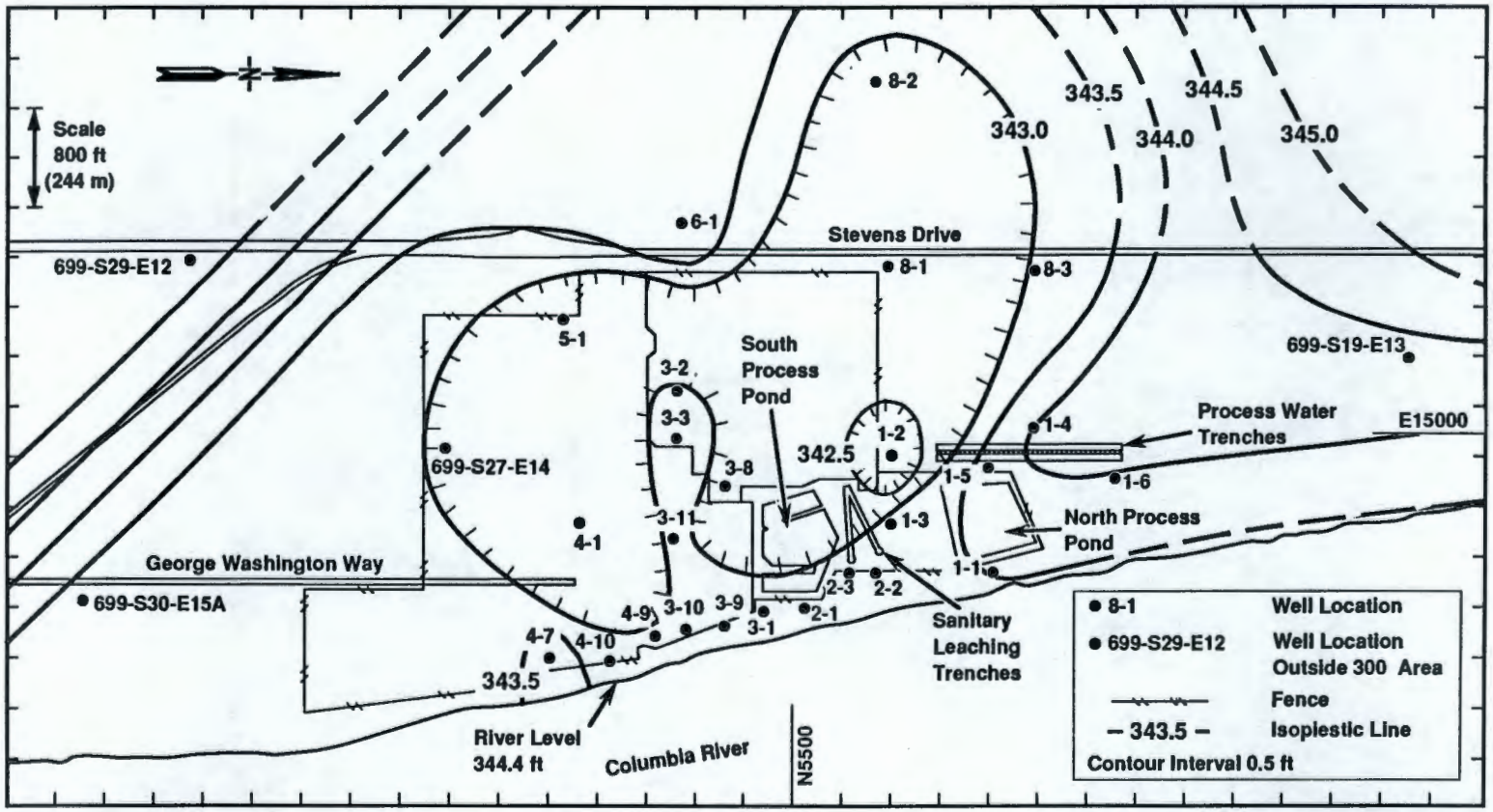

Figure 5-4. Flow Field Based on Initial Estimates of Hydraulic Conductivity and Heads at Boundaries.
(Boundary conditions based on maps prepared by Lindberg and Bond [1979]. The Columbia River's stage was 341.5 ft. Recharge from process trenches was assumed to be 3 M gal/d. Contour interval is 0.2 ft. Map coordinates based on Richland coordinate system.)

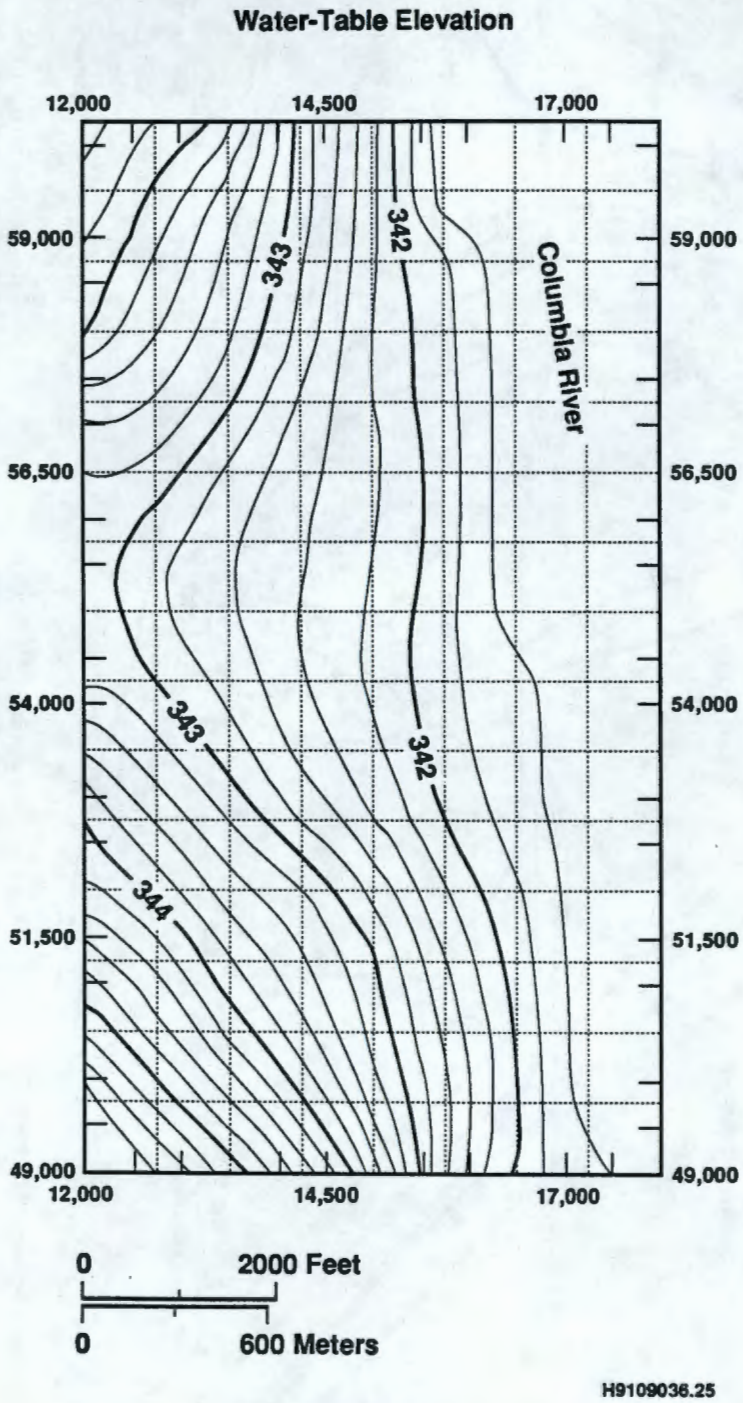

Figure 5-5. Flow Field Based on Aquifer Head Map Prepared by Lindberg and Bond (1979).
(The Columbia River's stage was 341.5 ft. Contour interval is 0.2 ft. Map coordinated based on Richland coordinate system.)

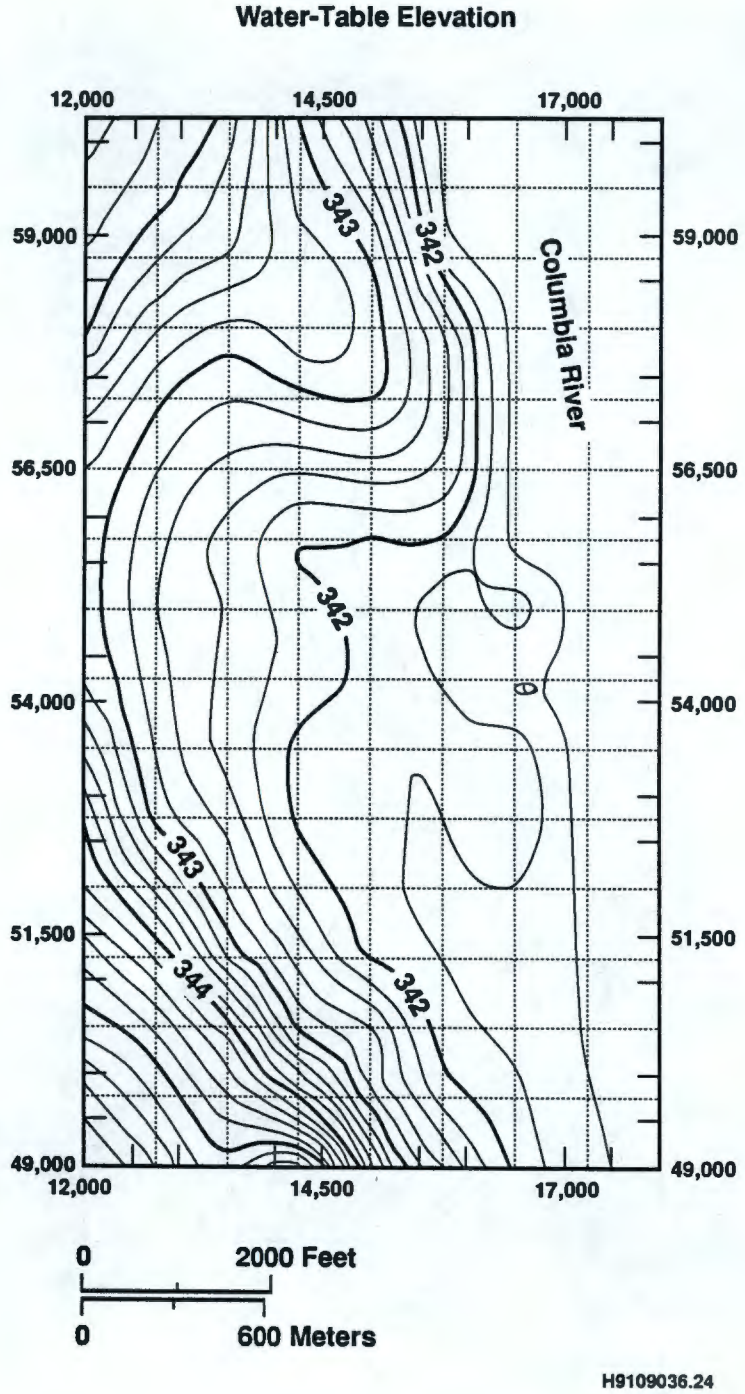

Figure 5-6. Flow Field Based on Inverse Estimates of Hydraulic Conductivity.
(Calculated heads based on prior estimates of hydraulic conductivity and aquifer head maps prepared by Lindberg and Bond [1979]. The Columbia River's stage was 341.5 ft. Recharge from process trenches assumed to be 3 M gal/d. Contour interval is 0.2 ft. Map coordinates based on Richland coordinate system.)

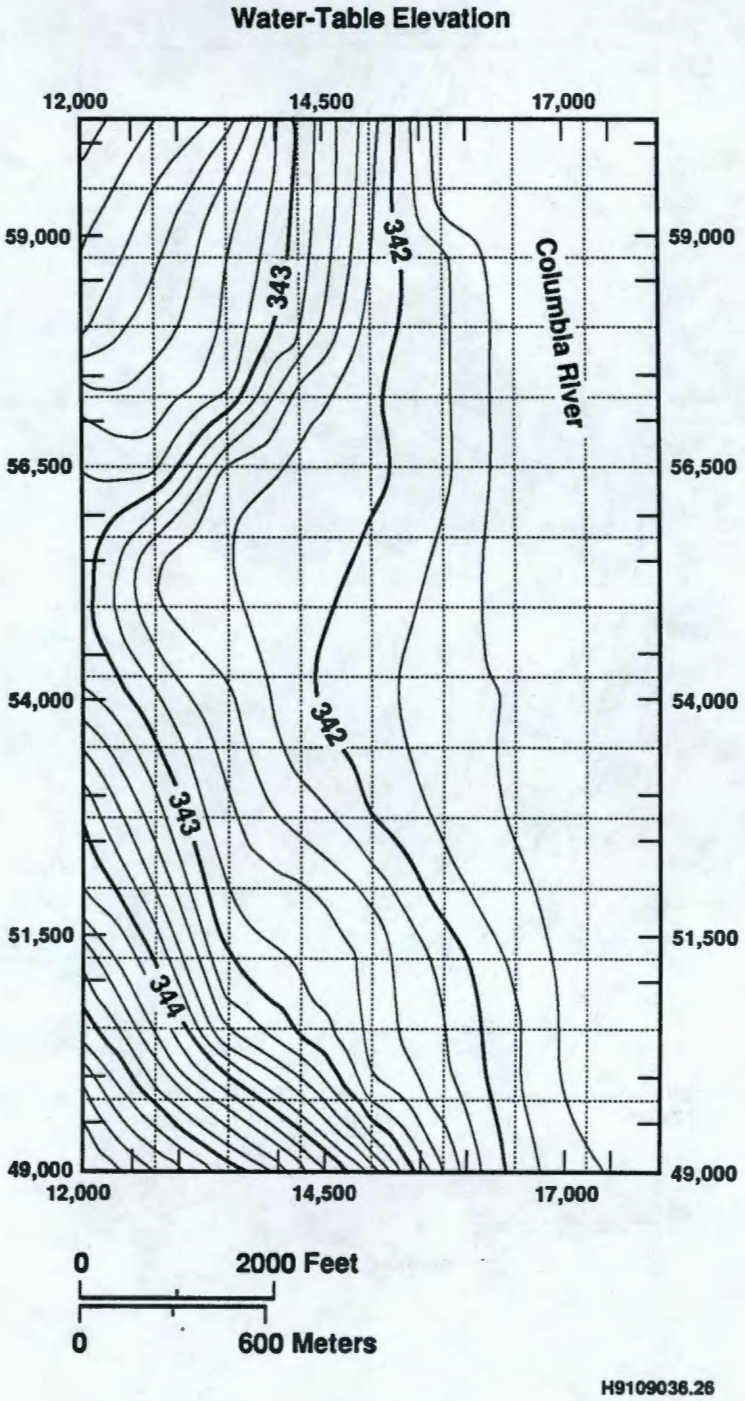

6.0 REFERENCES

Baker, V. R., 1973, *Paleohydrology and Sedimentology of Lake Missoula Flooding in Eastern Washington*, Geological Society of America, Special Paper 144.

Bjornstad, B. N., 1984, *Suprabasalt Stratigraphy Within and Adjacent to the Reference Repository Location*, RHO-SD-BWI-DP-039, Rockwell Hanford Operations, Richland, Washington.

_____, 1985, *Late Cenozoic Stratigraphy and Tectonic Evolution Within a Subsiding Basin, South-central Washington*, Geological Society of America, Abstracts with Programs, Vol. 17, No. 7.

Bjornstad, B. N., and K. R. Fecht, 1989, *Pre-Wisconsin Glacial-Outburst Floods: Pedogenic and Paleomagnetic Evidence from the Pasco Basin and Adjacent Channeled Scabland*, Geological Society of America, Abstracts with Programs, Vol. 21, No. 5.

CWRB, 1957, *Determination of Specific Yield and Storage Capacity*, California Water Rights Board, Special Report #2.

Delaney, C. D., K. A. Lindsey, and S. P. Reidel, 1991, *Geology and Hydrology of the Hanford Site: A Standardized Text for Use in Westinghouse Hanford Company Documents and Reports*, WHC-SD-ER-TI-0003, Rev. 0, Westinghouse Hanford Company, Richland, Washington.

DOE, 1988, *Consultation Draft, Site Characterization Plan, Reference Repository Location, Hanford Site, Washington*, DOE/RW-0164, 9 Vols., U.S. Department of Energy, Office of Civilian Radioactive Waste Management, Washington, D.C.

Eckis, R., 1934, *Geology and Ground Water Storage Capacity of Valley Fill*, California Division of Water Resources Bulletin, Vol. 45, p. 91-246.

Fecht, K. R., S. P. Reidel, and A. M. Tallman, 1985, *Paleodrainage of the Columbia River System on the Columbia Plateau of Washington State: A Summary*, RHO-BW-SA-318P, Rockwell Hanford Operations, Richland, Washington.

Folk, R. L., 1954, *The Distinction Between Grain Size and Mineral Composition in Sedimentary-Rock Nomenclature*, Journal of Geology, Vol. 62, p. 344-359.

Freeze, R. A. and J. A. Cherry, 1979, *Groundwater*, Prentice Hall Inc., Englewood Cliffs, New Jersey.

Galloway, W. E., 1981, "Depositional Architecture of Cenozoic Gulf Coastal Plain Fluvial Systems", in *Recent and Ancient Nonmarine Environments, Models for Exploration*, p. 127-155.

Grollier, M. J. and J. W. Bingham, 1971, *Geologic Map and Sections of Parts of Grant, Adams, and Franklin Counties, Washington*, U.S. Geological Survey Miscellaneous Geologic Investigations Series Map I-589, 6 sheets, 1:62500.

_____, 1978, *Geology of Parts of Grant, Adams, and Franklin Counties, East-central Washington*, Washington Division of Geology and Earth Resources Bulletin, Vol. 71, 91 p.

Gupta, S. K., C. R. Cole, C. T. Kincaid, and A. M. Monti, 1987, *Coupled Fluid, Energy, and Solute Transport (CFEST) Model: Formulation and User's Manual*, BMI/ONWI-660, Office of Nucler Waste Isolation, Battelle Memorial Institute, Columbus, Ohio.

Gustafson, E. P., 1973, *The Vertebrate Fauna of the Late Pliocene Ringold Formation, South-central Washington*, University of Washington, Seattle, Washington, 164 p.

_____, 1985, "Soricids (Mammalia, Insectivora) from the Blufftop Local Fauna, Blancon Ringold Formation of Central Washington, and the Correlation of Ringold Formation Faunas", *Journal of Vertebrate Paleontology*, Vol. 5, p. 88-92.

Hazen, 1910, "Discussion of Dams on Sand Formations", in *Transactions of the American Society of Civil Engineers*, Vol. 73, p. 199-221.

Holtz, R. D. and W. D. Kovacs, 1981, *An Introduction to Geotechnical Engineering*, Prentice Hall, 733 p.

Hooper, P. R., 1982, "The Columbia River Basalts", in *Science*, Vol. 215, pp. 1463-1468.

IGWMC, 1989, "Solving Ground Water Problems with Models", in *Proceedings of the Fourth International Conference on the Use of Models to Analyze and Find Working Solutions to Ground Water Problems*, International Ground Water Modeling Center, Indianapolis, Indiana, 1203 p.

Ingram, R. L., 1967, "Sieve Analysis", in *Procedures in Sedimentary Petrology*, Wiley Interscience, New York, p. 49-67.

Lambe, T. W. and R. V. Whitman, 1969, *Soil Mechanics*, John Wiley and Sons, 553 p.

Lindberg, J. W., and F. W. Bond, 1979, *Geohydrology and Ground-Water Quality Beneath the 300 Area, Hanford Site, Washington*, PNL-2949, Pacific Northwest Laboratory, Richland, Washington.

Leopold, E. B. and R. Nickmann, 1981, *A Late Miocene Pollen and Spore Flora from the Hanford Reservation, Eastern Washington*, report submitted to Golder Associates (by what company and does it have a document number and is it available to public? what does Golder have to do with anything?, etc.,?), 23 p.

Lindsey, K. A., 1991, *Revised Stratigraphy for the Ringold Formation, Hanford Site, South-Central Washington*, WHC-SD-EN-EE-004, Rev. 0, Westinghouse Hanford Company, Richland, Washington, 12 p.

Lindsey, K. A., D. R. Gaylord, and E. P. Poeter, 1989, *Sedimentary and Stratigraphic Examination of the Ringold Formation, Hanford Nuclear Reservation, Washington, Applied Lithofacies Analysis*, Geological Society of America, Abstracts with Programs, Vol. 21, No. 5.

Lindsey, K. A., and D. R. Gaylord, 1990, "Lithofacies and Sedimentology of the Miocene-Pliocene Ringold Formation, Hanford Site, South-Central Washington", *Northwest Science*, Vol. 64, No., 3, p. 165-180.

Masch, F. D. and K. J. Denny, 1966, "Grain Size Distribution and its Effect on the Permeability of Unconsolidated Sands", *Water Resources Research*, Vol. 2, No. 4, p. 665-672.

McKee, E. H., D. A. Swanson, and T. L. Wright, 1977, *Duration and Volume of Columbia River Basalt Volcanism: Washington, Oregon, and Idaho*, Geological Society of America, Abstracts with Programs, Vol. 9, No. 4, p. 463-464.

McKee, E 1979,

Merriam, J. C. and J. P. Buwalda, 1917, "Age of the Strata Referred to the Ellensburg Formation in the White Bluffs of the Columbia River", *University of California Bulletin of Geological Sciences*, Vol. 10, p. 255-266.

Miall, A. D., 1977, "A Review of the Braided River Depositional Environment", *Earth Science Reviews*, Vol. 13, p. 1-62.

_____, 1978, "Lithofacies Types and Vertical Profile Models in Braided River Deposits: A Summary", in *Fluvial Sedimentology*, Canadian Society of Petroleum Geologists Memoir 5, p. 597-604.

_____, 1985, "Architectural-Element Analysis: A New Method of Facies Analysis Applied to Fluvial Deposits, *Earth Science Reviews*, Vol. 22, pp. 261-308.

_____, 1987, "Recent Developments in the Study of Fluvial Facies Models", in *Recent Developments in Fluvial Sedimentology*, F. G. Ethridge, R. M. Flores, and M. D. Harvey (eds.), Society of Economic Paleontologists and Mineralogists Special Publication 39, pp. 1-9.

Mullineaux, D. R., R. E. Wilcox, W. F. Ebaugh, R. Fryxell, and M. Rubin, 1978, "Age of the Last Major Scabland Flood of the Columbia Plateau in Eastern Washington", *Quaternary Research*, Vol. 10, pp. 171-180.

Myers, C. W. and S. M. Price, 1979, *Geologic Studies of the Columbia Plateau: A Status Report*, RHO-BWI-ST-4, Rockwell Hanford Operations, Richland, Washington.

Newcomb, R. C., 1958, "Ringold Formation of Pleistocene Age in the Type Locality, the White Bluffs, Washington", *American Journal of Science*, Vol. 256, pp. 328-340.

Newcomb, R. C., J. R. Strand, and F. J. Frank, 1972, *Geology and Groundwater Characteristics of the Hanford Reservation of the Atomic Energy Commission, Washington*, U.S. Geological Survey Professional Paper 717.

NRC, 1990, *1990 Ground Water Models*, National Research Council, National Academy Press, Washington, D.C., 303 p.

Packer, D. R. and J. M. Johnson, 1979, *A Preliminary Investigation of the Magnetostratigraphy of the Ringold Formation*, RHO-BWI-C-46, Rockwell Hanford Operations, Richland, Washington, 48 p.

Piper, A. M., H. S. Gale, H. E. Thomas, and T. W. Rodinson, 1939, *Geology and Groundwater Hydrology of the Mokelumne Area, California*, U.S. Geological Survey Water Supply Paper 780, p. 101-121.

PSPL, 1982, *Stratigraphic Investigation of the Skagit/Hanford Nuclear Project, Skagit/Hanford Nuclear Project Preliminary Safety Analysis Report*, Vol. 5, Appendix 2R, Puget Sound Power and Light Company, Bellevue, Washington.

Reidel S. P., and K. R. Fecht, 1981, "The Wanapum and Saddle Mountains Basalts of the Cold Creek Syncline Area", in *Subsurface Geology of the Cold Creek Synclines: Richland, Washington*, C. W. Myers and S. M. Price (eds.), RHO-BWI-ST-14, Rockwell Hanford Operations, Richland, Washington, p. 3.1-3.45.

Reidel, S. P., 1984, "The Saddle Mountains: The Evolution of an Anticline in Yakima Fold Belt", *American Journal of Science*, Vol. 284, pp. 942-978.

Reidel, S. P., and P. R. Hooper, (eds.) 1989, *Volcanism and Tectonism in the Columbia River Flood Basalt Province*, Geological Society of America Special Paper 239, 386 p.

Reidel, S. P., T. L. Tolan, P. R. Hooper, M. H. Beeson, K. R. Fecht, R. D. Bentley, and J. L. Anderson, 1989a, "The Grande Ronde Basalt, Columbia River Basalt Group: Stratigraphic Descriptions and Correlations in Washington, Oregon, and Idaho" in *Volcanism and Tectonism in the Columbia River Flood Basalt Province*, Geological Society of America Special Paper 239, p. 21-53..

Reidel, S. P., K. R. Fecht, M. C. Hagood, and T. L. Tolan, 1989b, "The Geologic Evolution of the Central Columbia Plateau", in *Volcanism and Tectonism in the Columbia River Flood Basalt Province*, Geological Society of America Special Paper 239, p. 247-264.

Rust, B. R., 1978, "Depositional Models for Braided Alluvium", in *Fluvial Sedimentology*, A. D. Miall (ed.), Canadian Society of Petroleum Geologists Memoir 5, pp. 605-625.

Rust, B. R., and E. H. Koster, 1984, "Coarse Alluvial Deposits", in *Facies Models*, 2nd ed., R. G. Walker (ed.), Geoscience Canada Reprint Series 1, p. 53-70.

Smith, G. A., B. N. Bjornstad, and K. R. Fecht, 1989, "Neogene Terrestrial Sedimentation on and Adjacent to the Columbia Plateau: Washington,

Oregon, and Idaho", in *Volcanism and Tectonism in the Columbia River Flood Basalt Province*, S. P. Reidel and P. R. Hooper (eds.), Geological Society of America Special Paper 239, 386 p.

Swanson, D. A., T. L. Wright, P. R. Hooper, and R. D. Bentley, 1979, *Revisions in Stratigraphic Nomenclature of the Columbia River Basalt Group*, U.S. Geological Survey Bulletin 1457-G, 59 p.

Tallman, A. M., K. R. Fecht, M. C. Marratt, and G. V. Last, 1979, *Geology of the Separations Areas, Hanford Site, South-Central Washington*, RHO-ST-23, Rockwell Hanford Operations, Richland, Washington, 132 p.

Tallman, A. M., J. T. Lillie, and K. R. Fecht, 1981, "Suprabasalt Sediments of the Cold Creek Syncline Area", in *Subsurface Geology of the Cold Creek Syncline*, C. W. Myers and S. M. Price (eds.), RHO-BWI-ST-14, Rockwell Hanford Operations, Richlandm Washington, 28 p.

Taylor, S. R., and S. M. McLennan, 1985, *The Continental Crust: Its Composition and Evolution*, Blackwell Scientific, 312 p.

Tolan, T. L., S. P. Reidel, M. H. Beeson, J. L. Anderson, K. R. Fecht, and D. A. Swanson, 1989, "Revisions to the Estimates of the Areal Extent and Volume of the Columbia River Basalt Group" in *Volcanism and Tectonism in the Columbia River Flood Basalt Province*, S. P. Reidel and P. R. Hooper (eds.), Geological Society of America Special Paper 239, p 1-20.

Waitt, R. B., Jr., 1980, "About Forty Last-Glacial Lake Missoula Jokulhlaups Through Southern Washington", *Journal of Geology*, Vol. 88, p. 653-679.

APPENDIX A

PREPARATION OF SAMPLES FOR XRF ANALYSIS

1. Samples were split using a mechanical sample splitter to assure that the sediments used were representative.

2. Samples were sieved and all sediments greater than -1 phi (2 mm) in diameter and less than 4 phi (0.0625 mm) in diameter were removed. All samples tested were sand sized.

3. Sands were washed using a deflocculent and distilled water as described by Ingram (1971). Sediment samples were stirred gently before silt and clay residues were decanted. Decantation times were determined using the Stokes settling equation.

4. Once dry, the washed samples were placed in a Tema swingmill (shatterbox or ringmill) with tungsten carbide surfaces, and milled for 2 minutes. Three and one half grams of this rock powder were then mixed with 7.0 g of pure lithium tetraborate ($Li_2B_4O_7$) and, with an enclosed glass bead, mixed automatically for 10 minutes. The mixed powders were then emptied into graphite crucibles and placed in a preheated furnace at 1000°C. Fusion took place 5 minutes from the time the preheated furnace reached its 1000°C level after loading. Each bead was then reground in the Tema swingmill for 35 seconds, the glass powder replaced in the graphite crucibles and refused for 5 minutes.

5. After the second fusion, the cooled beads were labelled with an engraver, their flat surfaces were ground on coarse grit (#240) for approximately 10 seconds, on fine grit (#600) for approximately 10 seconds, washed in an ultrasonic cleaner, dried, and then loaded into the XRF spectrometer.

REFERENCE

Ingram, R. L., 1971, "Sieve Analysis" in *Procedures in Sedimentary Petrology*, Wiley Interscience, New York, New York.

APPENDIX B

PROCEDURES FOR ICP/MS ANALYSIS

1. Samples were split using a mechanical sample splitter to assure that the sediments used were representative.

2. Samples were sieved and all sediments greater than -1 phi (2 mm) in diameter and less than 4 phi (0.0625 mm) in diameter were removed. Thus, all samples tested were sand sized.

3. Sands were washed using a deflocculent and distilled water as described by Ingram (1971). Sediment samples were stirred gently before silt and clay residues were decanted. Decantation times were determined using the Stokes settling equation.

4. Once dry, the washed samples were placed in a Tema swingmill (shatterbox or ringmill) with tungsten carbide surfaces, and milled for 2 minutes.

5. 0.2 gram (200 milligrams) of this powder was digested in a solution of hydrochloric, nitric, perchloric and hydrofluoric acid at 110°C.

6. This solution was then evaporated to dryness, rehydrated with perchloric acid and brought to dryness again, then rehyrdated with dilute nitric acid to a final volume of 50 mL. Thus, the original powder was dissolved is a slightly acidic aqueous solution in the ratio of 0.2 gram rock to 50 grams water, or 1:250).

7. Sample solutions were aspirated for 60 seconds prior to intensity measurement, and the sample introduction system was rinsed with 2% nitric acid for 50 seconds between samples. Elemental intensities were sequentially measured ten times for 50 milliseconds each repeat. This gives a total integration time of 0.5 second per element.

8. Three rock standards were digested and measured concurrently with the unknown samples and used to form calibration curves. Two of the rock standards, MON-01 and GMP-01, are in-house standards that have been calibrated against 4 international rock standards. The third is a sample of Columbia River Basalt from the same quarry as the USGS standard BCR-1. Our tests have shown this rock to be indistinguishable from BCR-1

9. Elemental concentrations were calculated from the raw intensities using a commercial spreadsheet on a personal computer.

REFERENCE

Ingram, R. L., 1971, "Sieve Analysis" in *Procedures in Sedimentary Petrology*, Wiley Interscience, New York, New York.

APPENDIX C

PROCEDURES FOR ESTIMATING HYDRAULIC CONDUCTIVITY AND SPECIFIC YIELD FROM GRAIN SIZE DISTRIBUTION

HYDRAULIC CONDUCTIVITY FROM GRAIN SIZE DISTRIBUTIONS

Grain size distributions were used to estimate both hydraulic conductivity and specific yield. Hydraulic conductivities were estimated using established methods of Hazen (1910), Masch and Denny (1966), and McKee (1979). These methods were originally designed for estimating hydraulic conductivities in sand-sized sediments. The empirical relationships for each of these methods are summarized as follows.

Hazen's (1910) equation is based on the concept that hydraulic conductivity depends on intrinsic permeability (L2), which is solely dependent on the properties of the geologic material. Hazen tested well-sorted gravels and sands ranging from 4 to 0.0625 mm in diameter. He set limiting criteria for D5 and D10, defined as the diameter of the finest 5th and 10th percentile of the sample distribution. Hazen focused his research on sediments where D5 was greater than 3.75 phi (0.007 mm), and D10 ranged between 0.1 mm and 3.0 mm. These constraints greatly limit the range of sediment types for which his technique is applicable. Hazen used D10 as a representative grain size diameter that he concluded was characteristic of the hydraulic conductivity of sediments. To account for the influence of fluid density, viscosity, temperature, and choice of units, gravity, grain shape and packing arrangement, Hazen (1910) incorporated an empirically derived constant, C, which he multiplied by the square of D10.

$$K = C(D10)2 \qquad (1)$$

Masch and Denny (1966) sieved and washed Colorado River sands and then mixed sediment samples with predetermined grain size distributions. The statistical parameters of median grain size, standard deviation, expressed in phi units, skew, kurtosis, and modality (Folk 1954) were calculated for each sample. Hydraulic conductivity values for each distribution of grain sizes were determined by constant head permeameter tests and plotted against each statistical parameter for given grain size distributions.

Masch and Denny (1966) recognized that the mean grain size and all subsequent moments about the mean contributed to the variability of the value of the hydraulic conductivity. Masch and Denny further observed that the value of hydraulic conductivity was most sensitive to the median grain size and standard deviation. This suggests that for all the statistical parameters calculated, hydraulic conductivity is most dependent on the median grain size and the standard deviation. Masch and Denny compiled permeameter data for different sample distributions (by varying the values of median grain size and standard deviation) and created a nomogram which relates median grain size, standard deviation and hydraulic conductivity. After the grain size distribution is known, the hydraulic conductivity of well sorted to poorly sorted sands, as defined by Folk (1980) can be estimated from the median grain size and the standard deviation.

McKee's equation describes hydraulic conductivity as a function of a number of parameters including intrinsic permeability (k), density (p), gravity (g), and fluid viscosity (m):

$$k = [a/S(wi/di)]^2 \cdot [n^3/(36cT)(1-n)^2] \cdot [p\ g/m] \qquad (2)$$

Intrinsic permeability is further described as a function of porosity (n), tortuosity (T), grain shape (a), pore channel shape (c), and a representative grain size diameter (dm). Grain size analysis provided a means of quantifying dm which is depicted in the equation as the ratio of the average grain shape (a) to the sum of quotients of each weight fraction (wi) divided by its respective grain size (di). Each portion of the grain size distribution contributes to the weight fraction factor (wi/di) which, when summed, closely approximates the true grain size distribution. Wi usually varies arithmetically but di decreases exponentially (base 2). For samples that are relatively finer grained, as di decreases, the sum of wi/di increases, and other factors remaining constant, hydraulic conductivity decreases. McKee's technique was applied only to the portion of the sample that was coarse enough to be analyzed by mechanical sieving (>4.0 phi, 0.0625 mm). Therefore, conservative judgment was exercised when applying this method to samples that contain 5% or more silts or clays.

Specific Yield from Grain Size Distributions

Specific yield is the volume percentage of water that can be drained by gravity from a saturated unit volume of sediment. Both laboratory and field studies have demonstrated that specific yield is time dependent, increasing at a diminishing rate with time. Grain size distribution is the most critical parameter controlling specific yield as revealed by previously published correlations between grain size distribution parameters and specific yield (CWRB 1957; Eckis 1934; Piper 1939).

Eckis (1934) determined specific yields directly from laboratory experiments by using the relation:

$$n - Sr = Sy \qquad (3)$$

where:

n = porosity
Sr = specific retention
Sy = specific yield

Eckis defined the screen size retaining the cumulative finest 10th percentile as a representative grain size called grain size 10 (GS10). Porosity and specific retention were both plotted on the same axis versus GS10 and average curves fitted through the data points. Specific yield was estimated by subtracting the value of specific retention from porosity. Porosity was determined from bulk density measurements or estimated from grain size distributions. GS10 was determined from grain size analyses and then used to estimate specific retention and specific yield respectively.

Piper (1939) determined specific retention by two distinct methods which he termed: (1) volumetric analysis, and (2) specific retention. Piper correlated specific retention and grain size data from the 16 samples of undisturbed sediment, and using equation 3 correlated mean grain size to specific yield. Piper noted that a set of only 16 samples was not statistically significant. In spite of this, he still surmised that sediment samples with low standard deviations tended to have higher specific yields than samples with higher standard deviations.

The California Water Rights Board (CWRB) (1957) utilized well log records to estimate the specific yield of unconfined aquifers in an effort to evaluate ground-water resources. Before ground water resources could be evaluated, correlations between the grain size distributions and specific yield, and between geologic log documentation and grain size distributions were established. The grain size parameter GS10 was chosen as a representative grain size. Correlations from grain size distributions indicated the median grain size was approximately 1 phi unit smaller than GS10. This correlation allowed the use of existing geologic logs (which generally listed the median grain size) for estimating GS10.

REFERENCES

CWRB, 1957, *Determination of Specific Yield and Storage Capacity*, California Water Rights Board, Special Report #2.

Eckis, R., 1934, *Geology and Ground Water Storage Capacity of Valley Fill*, California Division of Water Resources Bulletin, Vol. 45, p. 91-246.

Folk, R. L., 1954, *The Distinction Between Grain Size and Mineral Composition in Sedimentary-Rock Nomenclature*, Journal of Geology, Vol. 62, p. 344-359.

Hazen, 1910, "Discussion of Dams on Sand Formations", in *Transactions of the American Society of Civil Engineers*, Vol. 73, p. 199-221.

Masch, F. D., and K. J. Denny, 1966, "Grain Size Distribution and Its Effect on the Permeability of Unconsolidated Sands" in *Water Resources Research*, Vol. 2, No. 4, p. 665-672.

McKee, 1979

Piper, A. M., H. S. Gale, H. E. Thomas, and T. W. Rodinson, 1939, *Geology and Groundwater Hydrology of the Mokelumne Area, California*, U.S. Geological survey Water Supply Paper 780, p. 101-121.

ATTACHMENT

This attachment presents a copy of a permeability theory provided by C. R. McKee, Associate Professor in Department of Civil Engineering, at the University of Wyoming.

C. R. McKee

2. PERMEABILITY THEORY

To better understand the meaning of permeability, we begin with Darcy's law for flow of groundwater in an aquifer. The equation is

$$Q = -T\frac{h_2 - h_1}{x_2 - x_1} \qquad (2.1)$$

where Q is the flow through an area element 1 ft wide and a depth equal to the thickness of the aquifer. The flow is in units of volume/unit width/unit time, while h is the head and T is the transmissivity of the aquifer. A minus sign is used in eq 2.1 since the flow is opposite to the direction of head increase. Transmissivity is given by

$$T = Kb \qquad (2.2)$$

where b is the aquifer thickness and K the hydraulic conductivity

$$K = \frac{k\rho g}{\mu} \qquad (2.3)$$

In this equation k is permeability, ρ fluid density, g acceleration of gravity, and μ is the fluid viscosity. Unlike transmissivity and hydraulic conductivity, permeability is theoretically a medium property and independent of the fluid or aquifer thickness. To a large extent, permeability can usually be regarded as a formation property. A major exception to this rule occurs when particles such as clay are strongly affected by the chemical properties of a particular fluid flowing through the sample.

When clays are not a major factor, permeability can be computed from a knowledge of the size distribution of the grains and porosity of the sample. Such a calculation assumes that the formation is unconsolidated with no cementation of grains, and that the various sizes are homogeneously mixed. Treatment of clays and other particles less than 1 micron in diameter is discussed below.

The derivation begins with the formula for average fluid velocity v, and head loss in a pipe (Bird, Stewart, Lightfoot p. 197)

$$v = -\frac{R^2 \rho g}{c\mu} \frac{h_\ell - h_o}{\ell} \qquad (2.4)$$

where ℓ is the sample length, and R the hydraulic radius of the conduit defined as

$$R = \frac{\text{cross-section available for flow}}{\text{wetted perimeter of pipe}} \quad . \qquad (2.5)$$

For a circular pipe, the hydraulic radius is ½ the actual pipe radius. The constant c in eq. 2.4 has the value c for pipes of circular cross-section. It is one of the strengths of the hydraulic radius concept that the constant c does not change appreciably for channels of different shapes (see table 2.1).

Table 2.1 Values of c for viscous flow in various cross-sectional shapes (after Carmen).

	Shape	c
1.	circle	2.00
2.	ellipse, semi-axes a,b:	
	(i) a = 2b	2.13
	(ii) a = 10b	2.45
3.	square	1.78
4.	rectangles, sides a,b:	
	(i) a = 2b	1.94
	(ii) a = 10b	2.65
5.	parallel slit (fracture)	3.00
6.	equilateral triangle	1.67
7.	annuli in pipes with concentric cores	2.0-3.0
8.	annuli in pipes with eccentric cores, radii a_1 and a_2:	
	(i) e < 0.7	1.7-3.0
	(ii) e > 0.7	1.2-2.0
	e = eccentricity = $b/(a_1 - a_2)$ b = distance between centers	

If shapes other than circular were choosen, the factor c would

change slightly. Even cases 7 and 8 (channels with cores) corresponding to partial plugging of channels with grains, does not modify c greatly.* However, as shown below, mean grain diameter and porosity can change significantly thus accounting for differences in permeability of various media.

Obviously it would be very difficult or impossible to measure the cross-sectional area and wetted perimeters of the highly irregular pore geometry. Instead the hydraulic radius will be related to the distribution of grain sizes -- a quantity which can be directly measured. This is accomplished by multiplying the numerator and denominator of eq. 2.5 by the length of a channel to obtain

$$R = \frac{\text{volume available for flow}}{\text{total wetted surface}} \qquad (2.6)$$

Dividing numerator and denominator of eq. 2.6 by the total sample volume (grains and voids) gives

hydraulic radius of conduit

$$R = \frac{\phi}{S} \qquad (2.7)$$

where ϕ is the porosity defined as (void volume)/(sample volume), and S is the specific surface area (wetted surface)/(sample volume). If a unit volume is considered, then grains occupy a volume equal to $(1 - \phi)$, and the specific surface/unit volume of grains is then

wetted surface / total volume

$$S_g = \frac{S}{(1 - \phi)} \qquad (2.8)$$

grain volume

The reason for using S_g is that it can be related to grain size. For uniformly sized spherical paritcles we have

$$S_g = \frac{4\pi r^2}{\frac{4}{3}\pi r^3} = \frac{6}{d_m} \qquad (2.9)$$

% grain volume

where d_m is the grain diameter. If grains of the same size are

[Specific surface/unit volume of grains]

not spherical, then a shape factor, a, must be introduced as follows

$$S_g = \frac{6}{a d_m} \tag{2.10}$$

to account for particle asymmetry. Table 2.2 gives values of the shape factor for various materials.

Table 2.2 Values of the particle shape factor from Carmen

Material	Shape Factor a
spheres	1.00
Ottawa sand, nearly spherical	0.95
sand, rounded	0.83
sand, average for various types	0.75
sand, angular	0.73
pulverized glass	0.73
flint sand, jagged	0.66
natural coal dust, less than 3/8 in.	0.65
Wilcox sand, jagged	0.63
flint sand, jagged flakes	0.43
mica flakes	0.28

To arrive at a mean grain diameter when a distribution of sizes is present we begin with the definition of specific surface area as

$$S_g = \frac{\text{total surface area of grains}}{\text{total volume of grains}} = \frac{\Sigma \pi n_i d_i^2 a^2}{\Sigma \frac{1}{6} \pi n_i d_i^3 a^3} \tag{2.11}$$

The symbol Σ is a summation sign and indicates that we are to add the surface areas (numerators) and grain volumes (denominators) separately for each grain size group and then perform the division to obtain the specific surface area with respect to grains (S_g). In equation 2.11, n_i is the number of grains with diameter d_i.

To avoid counting the number of grains within each size group, we convert eq. 2.11 to weight fractions by multiplying numerator and denominator by the grain density ρ_g. The denominator then becomes the total sample weight, and eq. 2.11 after multiplying and dividing the numerator by $6d_i a$ yields

$$S_g = 6 \Sigma \frac{w_i}{d_i a} = \frac{c}{d_m} \qquad (2.12)$$

The numerator w_i is the weight fraction of the sample with diameter d_i. Substituting eq. 2.12 into eq. 2.9, the mean grain diameter is obtained in terms of an equivalent mixture of spherical particles as

$$d_m = \frac{a}{\Sigma \frac{w_i}{d_i}} \quad . \qquad (2.13)$$

Substituting equations 2.7, 2.8, and 2.9 into eq. 2.4 yields

$$q = \phi v = \left[- \frac{d_m^2 \phi^3 \rho g}{36 c \mu (1-\phi)^2 T} \right] \frac{h_\ell - h_o}{\ell} \quad , \qquad (2.14)$$

where q is the volumetric flow/unit area/unit time. Velocity has been multiplied by porosity since it is the average flow over the entire cross-section of the core which is usually measured instead of flow with respect to the cross-sectional area of the pore space. A tortuosity factor has also been included in the denominator of the right hand side of eq. 2.14. Tortuosity T, is defined as

$$T = \left[\frac{\text{actual length traveled}}{\text{sample length} = \ell} \right]^2 \qquad (2.15)$$

Tortuosity accounts for the fact that the fluid does not travel in a straight line through the sample. Instead it is constantly deflected by the grains such that a "tortuous" path results.

The square of the path ratio occurs in eq. 2.15 for two reasons. First, since the channel length is longer than the direct sample length ℓ, it has the effect of reducing the hydraulic gradient in eq. 2.14. Secondly, while velocity in a given channel may be constant, the fluid's rate of migration in the direction ℓ is reduced. This is due to the bending of the fluid's path at varying angles with respect to the direction ℓ as it traverses the sample. The tortuosity factor must therefore always be greater than or equal to one.

The coefficient of the difference in head in eq 2.14 is the hydraulic conductivity. From the relation (eq. 2.3) for hydraulic conductivity the permeability from eq 2.14 can be obtained as

$$k = \frac{d_m^2 \phi^3}{36cT(1-\phi)^2} \quad . \qquad (2.16)$$

It now remains to choose suitable values for the constants in eq. 2.16. Experimental data suggests that T lies between 2 and 2.5 for unconsolidated media, while c from table 2.1 may vary from 1.7 to 3.0.

For artificial mixtures in large packed columns, a value of 150 for 36cT works best. This value is suggested by Ergun (see Bird, Stewart, Lightfoot p. 200), and is in agreement with my experiments on large columns and particles at Livermore Labs. For finer industrial powders a value of 180 is recommended by Carmen. The examples I will present in section 3 are best fitted if 36cT is assigned the value 270, which is at the upper range of possible values for T and c (values of T were measured on artificial samples and are probably larger for natural materials). For the natural samples in sect. 3, the mean grain diameter and range of sizes is considerably different than the artificial mixtures in packed columns. For natural materials the trend is toward larger

values of the constants as the mean grain diameters become smaller and the spread of grain sizes greater. As smaller grains fill the spaces between larger grains, the tendency will be for Tortuosity to increase and for channel geometry to correspond more closely to the cases of channel plugging with low eccentricity ($c \rightarrow 3$ and possibly higher values in table 2.1). While a value of 270 for 36cT fits the examples in sect. 3 quite well, the reader should expect it vary from one formation to another. It is therefore advisable to determine its value indirectly from permeability measurements using eq. 2.14, porosity, and mean grain diameter by eq. 2.13, on a few select cores from the formation of interest.